Thermal and Magnetic Properties of Rare Earth Ions in Crystals By Crystal Field Theory

Thesis submitted to the
University of Roorkee
for the award of the Degree of
Doctor of Philosophy
in
Physics

By

SAT PALL TANEJA

DEPARTMENT OF PHYSICS
UNIVERSITY OF ROORKEE
ROORKEE
(INDIA)

May, 1971

C E R T I F I C A T E

Certified that the thesis entitled 'THERMAL AND MAGNETIC PROPERTIES OF RARE EARTH IONS IN CRYSTALS BY CRYSTAL FIELD THEORY' which is being submitted by Shri Sat Pall Taneja in fulfilment for the award of the degree of Doctor of Philosophy in Physics of University of Roorkee, Roorkee, is a record of his own work carried out by him under my supervision and guidance. The matter embodied in this thesis has not been submitted for the award of any other degree.

Furthermore it is certified that he has worked for a period more than 24 months full time research for preparing his thesis for Ph.D. degree at the University.

Dated May 4'1971

S. P. Puri

(S.P. Puri)
Department of Physics
University of Roorkee
Roorkee (India).

RÉSUMÉ

With a view to verify the accuracy of the crystalfield parameters from optical spectra for a number of rare-earth ions in anhydrous trichlorides and tribromides, hydrated ethylsulphates and sulphates, hydroxides (C_{3h}); phosphate, vanadate and Yttrium Aluminium garnet (D_{2d}) and thiocompounds (O_h), a study of thermal and magnetic properties is carried out in the framework of crystal field theory. Chapter I is introductory in content and discusses the technique employed and various physical quantities (Schottky specific heat, principal magnetic susceptibilities, spectroscopic splitting factors etc.) to be calculated in the following chapters. The crystal field potential for C_{3h} symmetry is discussed in detail and expressed in terms of operator equivalents. Throughout these calculations, the exchange interaction was ignored.

The anhydrous trichlorides and tribromides constitute a widely investigated class of rare-earth systems. Chapter II of this thesis deals with the thermal and magnetic properties of Nd^{3+}, Dy^{3+}, Ho^{3+} and Er^{3+} in $LaCl_3$, and Pr^{3+} and Er^{3+} in $LaBr_3$. Both the host lattices possess UCl_3 type hexagonal structure (space group C^2_{6h}) with bimolecular unit cell and the point symmetry at the rare-earth ion site is C_{3h}. The calculations are compared with the available experimental data.

The thermal and magnetic properties of $Nd^{3+}:La_2(SO_4)_3.9H_2O$, $Tb(OH)_3$ and $Tb^{3+}:Y(OH)_3$ systems are discussed in Chapter III. The optical spectra of these systems have been interpreted by assuming the point symmetry around the rare-earth ion to

be C_{3h} and we find that the same may be used to give thermal and magnetic properties satisfactorily.

The ethylsulphates of rare-earths form a series of hexagonal structure isomorphic to trichlorides. The calculations for thermal and magnetic properties of $Dy(C_2H_5SO_4)_3.9H_2O$ and $Yb(C_2H_5SO_4)_3.9H_2O$ constitute Chapter IV. These properties are found to be closely related to the properties of the individual ions.

The last chapter relates to the calculations of thermal and magnetic properties of Er^{3+} in YAlG, YPO_4, YVO_4, $CdIn_2S_4$, $CdInGaS_4$ and $ZnIn_2S_4$. The Yttrium Aluminium Garnet (YAlG) crystallizes in cubic group O_h^{10} in which Y^{3+} ion occupies dodecahedral sites. The Er^{3+} ions replace Y^{3+} ions substitutionally and it has been found that the crystal field at this site may be taken as tetragonal. Employing the crystal field parameters reported under the assumption of tetragonal field, calculations of Schottky specific heat, magnetic susceptibilities, μ_{eff} and g-values were carried out for Er^{3+}:YAlG over a temperature range 10-300°K. This system is of special interest because the crystal field splitting is appreciably large. Similar calculations for Er^{3+}:YPO_4 and Er^{3+}:YVO_4 with tetragonal fields at rare-earth ion sites are also included.

The thiocompounds $CdIn_2S_4$, $CdInGaS_4$ and $ZnIn_2S_4$ crystallize in the spinel structure typified by $Cd_{1/2}In_{1/2}[Cd_{1/2}In_{3/2}]S_4$. The Er^{3+} ion occupies the In^{3+} site and

has been found to possess a slight trigonal distortion on strongly cubic symmetry. The optical spectra of these systems have successfully been explained by approximating the site symmetry to be O_h. The Schottky specific heat and magnetic susceptibility are computed for the three systems under the assumption of O_h field. The g-values are calculated by incorporating slight trigonal distortions. The findings are compared with available experimental results.

The nice agreement with the available experiments in the systems discussed in the four chapters indicates that

(i) the crystal field parameters reported for the systems studied are reliably good;

(ii) the bulk thermal and magnetic properties are insensitive of small splittings as found in the two lowest levels of Tb^{3+} systems;

(iii) the thermal and magnetic properties of the garnet system can be obtained reliably under the D_{2d} field;

(iv) the approximation of low symmetry fields with higher ones is acceptable for calculations of thermal and magnetic quantities.

A C K N O W L E D G E M E N T S

I express my sincere appreciation to Dr. S.P. Puri for his constant guidance and encouragement during the course of this work. I feel incumbent upon me to express my gratitude to my coworkers Vishwamittar and S.N. Singh; to the former for help during the later stages of the work, and the latter for fruitful discussions.

It gives me pleasure to thank Professor S.K. Joshi, Head of the Physics Department for all the facilities made available to me, and other members of the Physics Community for their interest. Further I convey my grateful indebtedness to Dr. R.K. Gupta of Mathematics Department and Dr. Deo Raj for their unstinted assistance in computer programming in the initial stages of the work. I am equally thankful to other members of the Mössbauer group for their interest and help specially during the final stage of the manuscript. Mr. Ramesh Babu deserves my appreciation for the excellent typing job.

It, indeed, is a matter of pleasure to thank Professor C.W. Kimball for all the hospitality and encouragement extended to me during the course of writing. I owe special gratitude to my parents for their filial affections and inspiration throughout my formative career.

The financial assistance in the form of Research fellowship firstly by U.G.C. and, later on, by C.S.I.R., New Delhi, left me completely free of economic worries,

to devote singlemindedly to my research work. Lastly, it is my cherished obligation to express my appreciation to Incharge Computer Centre, S.E.R.C., Roorkee, for giving liberal access to the computing facilities on IBM 1620.

Sat Pall Taneja

(Sat Pall Taneja)

C O N T E N T S

		Page
CHAPTER I:	INTRODUCTION	1-17
	1.1 General Review and Electronic Structure of Rare-Earth Elements ..	1
	1.2 Crystal Field Theory ..	3
	1.3 General Hamiltonian and Crystal Field Potential ..	3
	1.4 Symmetry of Crystal Potential ..	5
	1.5 Calculation of Energy Spectrum and Crystal Quantum Numbers ..	10
	1.6 The Specific Heat ..	14
	1.7 The Paramagnetic Susceptibility ..	15
CHAPTER II:	STUDY OF ANHYDROUS RARE-EARTH TRICHLORIDES AND TRIBROMIDES	18-50
	2.1 Introduction ..	18
	2.2 Crystal Structure ..	20
	2.3 Theory and Calculations ..	21
	(i) $Nd^{3+}:LaCl_3$ ..	22
	(ii) $Dy^{3+}:LaCl_3$ ..	25
	(iii) $Ho^{3+}:LaCl_3$ ..	28
	(iv) $Er^{3+}:LaCl_3$ and $Er^{3+}:LaBr_3$ ..	31
	(v) $Pr^{3+}:LaBr_3$ ..	35
	2.4 Results and Discussion ..	39
	2.5 Comments and Conclusions ..	49
CHAPTER III:	THERMAL AND MAGNETIC PROPERTIES OF $Nd^{3+}:La_2(SO_4)_3.9H_2O$, $Tb(OH)_3$ AND $Tb^{3+}:Y(OH)_3$ SYSTEMS	51-62
	3.1 $Nd^{3+}:La_2(SO_4)_3.9H_2O$ ..	51-55
	3.1.1 Introduction ..	51
	3.1.2 Calculations ..	52
	3.1.3 Discussion ..	53

3.2 $Tb(OH)_3$ and Tb^{3+}:$Y(OH)_3$ .. 55-62

3.2.1 Introduction .. 55

3.2.2 Crystal Structure .. 56

3.2.3 Crystal Field Calculations .. 56

3.2.4 Discussion .. 59

CHAPTER IV: THERMAL AND MAGNETIC STUDIES OF DYSPROSIUM AND YTTERBIUM ETHYL SULPHATES 63-72

4.1 Introduction .. 63

4.2 Crystal Structure .. 65

4.3 Crystal Field Analysis .. 65

(a) Dysprosium Ethylsulphate .. 65
(b) Ytterbium Ethylsulphate .. 67

4.4 Discussion .. 69

CHAPTER V: STUDY OF Er^{3+} ION IN CRYSTAL FIELDS WITH D_{2d} AND O_h SITE SYMMETRIES 73-97

5.1. Thermal and Magnetic Properties of Er^{3+}:YalG .. 73-81

5.1.1 Introduction .. 73

5.1.2 Crystal Structure .. 75

5.1.3 Crystal Field Analysis .. 76

5.1.4 Discussion .. 78

5.2 Thermal and Magnetic Properties of Er^{3+}:YVO_4 and Er^{3+}:YPO_4. .. 81-88

5.2.1 Introduction .. 81

5.2.2 Crystal Structure .. 82

5.2.3 Calculations .. 82

5.2.4 Discussion .. 85

5.3 Thermal and Magnetic Properties of Er^{3+}:$CdIn_2S_4$, Er^{3+}:$CdInGaS_4$ and Er^{3+}:$ZnIn_2S_4$ Systems .. 88-97

5.3.1 Introduction .. 88

5.3.2 Crystal Structure .. 89

5.3.3 Calculations .. 89

5.3.4 Discussion .. 95

REFERENCES 98-105

LIST OF PUBLICATIONS 106-107

*****

CHAPTER I

INTRODUCTION

1.1 General Review and Electronic Structure of Rare-Earth Elements

During the last few years, the properties of rare-earth ions and their compounds have been the subject of extensive investigation and considerable headway has been forged in understanding the behaviour of rare-earth ions in crystals. These studies include paramagnetic resonance and relaxation, absorption and fluorescence spectra, Schottky specific heat and magnetic susceptibility etc. Whereas spectroscopic and paramagnetic resonance studies give information about a single electronic level, the specific heat and magnetic susceptibility measurements characterize the population density of various levels. Thus the thermal and magnetic studies serve as an additional check on the electronic structure of ions in paramagnetic substances, as derived from optical studies.

The fourteen rare-earths, whose atomic numbers range from 58(Ce) to 71(Lu), are characterized by their similar chemical and physical properties (1,2). These similarities emerge from the identical electronic structure of the valence shells, given by $\left[\,|Xe|(4f^n)\right]\left\{(5s)^2(5p)^6(5d)^1\ (6s)^2\right\}$; where n ranges from 1 to 14 for the entire series.

The rare-earths occur chiefly as trivalent ions and are strongly paramagnetic; in some cases these do exhibit ferromagnetic or antiferromagnetic coupling at low temperatures. It is the incomplete 4f shell which is responsible for the magnetic properties of the rare-earth ions. On formation of chemical

compounds the 4f electrons are not fully incorporated in the chemical bonds and being deep lying are shielded from ligand fields. This leaves the orbital angular momentum of 4f electrons unquenched and enhances the magnetic behavior. The type of coupling which is common and most applicable to the rare-earth group is the Russell-Saunders coupling, which considers only interactions of the s_i and s_j, and l_i and l_j, since other types of interactions are of a weaker nature. The resultant spin vector $\vec{S}$ is the vector sum of the individual electron spins and in a similar way $\vec{L}$ is the resultant orbital angular momentum. These two resultants in turn couple to form the total angular momentum $\vec{J}$. The orbital angular momentum quantum number, l, of the 4f electron shell is 3. Therefore, the (2l+1) magnetic quantum numbers of the orbitals are -3, -2, -1, 0, 1, 2 and 3. According to Pauli principle, each orbital may contain two electrons, one with a spin quantum number s = 1/2 and other with s = -1/2. Hund's rule states that in the most stable state; (i) the spin arrangement must have the maximum total angular momentum and (ii) the orbital arrangement should have the maximum orbital angulr momentum within the restriction that rule (i) and the Pauli principle are not violated. Electrons thus fill the 4f shell in the following order (l,s) = (3,1/2); (2, 1/2); (1,1/2); (0,1/2); (-1,1/2);.....; (0,-1/2). The total angular momentum quantum number J = L - S for less than a half-filled shell and J = L + S for more than half-filled shell. However, recently intermediate coupling has also been employed.

1.2 Crystal Field Theory

The crystal field theory is based on the assumption that central paramagnetic metal ion in a compound or system, is subjected to an electric field produced by the surrounding atoms or molecules, called the ligands; and is known as the crystal field (3). This basic assumption first made by Becquerel (4), was employed by Bethe (5) through the use of symmetry concepts, to show the effect of the symmetry and strength of a crystalline field on the splitting of the electronic levels of the metal ions. Lateron Kramers (6), Van Vleck (7) and Schlapp and Penney (8) extended the assumption, in connection with magnetic phenomena, that the surrounding ions may be regarded as point charges or point dipoles placed at lattice sites; these charges being polarizable by the presence of cations. The effect of the ligands is to set up static electric field which acts on the central ion.

1.3 General Hamiltonian and Crystal Field Potential

The study of the energy level structure of an ion situated in a crystal of a given symmetry depends on the crystalline surroundings. The free ion Hamiltonian can be written as (9)

$$H_{free} = -\frac{\hbar^2}{2m}\sum_i \nabla_i^2 - \sum_i \frac{Ze^2}{r_i^2} + \sum_{i\neq j}\frac{e^2}{r_{ij}} + \sum_i \xi_i (\vec{l}_i\cdot\vec{s}_i)$$

$$= H_o + \zeta(\vec{L}.\vec{S}) \; ; \qquad (1.1)$$

H_o includes the total kinetic energy, potential energy and interelectronic repulsion energy for all the electrons; $\zeta(\vec{L}.\vec{S})$ is the spin orbit interaction. When a rare-earth free ion is

subjected to magnetic field $\vec{H}$, the Hamiltonian becomes

$$H_1 = H_o + \zeta(\vec{L}.\vec{S}) + \mu_B(\vec{L} + 2\vec{S}).\vec{H}$$
$$= H_{free} + \mu_B g_J \vec{H}.\vec{J} = H_{free} + H' \qquad (1.2)$$

For the case $H' << \zeta(\vec{L}.\vec{S})$, each term characterized by J is split by H' into (2J+1) equally spaced levels according to the magnetic quantum number J_z, the energy of each magnetic sublevel being

$$E(J_z) = -g_J \mu_B H J_z, \qquad J_z = J, (J-1), \ldots, -(J-1), -J. \quad (1.3)$$

Here μ_B is Bohr magneton and g_J, Landé splitting factor $g_J = 1 + \frac{J(J+1)+S(S+1)-L(L+1)}{2J(J+1)}$. The magnetic behavior of rare-earth ions embedded in crystals is strongly affected by crystalline field and exchange interactions. It can be accounted for by the Hamiltonian.

$$H = H_{free} + H_{mag} + H_{crys} + H_{exch} \quad . \qquad (1.4)$$

H_{crys} represents the interaction of the crystalline electric field produced by the surrounding ions with the 4f -electrons; H_{exch} accounts for the spin-spin exchange interaction. These interactions are invariably smaller as compared with $\zeta(\vec{L}.\vec{S})$. Therefore, J remains good quantum number for rare-earth ions incorporated in crystals. There are large variations in the relative strengths of the exchange and crystal field terms for various rare-earth compounds and usually $H_{exch} << H_{crys}$. The rare-earth compounds remain paramagnetic down to low temperatures ($\sim$ few ^oK). However, many rare-earths and their intermetallic compounds show magnetic ordering and in these cases $H_{exch} \sim H_{crys}$.

For the calculation of H_{crys}, the surrounding ions are usually regarded as point charges which donot overlap the paramagnetic ion. The electrostatic potential is then assumed to obey Laplace's law $\Delta V=0$, which has generalized Legendre polynomials as its solutions:

$$H_{crys} = \sum_{k,m,n} A_n^m \; r_k^n \, Y_n^m (\theta_k, \phi_k). \qquad (1.5)$$

The expansion coefficients A_n^m are given by the relation

$$A_n^m = \frac{4\pi}{2n+1} (-1)^m \sum_k e_k \, r_k^{-n-1} \, Y_n^{-m}(\theta_k, \phi_k)$$

and are constants depending upon the crystal structure, r_k is the distance of the kth 4f-electron from the origin and Y_n^m are spherical harmonics. The normalized harmonics Y_n^m are defined as

$$Y_n^m(\theta,\phi) = (-1)^n \left[\frac{1}{4\pi} \frac{(2n+1)(n-|m|)!}{(n+|m|)!}\right]^{1/2} P_n^m (\cos\theta) e^{im\phi} \qquad (1.6)$$

For 4f electrons (l=3) only terms upto n=6 have to be retained, since for higher values of n, the matrix elements with l = 3 wave functions vanish. Odd n terms are excluded because of inversion symmetry and n = 0 term represents only a constant shift. Accordingly, terms corresponding to only n = 2, 4 and 6 give contribution to H_{crys}.

1.4 Symmetry of Crystal Potential

In a crystal, a lattice site is characterized by one of the thirty-two point groups, and a rare-earth ion embedded in crystal retains the site symmetry. This symmetry restricts

the number of A_n^m terms contributing to the crystalline electric potential. Every symmetry element transforms Y_n^m into a linear combination of Y_n^m. Following are some of the symmetry relations for point groups (10)

(i) C_p: If p-fold axis is chosen as z-axis, the potential must be unaltered by a rotation of $2\pi/p$ around z-axis. This rotation transforms Y_n^m as

$$Y_n^m \Longrightarrow e^{i2m\pi/p} Y_n^m; \tag{1.7}$$

here m has to be an integral multiple of p:

$$m = 0, \pm p, \pm 2p, \ldots\ldots \tag{1.8}$$

(ii) C_i: The inversion transforms Y_n^m as

$$Y_n^m \Longrightarrow (-1)^n Y_n^m \tag{1.9}$$

which leads to the result

$$A_n^m = 0 \qquad \text{for odd } n. \tag{1.10}$$

(iii) C_s: If the symmetry plane is zx-plane, the reflection transforms

$$Y_n^m \Longrightarrow (-1)^m Y_n^{-m} \tag{1.11}$$

and thus

$$A_n^m = (-1)^m A_n^{-m} . \tag{1.12}$$

(iv) S_{2p}: A rotatory reflection or improper rotation by $2\pi/2p$ transforms

$$Y_n^m \Longrightarrow e^{i\pi(n+m+m/p)} Y_n^m \tag{1.13}$$

so that

$$n+m+m/p = \text{even} . \tag{1.14}$$

(v)C_{ph}: The p-fold axis leads to relation (1.8) and inversion to (1.10) for p = 4 and 6. A rotatory-reflection by $2\pi/p$ transforms Y_n^m as

$$Y_n^m \Longrightarrow e^{i\pi(n+m+2m/p)} Y_n^m \qquad (1.15)$$

so that we have

$$n+m+\frac{2m}{p} = \text{even}. \qquad (1.16)$$

(vi)D_p: The p-fold axis leads to (1.8) and if one of the p two-fold axes is x-axis, then two-fold rotation transforms Y_n^m as

$$Y_n^m \Longrightarrow (-1)^n \; Y_n^{-m} \qquad (1.17)$$

leading to

$$A_n^m = (-1)^n A_n^{-m} \; . \qquad (1.18)$$

(vii)D_{ph}:The relations (1.8),(1.12),(1.16) and (1.18) hold.

Thus the crystal potential takes varied forms, determined by the relative arrangement of the x-, y- and z-axes w.r.t. crystal axes.

Employing the above relations we undertake to find the form of the crystal potential of C_{3h} symmetry at the rare-earth ion site (11), which indeed is the case in anhydrous trichlorides, some of the tribromides, ethylsulphates and hydrated sulphates. The group of this symmetry is generated by the single operation: rotate the system by 60° about the z-axis (c-axis) and invert in the origin i.e.

$$\theta \rightarrow \theta - \pi \quad \text{and} \quad \phi \rightarrow \phi + \frac{4\pi}{3} \; . \qquad (1.19)$$

The spherical harmonics under this operation transform as

$$Y_n^m(\theta,\phi) \Longrightarrow (-1)^{n+m} e^{i\,4\pi m/3} Y_n^m(\theta,\phi) \quad (1.20)$$

where $Y_n^m(\theta,\phi)$ satisfy the relation

$$Y_n^m(\theta,\phi) = (-1)^m Y_n^{m\,*}(\theta,\phi). \quad (1.21)$$

For spherical harmonics to be invariant under this operation

$$\begin{aligned} e^{i4\pi m/3} &= 1 \qquad & m &= 0, \pm 3, \pm 6, \ldots \\ (-1)^{n+m} &= 1 \qquad & n+m &= \text{even} \end{aligned} \quad (1.22)$$

for integral n and m. The crystal potential can thus be expanded as

$$H_{crys} = \sum_i \sum_k \sum_n \frac{4\pi}{2n+1} (-q_k e^2) \frac{r_i^n}{R_k^{n+1}} \Big\{ Y_n^o(\theta_i,\phi_i) Y_n^o(\theta_k,\phi_k) + \sum_{m=1}^{n} (-1)^n \big[Y_n^{-m}(\theta_i,\phi_i) Y_n^m(\theta_k,\phi_k) + Y_n^m(\theta_i,\phi_i) Y_n^{-m}(\theta_k,\phi_k) \big] \Big\} \quad (1.23)$$

where (r_i, θ_i, ϕ_i) and (R_k, θ_k, ϕ_k) are spherical polar coordinates of the ith electron andthe center of the kth ion, respectively; q_k is the charge on kth ion. The above equation may be expressed alternatively as

$$\begin{aligned} H_{crys} = \sum_i \; & \alpha_{20} Y_2^o(i) + \alpha_{33}\big[Y_3^3(i) + Y_3^{-3}(i)\big] + i\beta_{33}\big[Y_3^3(i) - Y_3^{-3}(i)\big] + \alpha_{40} Y_4^o(i) \\ & + \alpha_{53}\big[Y_5^3(i) + Y_5^{-3}(i)\big] + i\beta_{53}\big[Y_5^3(i) - Y_5^{-3}(i)\big] + \alpha_{60} Y_6^o(i) \\ & + \alpha_{66}\big[Y_6^6(i) + Y_6^{-6}(i)\big] + i\beta_{66}\big[Y_6^6(i) - Y_6^{-6}(i)\big] \end{aligned} \quad (1.24)$$

$Y_n^m(\theta_i,\phi_i)$ is abbreviated to $Y_n^m(i)$ and terms for $n>6$ have been

left as explained earlier. The α_{nm}'s and β_{nm}'s are real quantities proportional to r_i^n, given by

$$\alpha_{no} = (-1)^{n/2}(4\pi/2n+1) \sum_k (-q_k e^2)(r_i^n/R_k^{n+1}) Y_n^o(k),$$

$$\alpha_{nm} = (-1)^{n+m} (2\pi/2n+1) \sum_k (-q_k e^2) (r_i^n/R_k^{n+1}) [Y_n^m(k)+Y_n^{-m}(k)], \quad (1.25)$$

and

$$\beta_{nm} = (-1)^{n+m} (2\pi i/2n+1) \sum_k (-q_k e^2)(r_i^n/R_k^{n+1}) [Y_n^m(k)-Y_n^{-m}(k)].$$

However, all terms with odd parity (odd values of n) vanish because of inversion symmetry relation. The z-axis is generally taken as c-axis and the x-axis is chosen in such a way that $i(Y_6^6 - Y_6^{-6})$ does not appear in (1.24). Since ϕ dependence of $Y_6^{\pm 6}$ is $\exp(\pm i6\phi)$, there are six such x-axes, 30° apart. These restrictions limitthe value of n to 2,4 and 6 only for the rare-earth ions at C_{3h} site symmetry and hence

$$H_{crys}(C_{3h}) = \sum_i \{\alpha_{20} Y_2^o(i)+\alpha_{40}Y_4^o(i)+ \alpha_{60}Y_6^o(i) + \alpha_{66}[Y_6^6(i) + Y_6^{-6}(i)]\}. \quad (1.26)$$

Expressing the spherical harmonics in cartesian coordinates, we get

$$H_{crys} = A_2^o(3z^2-r^2)+A_4^o (35z^4-30r^2z^2+3r^4)+A_6^o (231z^6-315r^2z^4+ +105r^4z^2-5r^6) +A_6^6 (x^6-15x^4y^2+ 15x^2y^4-y^6)$$

$$= A_2^o V_2^o + A_4^o V_4^o + A_6^o V_6^o + A_6^6 V_6^6 . \quad (1.27)$$

A_n^m's correspond to α_{nm}'s in Eq.(1.26) and are obtained from experiments; V_n^m are propertional to $(r^n Y_n^m)$. Proceeding analogously the crystal potential for various symmetries can be easily derived. It is found that higher the symmetry, the simpler the expression for H_{crys}. In octaheral (O_h) symmetry only two parameters A_4 and A_6 determine the interaction:

$$H_{crys}(O_h) = A_4 (V_4^o + 5V_4^4) + A_6(V_6^o - 21V_6^4). \qquad (1.28)$$

The rare-earth ions doped in YPO_4, YVO_4, scheelites and Yttrium Aluminium Garnet experience an axial field with tetragonal distortion on a basic cubic potential. The site symmetry in these cases may be taken as D_{2d} and the interaction is given by

$$H_{crys}(D_{2d}) = A_2^o V_2^o + A_4^o V_4^o + A_4^4 V_4^4 + A_6^o V_6^o + A_6^4 V_6^4. \qquad (1.29)$$

1.5 Calculation of Energy Spectrum and Crystal Quantum Numbers

Once the point symmetry and the appropriate form of the crystal field potential are established, it becomes possible to find the Stark splittings and further Zeeman energy spectrum with the help of first and second order perturbation. In order to find the Stark splittings the energy matrix for the ion in crystal is constructed first. Within a manifold of states of constant J, the calculation of matrix elements is particularly simplified by using the operator equivalent method developed by Elliot and Stevens (12-14) and Judd (15). The transition to the operator equivalents

is carried out by replacing

x	by	J_x
y	by	J_y
and z	by	J_z

with proper regard for the commutation rules of these operators. Thus one gets

$$H_{crys} = \sum_{m,n} A_n^m \langle r^n \rangle \langle J||\theta_n||J\rangle \quad O_n^m \qquad (1.30)$$

where $\langle J||\theta_n||J\rangle$ are the reduced matrix elements α_J, β_J and γ_J for n = 2, 4 and 6 respectively (13), associated with the angular momentum operators O_n^m (16). The matrix elements for O_n^m have been tabulated by Hutchings (17). The complete Hamiltonian due to the crystal field and magnetic field can be written as

$$H = H_{crys} + g_J \mu_B \vec{H}.\vec{J}. \qquad (1.31)$$

To construct the energy matrix appropriate to this Hamiltonian, initially the magnetic interaction is omitted and the matrices diagonalized to yield the eigenvalues E_i° and their corresponding eigenvectors ψ_i°. Then the magnetic field effect is determined as a perturbation on the crystal field levels. The first and second order perturbation effects give

$$W_{ij}^{(1)} = g_J \mu_B \langle \psi_i^\circ | J | \psi_j^\circ \rangle \qquad i = j \qquad (1.32)$$

$$W_{ij}^{(2)} = g_J^2 \mu_B^2 \sum_{j \neq i} \frac{|\langle \psi_i^\circ | J | \psi_j^\circ \rangle|^2}{E_i - E_j} \qquad (1.33)$$

By introducing suitable crystal quantum numbers it becomes possible to divide the states of the free ion into classes so that all the states within a given class may interact with

one another but not with the states belonging to another class. Following Hellwege (18) we introduce a set of crystal quantum numbers μ such that

$$J_z = \mu \text{ (mod. m)}. \qquad (1.34)$$

For an ion containing odd number of electrons, three distinct classes are characterized by the crystal quantum numbers $\mu = \pm 1/2$, $\pm 3/2$ and $\pm 5/2$, and for an even number of electrons the four classes are specified by $\mu = 0, \pm 1, \pm 2, 3$. The states for which μ is double valued (e.g. $\mu = \pm 1$) will be doubly degenerate. The crystal quantum numbers classification of various J states of the free rare-earth ion in C_{3h} symmetry are given as a typical case, Table 1.1.

As an illustration consider J = 6 term of a free ion, which will be split into nine distinct levels. Three of these levels will be nondegenerate with $\mu = 0$, two pairs of the levels will be doubly degenerate and classifield by $\mu = \pm 1$ and $\mu = \pm 2$. In addition to these seven levels there will be two more non-degenerate levels with $\mu = 3$. Thus the 13x13 crystal field energy matrix for a pure J = 6 term may be reduced to a 3x3 matrix ($\mu = 0$) and five 2x2 matrices. However, two matrices for $\mu = \pm 1$ are equivalent as are the two matrices for $\mu = \pm 2$. Therefore, we are left with only a 3x3 submatrix and three distinct 2x2 submatrices to be solved. The eigenvectors of these submatrices will consist of linear combination of the J_z states.

TABLE 1.1 Crystal quantum numbers for C_{3h} symmetry

Even number of electrons

$\mu \rightarrow$	0	±1	±2	3	number of Levels
J	J_z	J_z	J_z	J_z	
0	0				1
1	0	±1			2
2	0	±1	±2		3
3	0	±1	±2	-3,+3	5
4	0	±1	±2,∓4	-3,+3	6
5	0	±1,∓5	±2,∓4	-3,+3	7
6	-6,0,+6	±1,∓5	±2,∓4	-3,+3	9
7	-6,0,+6	∓7,±1,∓5	±2,∓4	-3,+3	10
8	-6,0,+6	∓7,±1,∓5	±8,±2,∓4	-3,+3	11
9	-6,0,+6	∓7,±1,∓5	±8, ±2,∓4	+9,-3, +3,-9	13

Odd number of electrons

$\mu \rightarrow$	±1/2	±3/2	±5/2	number of levels.
J	J_z	J_z	J_z	
1/2	±1/2			1
3/2	±1/2	±3/2		2
5/2	±1/2	±3/2	±5/2	3
7/2	±1/2	±3/2	±5/2,∓7/2	4
9/2	±1/2	±3/2,∓9/2	±5/2,∓7/2	5
11/2	±1/2,∓11/2	±3/2,∓9/2	±5/2,∓7/2	6
13/2	±13/2,±1/2 ∓ 11/2	±3/2,∓9/2	±5/2,∓7/2	7
15/2	±13/2, ±1/2,∓11/2	±15/2, ±3/2,∓9/2	±5/2,∓7/2	8

1.6 The Specific Heat

The total heat capacity of a system containing a paramagnetic ion (e.g. rare-earth ion) is the sum of the lattice contribution which nearly follows a T^3 law, and the contribution associated with the localized f electrons (19,20). The latter, generally calledthe magnetic contributions C_M, are observed as sharp peaks in the total specific heat vs. temperature plots. To a good approximation, one may write

$$C_M = C_S + C_{hfs} + C_{dip} + C_{add}. \qquad (1.35)$$

Here C_S is the Schottky specific heat;

C_{hfs}, the contribution from the interaction between the localized f-electrons and the nuclear spin of the ion;

C_{dip}, the effect of dipolar interactions between the paramagnetic ions in the system;

and

C_{add} accounts for other couplings.

At temperatures above He temperature, the last three terms being negligibly small are ignored in the further discussion.

When an ion is placed in a crystalline electric field (CEF) the energy levels get split up and at very low temperatures only the ground level will be occupied. If one or more levels are separated from the ground level by a small energy $\epsilon = kT_{ex}$, then for $T \ll T_{ex}$ the ions cannot be excited to the higher levels and only the lowest state will be occupied. As $T \to T_{ex}$

some of the ions will be excited to the higher states and the extra energy required for these transitions will result in an additional specific heat in the region $T \sim T_{ex}$. However, for $T >> T_{ex}$, all levels will be equally populated and hence there will be no further excitation with the consequence that there will be no more additional thermal capacity. The specific heat associated with the CEF levels is called Schottky specific heat (21).

Taking the system to be an assembly of independent ions and applying the Maxwell-Boltzmann distribution function, the total energy of excitation for a system with n energy levels (obtained in CEF) is (22)

$$U_{Schottky} = N\sum_{i=1}^{n} E_i g_i \exp(-E_i^\circ/kT) \Big/ \sum_{i=1}^{n} g_i \exp(-E_i^\circ/kT). \quad (1.36)$$

E_i° is the energy of the ith CEF level with degeneracy g_i. The specific heat associated with this energy is

$$C_S = Nk\, Z^{-2}\left\{Z \sum_{i=1}^{n} g_i (E_i^\circ/kT)^2 \exp(-E_i^\circ/kT) - \left[\sum_{i=1}^{n} g_i (E_i^\circ/kT) \exp(-E_i^\circ/kT)\right]^2\right\} \quad (1.37)$$

where

$$Z = \sum_{i=1}^{n} g_i \exp(-E_i^\circ/kT). \quad (1.38)$$

The specific heat curve can, in turn, be integrated to give extra entropy associated with the anomaly.

1.7 The Paramagnetic Susceptibility

The field where CEF theory was reasonably successful is the interpretation of magnetic susceptibilities. We outline the derivation of Van Vleck (23) formula for calculating the paramagnetic susceptibility of an ion in the crystal field technique.

The energy level W_i of an ion or molecule can be expressed as a power series of the applied magnetic field H as

$$W_i = W_i^{(o)} + W_i^{(1)} H + W_i^{(2)} H^2 + \ldots, \tag{1.39}$$

where $W_i^{(o)}$ is the energy in the zero field. The magnetic moment μ of the ion in the direction of applied field is

$$\mu = - \partial W/\partial H \tag{1.40}$$

and the total magnetic moment P is defined as thermal average over all the states involved:

$$P = N \sum_i \mu_i \exp(-W_i/kT) / \sum_i \exp(-W_i/kT). \tag{1.41}$$

Now

$$\mu_i = - \partial W_i/\partial H = - W_i^{(1)} - 2HW_i^{(2)} + \ldots\ldots \tag{1.42a}$$

and

$$\exp(-W_i/kT) = \exp\left[-(W_i^{(o)} + HW_i^{(1)} + H^2 W_i^{(2)} + \ldots)/kT\right]$$
$$\simeq \exp(-W_i^{(o)}/kT) \left\{1 - \frac{HW_i^{(1)}}{kT}\right\} . \tag{1.42b}$$

In this approximation, P can be written as

$$P = N \frac{\sum_i (-W_i^{(1)} - 2HW_i^{(2)})(1 - \frac{HW_i^{(1)}}{kT}) \exp(-W_i^{(o)}/kT)}{\sum_i \exp(-W_i^{(o)}/kT)} \tag{1.43}$$

If the system does not have a permanent polarization in zero magnetic field, we have

$$\sum_i - W_i^{(1)} \exp(-W_i^{(o)}/kT) = 0. \tag{1.44}$$

Hence retaining terms linear in H, we get

$$P = NH \frac{\sum_i \left(\frac{[W_i^{(1)}]^2}{kT} - 2 W_i^{(2)}\right) \exp(-W_i^{(o)}/kT)}{\sum_i \exp(-W_i^{(o)}/kT)} . \tag{1.45}$$

The susceptibility $K_i = \chi_i$ $(i = x,y,z)$ is given by

$$\chi_i = P_i/H_i$$

$$= N \frac{\sum_i \left(\frac{|W_i^{(1)}|^2}{kT} - 2W_i^{(2)} \right) \exp\left(-W_i^{o}/kT\right)}{\sum_i \exp\left(-W_i^{(o)}/kT\right)} \qquad (1.46)$$

$W_i^{(1)}$ and $W_i^{(2)}$ are the first and second order Zeeman energies.

In the following chapters we have calculated the thermal and magnetic properties of rare-earth ions in anhydrous trichlorides, tribromides, ethylsulphates, hydrated sulphates, thioindates, garnets, vanadates etc. by the application of crystal field theory, and compared the results with available experimental data.

CHAPTER II

STUDY OF ANHYDROUS RARE-EARTH TRICHLORIDES AND TRIBROMIDES

2.1 INTRODUCTION

The rare-earth trichlorides and tribromides form a subclass of one of the major groups of inorganic paramagnetic compounds. Hutchison and Wong (24) studied the paramagnetic resonance in dilute solid solutions of various rare-earth ions in $LaCl_3$, whereas exhaustive studies of absorption and fluorescence spectra of dilute trichlorides and tribromides have been made by a number of workers (25-35). This work in rare-earth trichlorides and tribromides pertains to C_{3h} symmetry in the crystals. They are similar in several ways to ethylsulphates, whose magnetic properties have been examined in considerable detail by Elliot and Stevens (14).

The main purpose of these investigations has been to study the departure of the physical properties of various ions in crystals, from those of free ion and to provide, whenever possible, a relevant explanation by the application of the crystal field theory developed by Bethe (5), Penney and Schlapp (8,36) and Stevens et.al. (12-14). Most of the anhydrous trichlorides and some tribromides of rare-earths possess UCl_3 hexagonal structure with two molecules per unit cell (37,38). These give, in general, considerably sharp and well-defined absorption lines and are largely free from the superimposed molecular and lattice vibrations. Moreover, due to the existence

of strong fluorescence (25) in these crystals, it is possible to obtain low lying levels of the rare-earth ions in the crystal lattice.

The point symmetry at the rare-earth ion site in trichlorides is assumed to be C_{3h} and because of this high symmetry of the crystalline field, the Stark and Zeeman effect calculations are relatively simplified. As the interactions between the rare-earth ions themselves are important only at very low temperatures, the magnetic properties of a given ion are, therefore, determined almost completely by the crystalline electric field. The determination of the CEF involves some unknown parameters (CEF parameters), which are best achieved if a complete Stark level spectrum is available from optical spectra measurements (40,41). It may be pointed out that the consideration of g-values of the lowest Stark level only, may not necessarily ensure a near estimation of the CEF strength (41,42). Fortunately, absorption and fluorescence spectra are available almost in all the rare-earth trichlorides and some of the tribromides diluted with $LaCl_3$ and $LaBr_3$; from which most of the low lying levels and their electric field splittings have been obtained. The accuracy of the CEF parameters obtained from these investigations, can be checked by studying the thermal and magnetic properties of these compounds.

Using the CEF parameters reported in literature, we have studied the temperature dependence of magnetic and thermal properties, viz. principal paramagnetic susceptibilities, magnetic anisotropy, effective magnetic moment μ_{eff}, Schottky specific

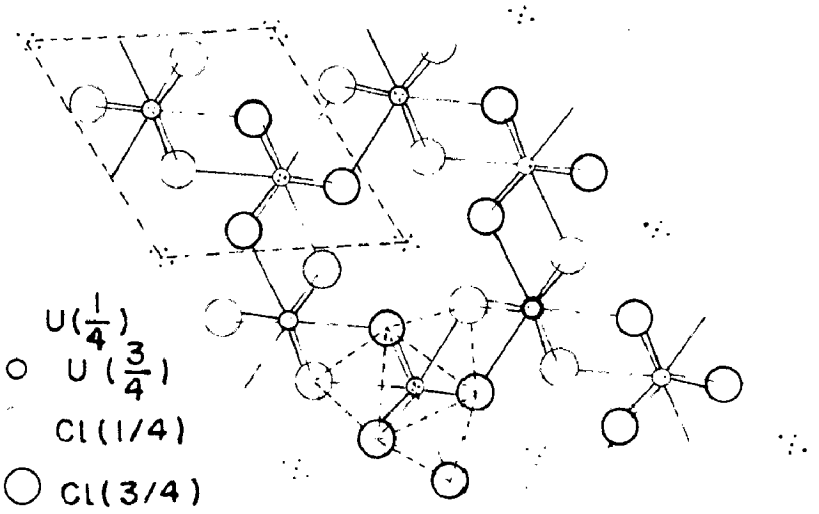

FIG. 2-1 CRYSTAL STRUCTURE OF UCl_3

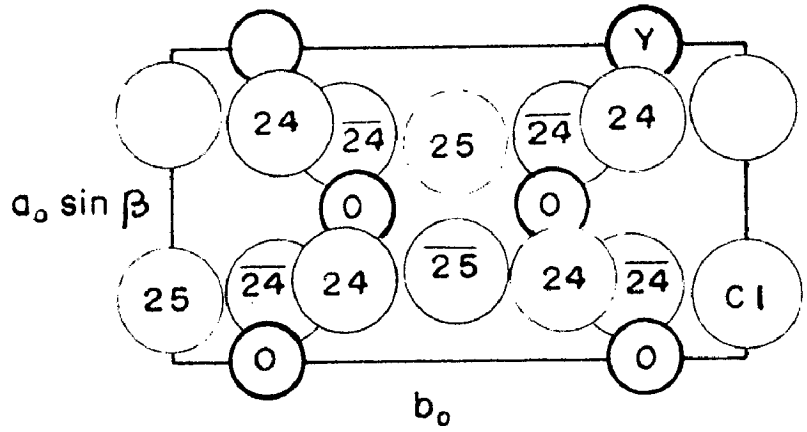

FIG. 2-2 MONOCLINIC STRUCTURE OF YCl_3 VIEWED ALONG ITS C_o AXIS.

heat in the temperature range 20-300°K for Nd^{3+}, Dy^{3+}, Ho^{3+} and Er^{3+} in $LaCl_3$ and Pr^{3+}, Er^{3+} in $LaBr_3$ host lattices. Furthermore, the anisotropy in the spectroscopic splitting factor of the lowest Stark level and the additional entropy connected with the thermal anomaly have been calculated. The paramagnetic Curie temperature and the temperature dependence of torque in unit magnetic field are also determined for some systems.

2.2 Crystal Structure

The trichlorides and tribromides of lanthanides exhibit four types of structure. Zachariasen has shown that the trichlorides of La - Gd and tribromides of La - Pr possess the hexagonal uranium trichloride - type (or Yttrium hydroxide) structure; Fig. 2.1 (43,44). The lattice parameters for UCl_3 are $a_o = 7.428 \pm 0.003$Å and $c_o = 4.312 \pm 0.003$Å. The space group is $C6_3/m$ (C_{6h}^2) and each metal atom is bonded to nine chlorine atoms, three at a distance U - Cl = 2.95Å and the remaining six at U - Cl = 2.96Å. The closest distance of approach of two Cl atoms is Cl - Cl = 3.45 Å. Also the bonding is predominantly ionic in character.

The trichlorides of Dy - Lu crystallize with monoclinic YCl_3 (or $AlCl_3$) structure; the space group being $C2/m$ (C_{3h}^2). This is distorted NaCl structure in which two thirds of the metal atom sites are vacant. The structure of YCl_3 is shown in Fig. 2.2 (45). The three sets of two chlorine atoms are at distances 2.58, 2.63 and 2.69 Å respectively from Yttrium atom and the lattice parameters are $a_o = 6.91$Å, $b_o = 11.94$Å, $c_o = 6.44$Å, $\beta = 111.0°$.

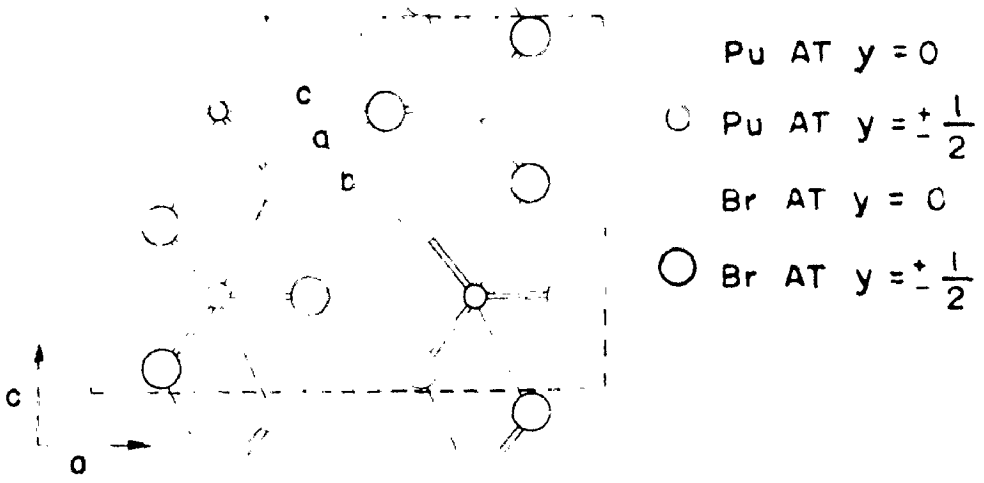

FIG. 2-3 THE LAYER STRUCTURE OF $PuBr_3$

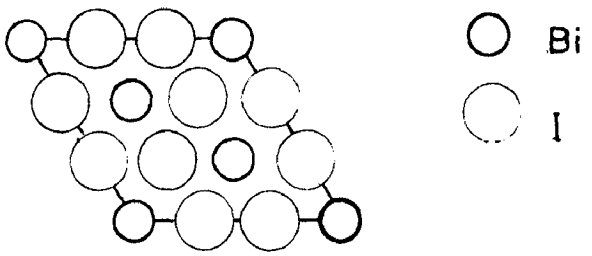

FIG. 2-4 PROJECTION OF THE HEXAGONAL CELL OF BiI_3

More recently, another type of structure has been identified as the orthorhombic plutonium tribromide structure (46). Terbium trichloride and tribromides of Nd- Eu possess the $PuBr_3$ structure. This structure, Fig.2.3, has layer-lattice; each metal atom being bonded to eight halogen atoms — two at 3.06Å and six at 3.08 Å in $PuBr_3$, and the lattice parameters are $a_o = 12.62$Å, $b_o = 4.09$Å and $c_o = 9.13$Å.

The tribromides of Nd-Lu possess the hexagonal ferric chloride or Bismuth iodide type structure (47) as shown in Fig.2,4.

2.3 Theory and Calculations

A number of workers (48,49) calculated the electrostatic and spin orbit matrix elements for various ions with $4f^n$ configuration, and predicted that J, the total angular momentum, remains a good quantum number in crystal field calculations. The Hamiltonian of the system subjected to magnetic field is

$$H = H_o + H_{crys} + H_{mag} \cdot \qquad (2.1)$$

H_o is the free ion Hamiltonian;

$$H_{crys} = A_2^o\langle r^2\rangle \alpha_J O_2^o + A_4^o\langle r^4\rangle \beta_J O_4^o + A_6^o \langle r^6\rangle \gamma_J O_6^o + A_6^6\langle r^6\rangle \gamma_J O_6^6 \qquad (2.2)$$

and $H_{mag} = \mu_B g_J \vec{J}.\vec{H}$. Using the operator equivalent method and tables of Stevens (12) and Elliot and Stevens (13,14), the eigenvalues E_i^o and corresponding eigenfunctions are calculated under the CEF interaction H_{crys}. The Schottky specific heat C_S can be generated from formula (1.37). Next, Zeeman splittings

are computed under the magnetic perturbation, H_{mag}, through perturbation technique and in turn used to generate the paramagnetic susceptibilities from equation (1.46). The torque L acting on a crystal placed in a magnetic field H is given by

$$L = 0.5(n/N)\Delta K \; H^2 \sin 2\theta; \qquad (2.3)$$

θ is the angle between H and z-axis and (n/N), the gram-atom fraction of the paramagnetic ion in the crystal; ΔK, the magnetic anisotropy. Further $\bar{\mu}_{eff}$ is readily extracted at different temperatures from the relation

$$\bar{\mu}_{eff} = (3kTK/N)^{1/2}. \qquad (2.4)$$

(i) $Nd^{3+}:LaCl_3$

The ground multiplet of Nd^{3+} ion ($4f^3$) is $^4I_{9/2}$ and the first excited term $^4I_{11/2}$ is about 1800 cm^{-1} higher (13) and, therefore, the effect of higher multiplets on the ground term may be considered negligible. The absorption and EPR spectra show that the ground level of $Nd^{3+}:LaCl_3$ may be assigned crystal quantum number $\mu = \pm 5/2$. In a C_{3h} field, the spherical rotation group for J = 9/2 is transformed in accordance with the reduction

$$D_{15/2} \rightarrow \Gamma_7 + 2\Gamma_8 + 2\Gamma_9$$

and gives five Kramers doublets. These doublets can alternatively be represented by the crystal quantum numbers $\mu = \pm 5/2, \pm 3/2, \pm 1/2$. Carlson and Dieke (25,27) found that in $Nd^{3+}:LaCl_3$, $^4I_{11/2}$ term is 1973.8 cm^{-1} above the ground term $^4I_{9/2}$ and that there

is no mixing of higher J multiplets with the ground term. The CEF parameters obtained by Judd (26) in LS coupling scheme are listed in Table 2.1 and used in these calculations. The calculated matrix elements are given as

$$A_1 = \langle \pm 9/2| H_{crys} |\pm 9/2\rangle = 17.41$$
$$A_2 = \langle \pm 7/2| H_{crys} |\pm 7/2\rangle = -121.09$$
$$A_3 = \langle \pm 5/2| H_{crys} |\pm 5/2\rangle = 74.23$$
$$A_4 = \langle \pm 3/2| H_{crys} |\pm 3/2\rangle = 65.76$$
$$A_5 = \langle \pm 1/2| H_{crys} |\pm 1/2\rangle = -36.31$$
$$B_1 = \langle \pm 9/2| H_{crys} |\mp 3/2\rangle = -53.40$$
$$B_2 = \langle \pm 7/2| H_{crys} |\mp 5/2\rangle = -81.58.$$

The Stark splittings and corresponding eigenvectors obtained from these matrices are:

E_i^o (cm^{-1})	μ	ψ_i^o
-150.71	$\pm 5/2$	$0.940\|\pm 7/2\rangle + 0.341\|\mp 5/2\rangle$
- 36.33	$\pm 1/2$	$\|\pm 1/2\rangle$
- 17.00	$\pm 3/2$	$0.840\|\pm 9/2\rangle + 0.542\|\mp 3/2\rangle$
100.20	$\pm 3/2$	$0.542\|\pm 9/2\rangle - 0.840\|\mp 3/2\rangle$
103.85	$\pm 5/2$	$0.341\|\pm 7/2\rangle - 0.940\|\mp 5/2\rangle$.

The Zeeman splittings of these Stark levels under the magnetic field H parallel and perpendicular to the symmetry axis are obtained by employing perturbation technique. The complete energy spectrum is:

TABLE 2.1 CEF parameters (in cm^{-1}) for various anhydrous rare-earth trichlorides and tribromides, which are used in the present calculations.

Crystals	$A_2^0\langle r^2\rangle$	$A_4^0\langle r^4\rangle$	$A_6^0\langle r^6\rangle$	$A_6^6\langle r^6\rangle$	Ref.
		(a) Trichlorides			
$NdCl_3$	103.7	-36.01	-44.51	426.21	40
$DyCl_3$	89.8	-40.0	-23.3	253.0	28
$HoCl_3$	113.6	-33.9	-27.8	276.7	50
$ErCl_3$	93.	-35.	-25.	235.	30
		(b) Tribromides			
$PrBr_3$	54.18	-44.52	-35.43	388.7	29
$ErBr_3$	117.	-39.6	-19.2	212.	34

H || z-axis	H $\perp$ z-axis
$E_1^o \pm 2.802\ G - 0.0145\ G^2$	$E_1^o \pm 1.282\ G - 0.0288\ G^2$
$E_2^o \pm 0.5\ G + 0.0\ G^2$	$E_{2\pm}^o 2.5\ G - 0.1217\ G^2$
$E_3^o \pm 2.735\ G - 0.0637\ G^2$	$E_{3+}^o 0 + 0.1049\ G^2$
$E_{4\pm}^o 0.264\ G + 0.0637\ G^2$	$E_4^o + 0 - 1.1619\ G^2$
$E_{5\pm}^o 1.802\ G + 0.0145\ G^2$	$E_{5\pm}^o 1.282\ G + 1.2076\ G^2$

where $G = \mu_B g_J H$.

From the above energy expressions, the principal magnetic susceptibilities and Schottky specific heat at different temperatures are calculated from the formulae (1.46) and (1.37) respectively. The K values alongwith the calculations for ΔK and $\tilde{\mu}_{eff}$ are given in Table 2.2. The calculated $K_{||} T$, $K_{\perp} T$, $\bar{K}T$ and C_S vs T are plotted in Figs.2.5 and 2.6. The extra entropy associated with the Schottky anomaly can be calculated from the following relations:

$$C_S = \frac{dQ}{dT} = \frac{TdS}{dT}$$

or

$$S = \int \frac{C_S}{T}\, dT \qquad (2.5)$$

Numerical integration by Simpson's rule would give the magnitude of additional entropy. The result for $NdCl_3$ for temperature upto 400°K is given in Table 2.8.

(ii) $\underline{Dy^{3+}:LaCl_3}$

The ground multiplet of $Dy^{3+}(4f^9)$ is $^6H_{15/2}$ and the first excited term is about 3300 cm^{-1} above it (13) and as such the effect of higher multiplets on the ground term is negligible.

TABLE 2.2 : Variation of principal magnetic susceptibilities, anisotropy, and μ_{eff} of $NdCl_3$ with temperature.

T(°K)	$K_{\parallel} .10^3$ cgs emu	$K_{\perp} .10^3$ cgs emu	$\bar{K}' .10^3$ cgs emu	$\Delta K. 10^3$ cgs emu	$\bar{\mu}_{eff}$ (μ_B)
300	5.7	5.1	5.3	0.6	3.57
260	6.6	5.8	6.1	0.7	3.55
220	7.8	6.7	7.1	1.1	3.53
200	8.6	7.3	7.7	1.3	3.51
180	9.6	7.9	8.5	1.7	3.49
160	10.8	8.6	9.3	2.1	3.46
140	12.3	9.5	10.4	2.9	3.42
120	14.4	10.4	11.8	3.9	3.36
100	17.3	11.6	13.4	5.7	3.28
80	21.5	12.8	15.7	8.8	3.17
60	28.6	14.2	19.0	14.4	3.02
40	42.4	16.5	25.2	25.8	2.84
20	81.9	24.3	43.5	57.6	2.64

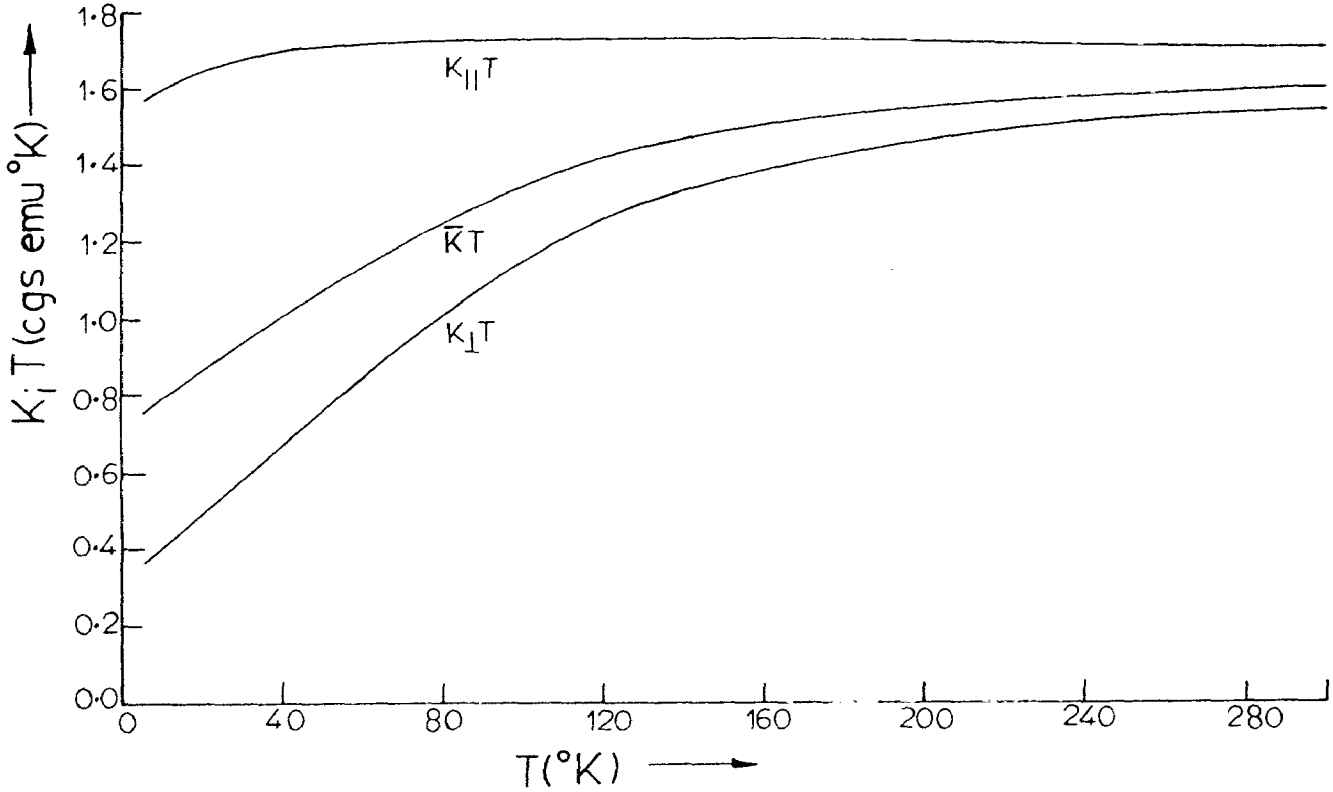

FIG. 2.5 Temperature dependence of $K_1 T$ of single crystal of $NdCl_3$.

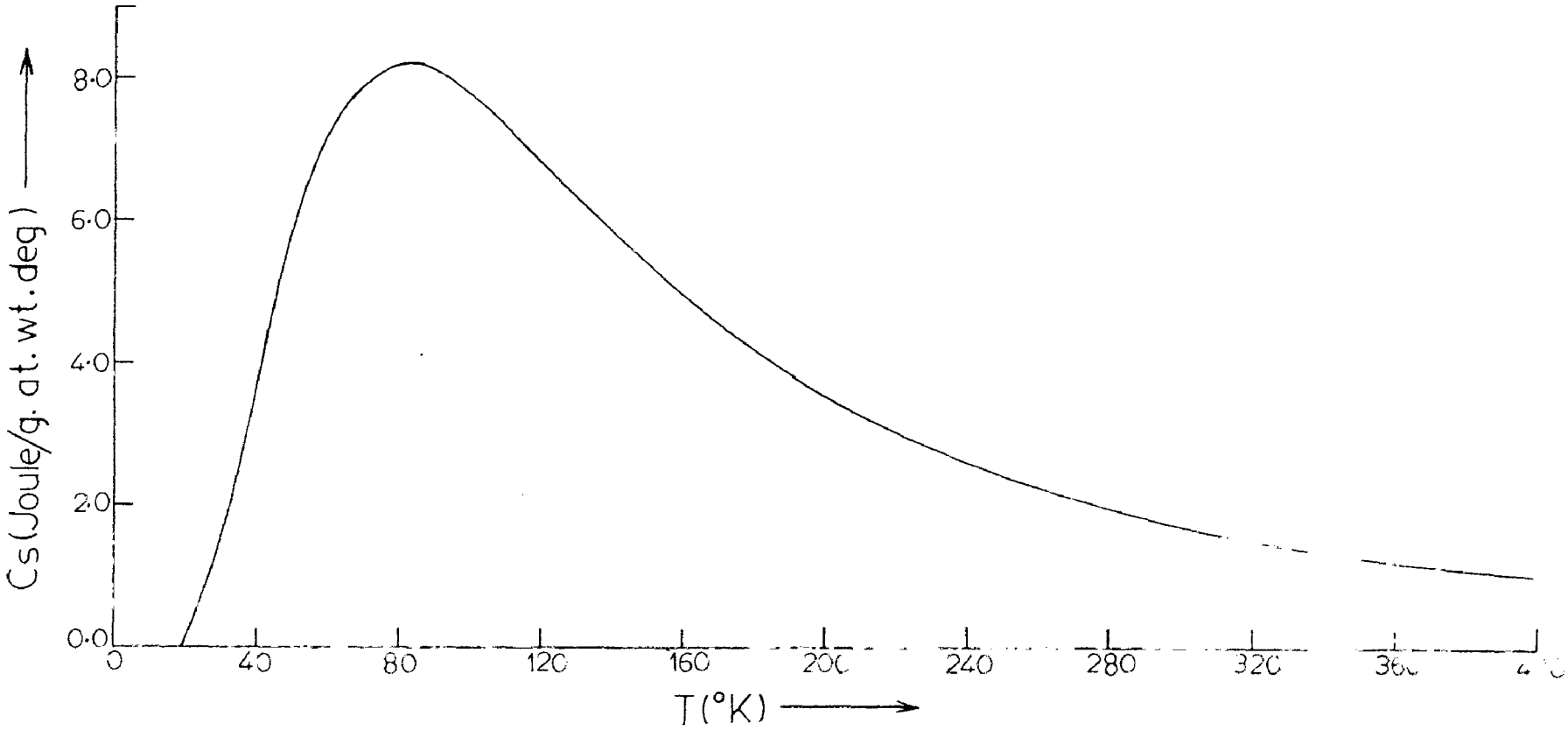

FIG. 2.6 Temperature dependence of schottky specific heat of $NdCl_3$.

Under the influence of C_{3h} crystal field, the $^6H_{15/2}$ term would split into eight Kromers doublets. Crosswhite and Dieke (28) interpreted the Stark splitting of the ground term by using the CEF parameters listed in Table 2.1; they derived these by applying LS coupling approximation. The Stark levels are described by the following eigenvalues and eigenfunctions:

$E_i^o(cm^{-1})$	μ	ψ_i^o
-52.95	$\pm 3/2$	$0.154\|\pm 15/2\rangle - 0.234\|\pm 3/2\rangle + 0.960\|\mp 9/2\rangle$
-43.13	$\pm 5/2$	$0.889\|\pm 7/2\rangle - 0.458\|\mp 5/2\rangle$
-42.97	$\pm 3/2$	$0.986\|\pm 15/2\rangle - 0.022\|\pm 3/2\rangle - 0.164\|\mp 9/2\rangle$
-37.35	$\pm 1/2$	$0.085\|\pm 13/2\rangle - 0.171\|\pm 1/2\rangle + 0.982\|\mp 11/2\rangle$
-11.31	$\pm 1/2$	$0.988\|\pm 13/2\rangle - 0.114\|\pm 1/2\rangle - 0.108\|\mp 11/2\rangle$
28.99	$\pm 5/2$	$0.458\|\pm 7/2\rangle + 0.889\|\mp 5/2\rangle$
65.73	$\pm 3/2$	$0.060\|\pm 15/2\rangle + 0.972\|\pm 3/2\rangle + 0.227\|\mp 9/2\rangle$
93.02	$\pm 1/2$	$0.130\|\pm 13/2\rangle + 0.979\|\pm 1/2\rangle + 0.159\|\mp 11/2\rangle$.

The Zeeman splittings of these levels under the magnetic field H $\parallel$ and $\perp$ to z-axis are

H $\parallel$ to z-axis	H $\perp$ to z-axis
$E_1^o \pm 3.889\ G - 0.356\ G^2$	$E_1^o + 0 \qquad -1.792\ G^2$
$E_2^o \pm 2.245\ G - 0.083\ G^2$	$E_2^o \pm 3.016\ G \quad - 0.117 G^2$
$E_3^o \pm 7.173\ G + 0.339\ G^2$	$E_3^o + 0 \qquad +1.060\ G^2$
$E_4^o \pm 5.238\ G - 0.056\ G^2$	$E_4^o \pm 0.557\ G \quad + 0.382\ G^2$
$E_5^o \pm 6.282\ G + 0.042\ G^2$	$E_5^o \pm 0.514\ G \quad + 0.382\ G^2$
$E_6^o \pm 1.242\ G + 0.083\ G^2$	$E_6^o \pm 3.018\ G \quad = 0.302\ G^2$
$E_7^o \pm 1.211\ G + 0.016\ G^2$	$E_7^o \pm 0 \qquad -0.172\ G^2$
$E_8^o \pm 0.449\ G + 0.013\ G^2$	$E_8^o \pm 3.940\ G \quad + 0.560\ G^2$

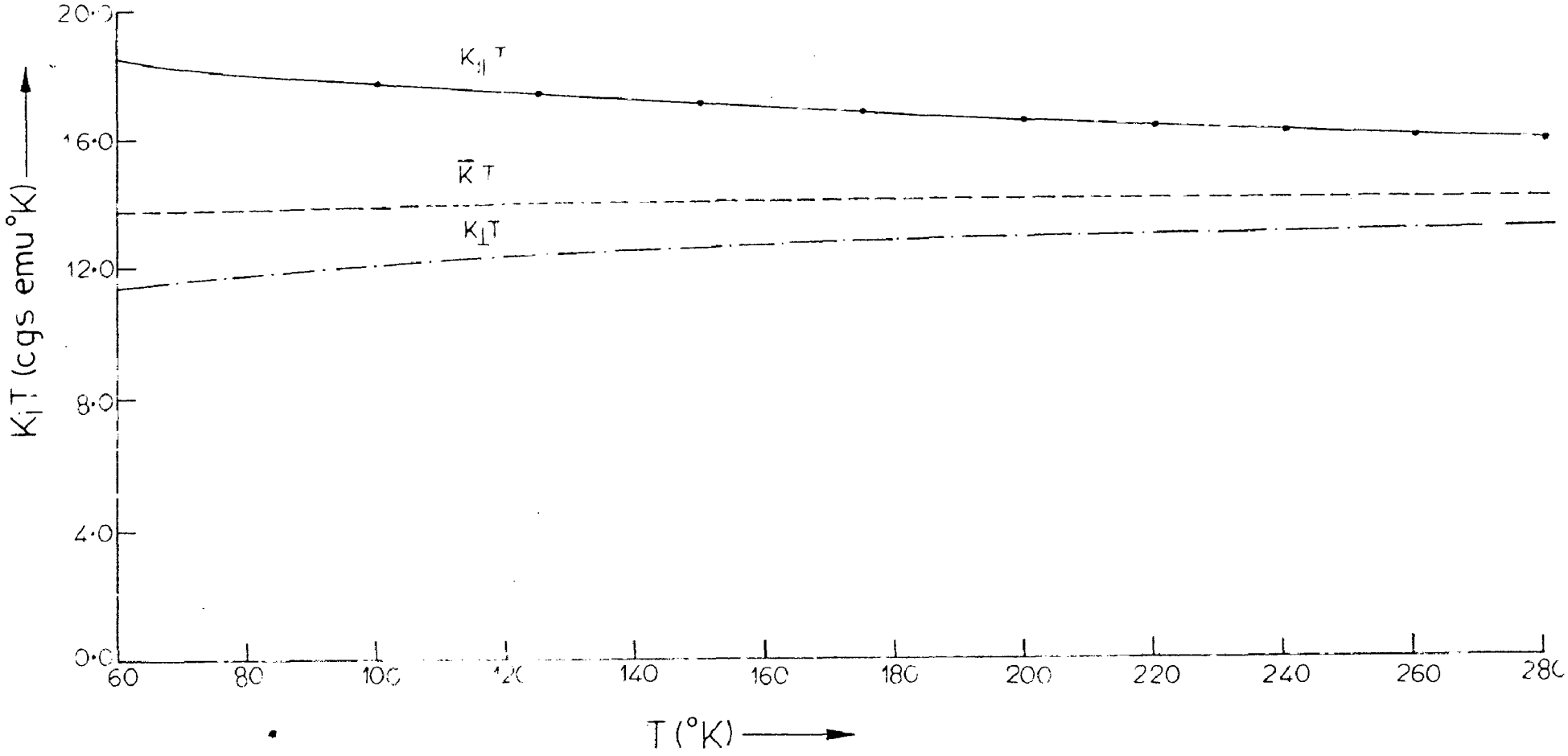

FIG. 2.7 Temperature dependence of K_iT of $DyCl_3$.

The calculated values of principal and mean susceptibilities, anisotropy, $\bar{\mu}_{eff}$ and C_S are listed in Table 2.3. The derived value of S upto 400°K is given in Table 2.8 and the temperature dependence of $K_{\parallel}T$, $K_{\perp}T$ and $\bar{K}T$ is displayed in Fig.2.7.

(iii) $Ho^{3+}:LaCl_3$

The ground multiplet of the Ho^{3+} ion is a $4f^{10}$, $^5I_8$ state. Each J level of an ion with even number of electrons is split into singlets and non Kramers doublets in a CEF of C_{3h} symmetry. In such ions the Jahn-Teller effect becomes operative and removes the degeneracy of the non Kramers levels. Since the 4f electrons are inner electrons and donot take part significantly in chemical bonding, therefore this effect, if it manifests itself, is probably very small. Thus C_{3h} symmetry in such systems still remains a good approximation. The nearest excited term is 5050 cm^{-1} higher than the ground multiplet (13) so that the influence of excited multiplets on the ground term may be neglected. Rajnak and Krupke (50) found that $^5I_7$ multiplet is 5161 cm^{-1} higher than $^5I_8$ in $Ho^{3+}:LaCl_3$. The CEF parameters obtained by them in the LS coupling scheme are given in Table 2.1. These are slightly improved over those previously obtained by Dieke et al. (33). Employing these parameters, the Stark levels of $^4I_8$ term in $Ho^{3+}:LaCl_3$ are determined and are as given below:

TABLE 2.3: Temperature dependence of principal magnetic susceptibilities, magnetic anisotropy effective magnetic moment and specific heat of $DyCl_3$.

T(°K)	$K_{\parallel} .10^3$ cgs emu	$K_{\perp} .10^3$ cgs emu	$\bar{K} .10^3$ cgs emu	$\Delta K.10^3$ cgs emu	$\bar{\mu}_{eff}$ (μ_B)	C_S (J/g.at.wt.deg.)
300	53.0	44.3	47.2	8.7	10.63	0.42
280	57.1	47.2	50.5	9.9	10.63	0.48
260	62.0	50.6	54.4	11.3	10.63	0.54
240	67.7	54.5	58.9	13.1	10.63	0.62
220	74.5	59.1	64.2	15.4	10.63	0.71
200	82.8	64.5	70.6	18.3	10.62	0.83
180	93.1	71.1	78.4	22.0	10.62	0.98
160	106.1	79.1	88.1	27.0	10.61	1.16
140	123.2	89.2	100.5	33.9	10.60	1.40
120	146.2	102.4	117.0	43.7	10.58	1.70
100	178.8	120.6	140.0	59.2	10.57	2.06
80	227.7	147.1	174.0	80.6	10.52	2.48
60	308.0	190.6	229.7	117.4	10.46	2.83
40	459.5	277.1	337.9	182.4	10.29	2.85
20	854.8	432.3	573.1	422.5	9.56	2.91

E_i^o (cm^{-1})	μ	ψ_i^o
-107.67	±1	$0.959\|\pm7\rangle - 0.267\|\pm1\rangle + 0.101\|\mp5\rangle$
- 95.15	0	$0.584\|+6\rangle - 0.564\|0\rangle + 0.584\|-6\rangle$
- 61.61	0	$0.707\|+6\rangle - 0.707\|-6\rangle$
- 40.62	±1	$0.269\|\pm7\rangle + 0.730\|\pm1\rangle - 0.628\|\mp5\rangle$
- 18.05	±2	$0.140\|\pm8\rangle - 0.800\|\pm2\rangle + 0.583\|\mp 4\rangle$
- 3.13	3	$0.707\|+3\rangle + 0.707\|-3\rangle$
10.39	0	$0.399\|+6\rangle + 0.826\|0\rangle + 0.399\|-6\rangle$
43.61	±2	$0.982\|\pm8\rangle + 0.038\|\pm2\rangle - 0.184\|\mp 4\rangle$
49.38	±1	$0.094\|\pm7\rangle + 0.629\|\pm1\rangle + 0.772\|\mp5\rangle$
94.30	±2	$0.126\|\pm8\rangle + 0.599\|\pm2\rangle + 0.791\|\mp4\rangle$
107.58	3	$0.707\|+3\rangle - 0.707\|-3\rangle$.

The complete energy spectrum, including Zeeman splittings, is

H $\parallel$ to z-axis		H $\perp$ to z-axis	
E_1^o	$\pm$ 6.451 G - 0.0565 G^2	E_1^o	+ 0 -0.5450 G^2
E_2^o	+ 0 -0.7316 G^2	E_2^o	+ 0 +0.3303 G^2
E_3^o	+ 0 +0.5727 G^2	E_3^o	+0 -0.1484 G^2
E_4^o	$\pm$ 0.929 G - 0.0483 G^2	E_4^o	+ 0 -0.4001 G^2
E_5^o	$\pm$ 0.077 G -0.0982 G^2	E_5^o	+ 0 +0.4673 G^2
E_6^o	+ 0 -0.0813 G^2	E_6^o	+ 0 -0.1254 G^2
E_7^o	+ 0 +0.1588 G^2	E_7^o	+ 0 -0.1975 G^2
E_8^o	$\pm$ 7.584 G -0.0164 G^2	E_8^o	+ 0 +0.0224 G^2

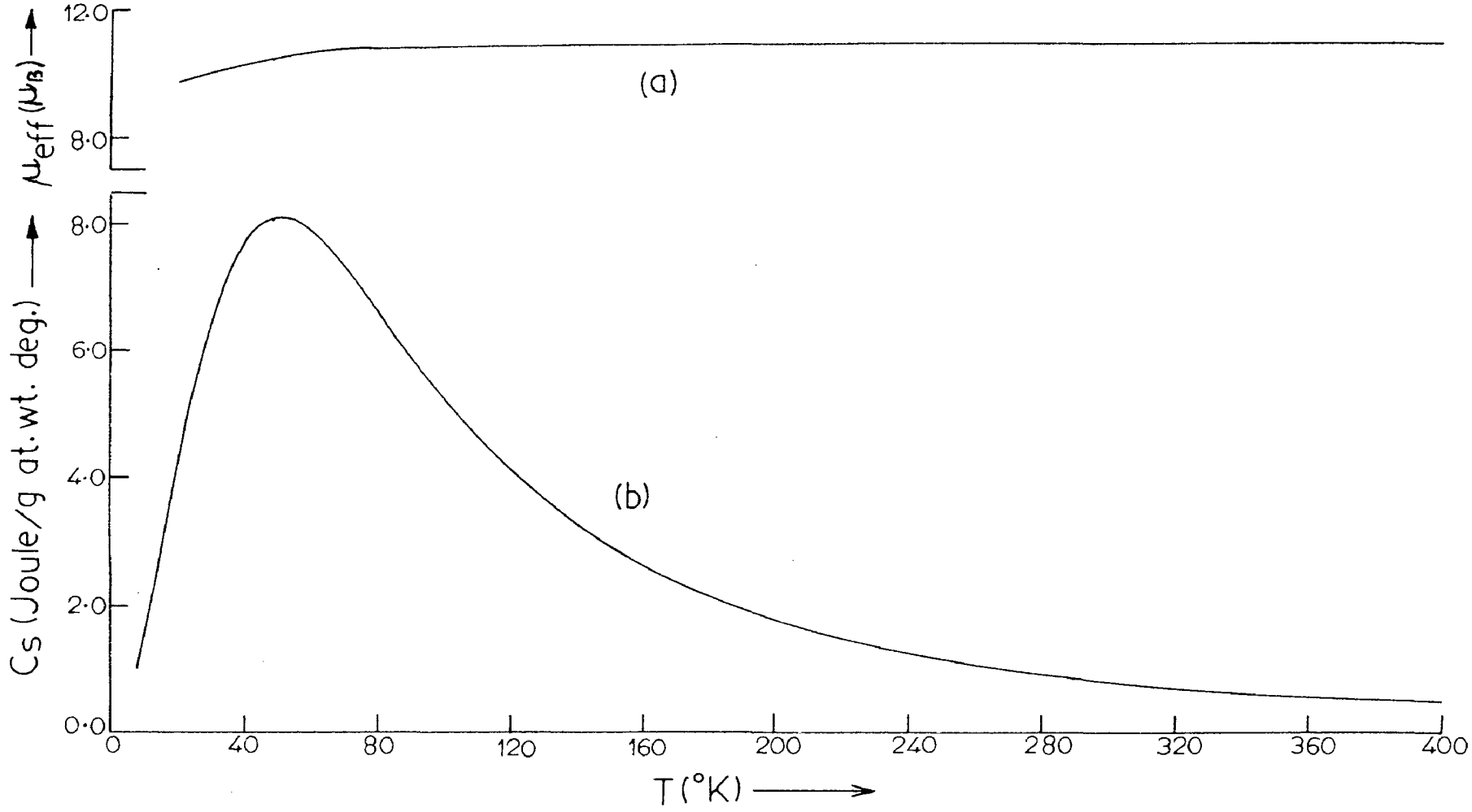

FIG 2.8 Temperature dependence of (a) $\bar{\mu}_{eff}$ and (b) C_S of $HoCl_3$.

$E_9^o \pm 2.522\ G + 0.1039\ G^2$ $\qquad$ $E_9^o + 0 \qquad -0.0066\ G^2$

$E_{10}^o \pm 1.661\ G + 0.1146\ G^2$ $\qquad$ $E_{10}^o + 0 \qquad + 0.4616\ G^2$

$E_{11}^o \pm 0 \qquad + 0.0813\ G^2$ $\qquad$ $E_{11}^o + 0 \qquad + 0.1417\ G^2$

Once again this energy spectrum is employed to calculate the value of $K_{\parallel}$, $K_{\perp}$, $\bar{K}$ and ΔK and the results are catalogued in Table 2.4. The temperature dependence of μ_{eff} and C_S is displayed in Fig.2.8. The extra entropy associated with specific heat is given in Table 2.8.

(iv) $Er^{3+}LaCl_3$ and $Er^{3+}:LaBr_3$

The ground multiplet of Er^{3+} ion ($4f^{11}$) is $^4I_{15/2}$. Wybourne (51) and Wong (48) calculated the electrostatic and spin-orbit interaction for f^{11} configuration and found that the term $^4I_{13/2}$, the first excited term of Er^{3+}, is approximately 6770 cm^{-1} above the ground term $^4I_{15/2}$ and as such the crystal field effect of excited multiplet on the ground term is neglected. A crystal field of C_{3h} symmetry with time reversal has three symmetry classes for an odd number of electrons, each with doubly degenerate levels. These are designated by the crystal quantum numbers $\mu = \pm 1/2, \pm 3/2, \pm 5/2$. The ground term of Er^{3+} is split into eight Kramers doublets, three with $\mu = \pm 1/2$, three with $\mu = \pm 3/2$ and two with $\mu = \pm 5/2$. From absorption spectra of $Er^{3+}:LaCl_3$ by Dieke and Singh (52), the lowest doublet has been assigned $= \pm 5/2$ and the next two doublets with $\mu = \pm 3/2$. The $^4I_{13/2}$ term lies higher than the ground term $^4I_{15/2}$ by 6481.6 cm^{-1} in $Er^{3+}:LaCl_3$ (52) and

TABLE 2.4 : Calculated paramagnetic susceptibility parameters of $HoCl_3$.

T(^{o}K)	$K_{\parallel} .10^3$ (cgs emu)	$K_{\perp} .10^3$ (cgs emu)	$\bar{K} .10^3$ (cgs emu)	$\Delta K .10^3$ (cgs emu)	$K_{\parallel} T$ (cgs emu ^{o}K)	$K_{\perp} T$ (cgs emu ^{o}K)	$\bar{K} T$ (cgs emu ^{o}K)
300	49.9	48.9	49.3	1.0	15.0	14.7	14.8
280	53.8	52.4	52.8	1.4	15.0	14.7	14.8
260	58.2	56.3	56.9	1.9	15.1	14.6	14.8
240	63.4	60.9	61.7	2.6	15.2	14.6	14.8
220	69.7	66.2	67.4	3.5	15.3	14.6	14.8
200	77.4	72.6	74.2	4.8	15.5	14.5	14.8
180	86.9	80.2	82.4	6.6	15.6	14.4	14.8
160	99.1	89.6	92.8	9.4	15.8	14.3	14.8
140	115.2	101.3	105.9	13.9	16.1	14.2	14.8
120	137.5	116.2	123.3	21.3	16.5	13.9	14.8
100	170.2	135.6	147.2	34.6	17.0	13.6	14.7
80	222.4	161.6	181.9	60.8	17.8	12.9	14.6
60	316.2	197.0	236.7	119.2	19.0	11.8	14.2
40	517.0	245.7	336.1	271.3	20.7	9.8	13.4
20	1119.6	319.8	586.4	799.8	22.4	6.4	11.7

6475.1 cm^{-1} in $Er^{3+}:LaBr_3$(34). Thus the CEF mixing of higher terms with the ground multiplet may be neglected. The relevant CEF parameters for $Er^{3+}:LaCl_3$ and $Er^{3+}:LaBr_3$ obtained by Varsanyi and Dieke (30) and Kiess and Dieke (34), respectively, in the LS coupling scheme are listed in Table 2.1. Using these parameters the Stark energy levels and corresponding eigenvectors are computed for both the systems and the results are as following:

(a) $\underline{Er^{3+}:LaCl_3}$

$E_i^o(cm^{-1})$	μ	ψ_i^o
-107.22	$\pm 5/2$	$0.752\|\pm 7/2\rangle - 0.660\|\mp 5/2\rangle$
- 68.55	$\pm 3/2$	$0.364\|\pm 15/2\rangle - 0.626\|\pm 3/2\rangle + 0.690\|\mp 9/2\rangle$
- 45.25	$\pm 3/2$	$0.924\|\pm 15/2\rangle + 0.151\|\pm 3/2\rangle - 0.351\|\mp 9/2\rangle$
- 7.79	$\pm 1/2$	$0.185\|\pm 13/2\rangle - 0.838\|\pm 1/2\rangle + 0.513\|\mp 11/2\rangle$
2.81	$\pm 5/2$	$0.660\|\pm 7/2\rangle + 0.752\|\mp 5/2\rangle$
34.68	$\pm 3/2$	$0.116\|\pm 15/2\rangle + 0.765\|\pm 3/2\rangle + 0.633\|\mp 9/2\rangle$
74.97	$\pm 1/2$	$0.341\|\pm 13/2\rangle - 0.435\|\pm 1/2\rangle - 0.833\|\mp 11/2\rangle$
116.36	$\pm 1/2$	$0.922\|\pm 13/2\rangle + 0.329\|\pm 1/2\rangle + 0.206\|\mp 11/2\rangle$.

The Zeeman splitting calculated from these eigenvalues and eigenfunctions are:

H $\parallel$ to z-axis	H $\perp$ to z-axis
$E^o_{1\pm}$ 0.890 G - 0.0804 G^2	$E^o_1 \pm$ 3.677 G - 0.3279 G^2
$E^o_{2\pm}$ 0.557 G - 0.5722 G^2	$E^o_2 \pm$ 0 + 0.1140 G^2
$E^o_{3\pm}$ 5.882 G + 0.4691 G^2	$E^o_3 \pm$ 0 - 0.0193 G^2
$E^o_{4\pm}$ 0.873 G - 0.1059 G^2	$E^o_4 \pm$ 3.313 G + 0.1146 G^2

$E_5^o \pm 0.1098\ G + 0.0841\ G^2$ $\qquad$ $E_5^o \pm 3.677\ G - 0.4193\ G^2$

$E_6^o \pm 0.825\ G + 0.1031\ G^2$ $\qquad$ $E_6^o + 0 \qquad + 0.2386\ G^2$

$E_7^o \pm 2.968\ G - 0.1009\ G^2$ $\qquad$ $E_7^o \pm 0.750\ G + 0.1089\ G^2$

$E_8^o \pm 5.341\ G + 0.2068\ G^2$ $\qquad$ $E_8^o \pm 1.438\ G + 0.1904\ G^2$

(b) $\underline{Er^{3+}:LaBr_3}$

$E_i^o(cm^{-1})$	μ	ψ_i^o
-92.20	$\pm 5/2$	$0.724\|\pm 7/2\rangle - 0.690\|\mp 5/2\rangle$
-60.99	$\pm 3/2$	$0.288\|\pm 15/2\rangle - 0.711\|\pm 3/2\rangle + 0.641\|\mp 9/2\rangle$
-31.90	$\pm 3/2$	$0.950\|\pm 15/2\rangle + 0.128\|\pm 3/2\rangle - 0.285\|\mp 9/2\rangle$
-18.79	$\pm 1/2$	$0.182\|\pm 13/2\rangle - 0.885\|\pm 1/2\rangle + 0.428\|\mp 11/2\rangle$
6.32	$\pm 5/2$	$0.690\|\pm 7/2\rangle + 0.724\|\mp 5/2\rangle$
30.53	$\pm 3/2$	$0.121\|\pm 15/2\rangle + 0.691\|\pm 3/2\rangle + 0.712\|\mp 9/2\rangle$
66.98	$\pm 1/2$	$0.319\|\pm 13/2\rangle - 0.359\|\pm 1/2\rangle - 0.877\|\mp 11/2\rangle$
100.05	$\pm 1/2$	$0.930\|\pm 13/2\rangle + 0.296\|\pm 1/2\rangle + 0.217\|\mp 11/2\rangle$.

The Zeeman splittings computed from the above Stark levels are as follows:

H $\parallel$ to z-axis	H $\perp$ to z-axis
$E_1^o \pm 0.643\ G - 0.0911\ G^2$	$E_1^o \pm 3.704\ G - 0.4133\ G^2$
$E_2^o \pm 0.469\ G - 0.3280\ G^2$	$E_2^o + 0 \qquad + 0.2109\ G^2$
$E_3^o \pm 6.426\ G + 0.1996\ G^2$	$E_3^o + 0 \qquad - 0.0765\ G^2$
$E_4^o \pm 0.401\ G - 0.0806\ G^2$	$E_4^o \pm 3.546\ G + 0.2431\ G^2$
$E_5^o \pm 0.357\ G + 0.0911\ G^2$	$E_5^o \pm 3.704\ G - 0.5414\ G^2$
$E_6^o \pm 1.457\ G + 0.1283\ G^2$	$E_6^o \pm 0 \qquad + 0.6639\ G^2$
$E_7^o \pm 3.509\ G - 0.1789\ G^2$	$E_7^o \pm 0.964\ G + 0.0860\ G^2$
$E_8^o \pm 5.411\ G + 0.2595\ G^2$	$E_8^o \pm 1.417\ G + 0.2285\ G^2$.

From these energy expressions, the principal paramagnetic susceptibilities $K_{\parallel}$ and $K_{\perp}$, the magnetic anisotropy ΔK, mean effective moment $\bar{\mu}_{eff}$ and Schottky specific heat C_S, are calculated at different temperatures for both the systems; Tables 2.5 and 2.6. The temperature dependence of $K_{\parallel}T$, $K_{\perp}T$ and $\bar{K}.T$ as well as of C_S and $\bar{\mu}_{eff}$ is exhibited in Figs. 2.9 and 2.10 for $Er^{3+}:LaCl_3$, and Figs. 2.11 and 2.12 for $Er^{3+}:LaBr_3$. The additional entropy associated with C_S is listed in Table 2.8.

(v) $Pr^{3+}:LaBr_3$

During the recent years, perhaps more attention has been directed towards an analysis of the absorption and fluorescence spectra of Pr^{3+}:ion than any other ion in the rare-earth series. Spedding (53), Hellwege and Hellwege (54) and Sayre et.al. (55) studied the absorption spectra of $Pr^{3+}:LaCl_3$ and proposed the energy positions of different levels. Later on Dieke and Sarup (56) observed the fluorescence spectra and gave firm footing to the energy levels of $Pr^{3+}:LaCl_3$. Wong and Richman (29) carried out similar studies for $Pr^{3+}:LaBr_3$ and found the spectra to be in correspondence with that for $Pr^{3+}:LaCl_3$; the centres of gravity of the J levels were shifted by about 100 cm^{-1}.

$Pr^{3+}(4f^2)$ has a free ion ground term $^3H_4$ lying about 2152 cm^{-1} below the first excited term $^3H_5$ (57). In crystal field with C_{3h} symmetry, $^3H_4$ term splits into three singlets,

TABLE 2.5 : Magnetic Susceptibilities and anisotropy of $Er^{3+}:LaCl_3$ at different temperatures (in cgs emu).

T(^{o}K)	$K_{\parallel} .10^3$	$K_{\perp} .10^3$	$\Delta K .10^3$	$\bar{K}. 10^3$
300	35.8	39.0	- 3.2	38.0
280	38.2	41.9	- 3.6	40.7
260	41.0	45.1	- 4.1	43.8
240	44.2	48.9	- 4.7	47.4
220	47.9	53.4	- 5.5	51.6
200	52.3	58.8	- 6.5	56.6
180	57.5	65.4	- 7.9	62.8
160	63.9	73.6	- 9.8	70.4
140	71.7	84.2	-12.5	80.1
120	81.5	98.3	-16.8	92.7
100	93.9	118.1	-24.2	110.0
80	109.4	147.7	-38.3	134.9
60	126.9	197.3	-70.4	173.9
40	136.6	297.0	-160.5	243.5
20	107.7	564.7	-457.0	412.4

TABLE 2.6 : Temperature dependence of calculated gram-atomic susceptibility parameters of Er^{3+}:$LaBr_3$ (in cgs emu).

T(^{o}K)	$K_{\parallel} .10^3$	$K_{\perp} .10^3$	$\bar{K}.10^3$	$\Delta K.10^3$
300	35.5	39.3	38.0	- 3.7
275	38.5	43.0	41.5	- 4.5
250	42.0	47.4	45.6	- 5.4
225	46.2	52.8	50.6	- 6.6
200	51.2	59.6	56.8	- 8.4
175	57.5	68.4	64.8	-10.9
150	65.5	80.2	75.3	-14.7
125	75.9	96.8	89.9	-20.9
100	89.8	121.9	111.2	-32.2
80	104.1	153.5	137.0	-49.5
60	120.5	206.5	177.8	-86.0
50	127.9	249.0	208.6	-121.0
40	131.5	312.3	252.0	-180.8
30	125.8	414.5	318.3	-288.7
20	106.0	599.3	434.9	-493.4

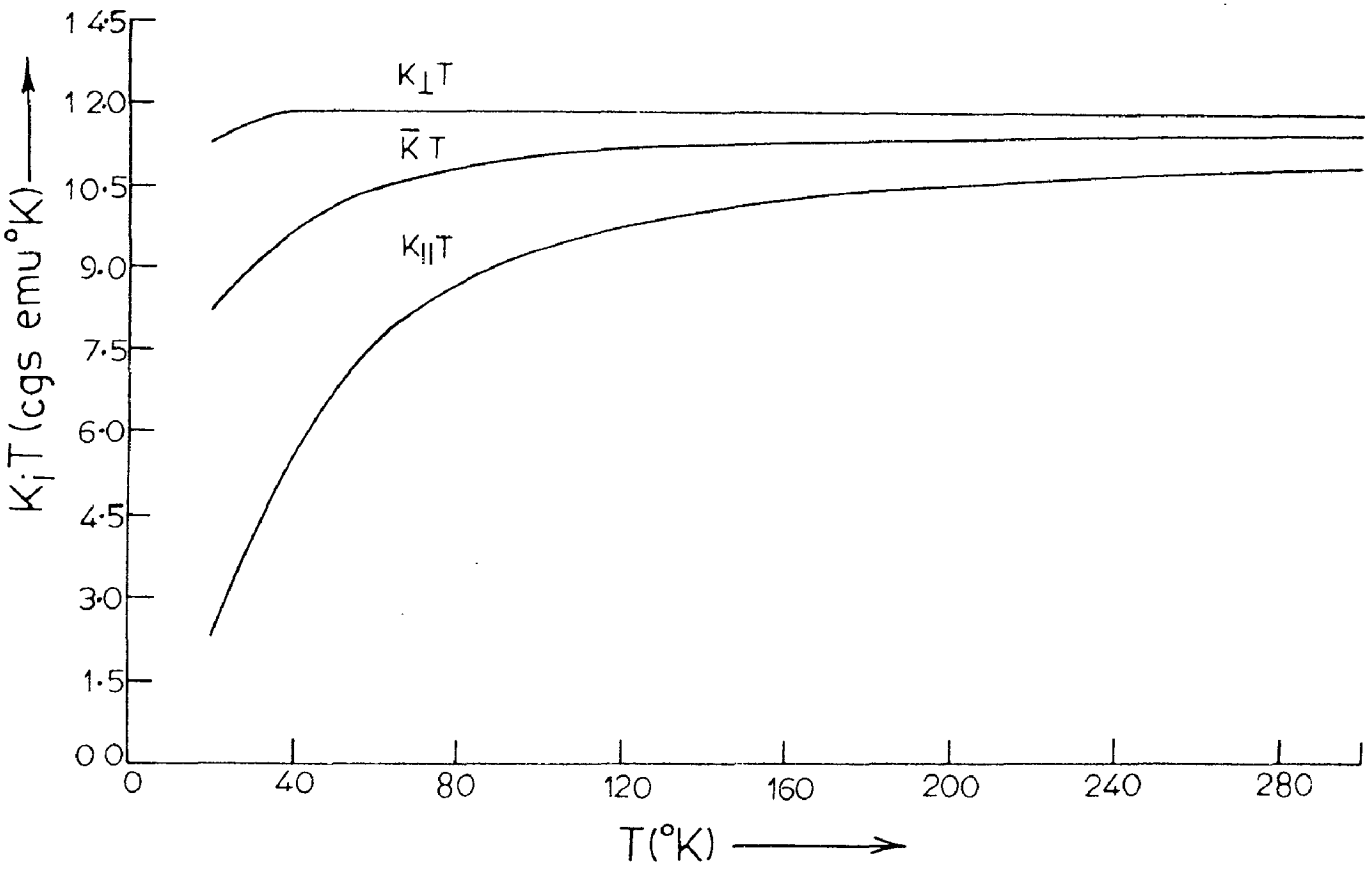

FIG. 2.9 Temperature dependence of $K_i T$ of single crystal of Er^{3+} : $LaCl_3$.

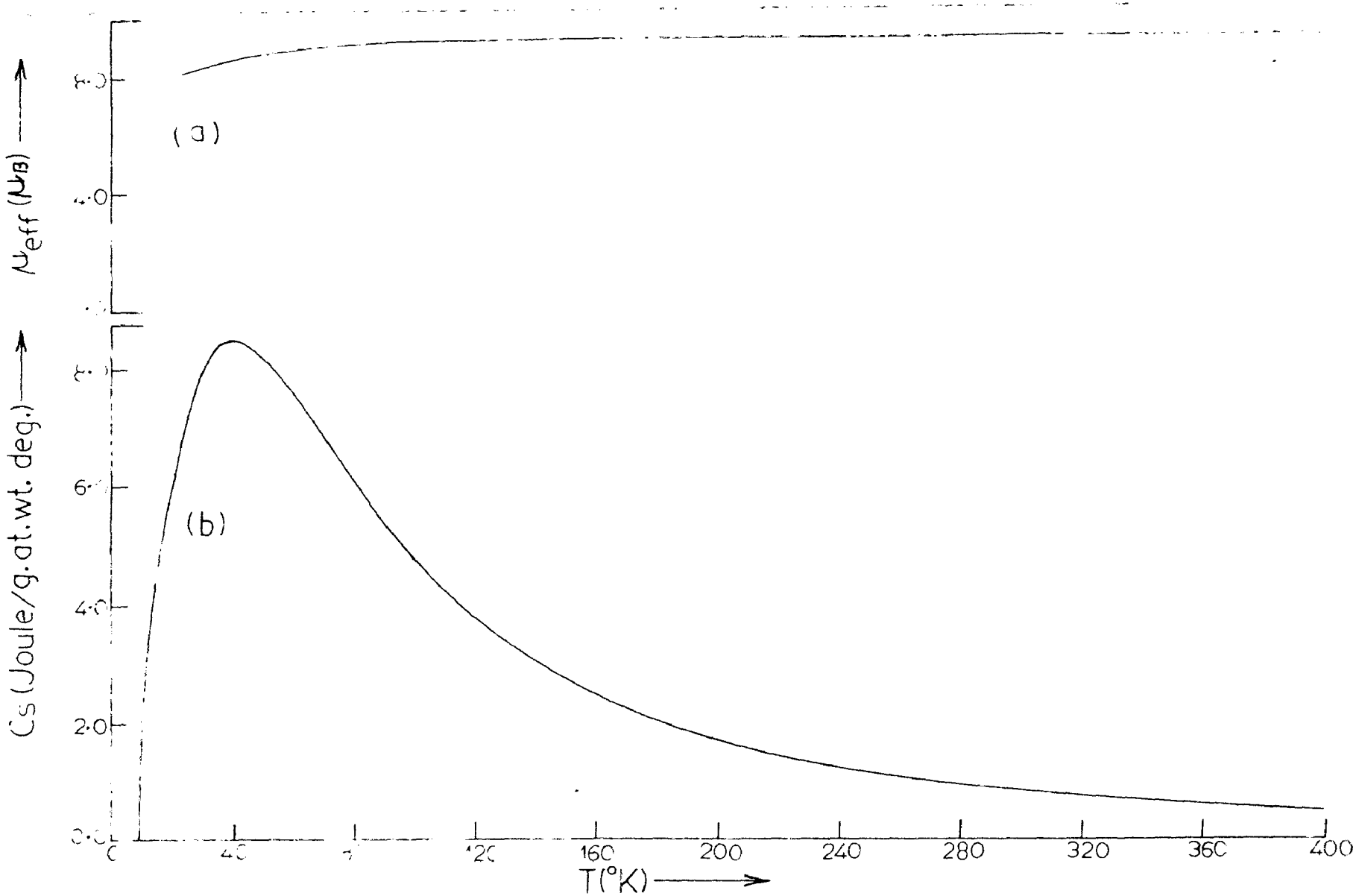

FIG. 2.10. Temperature dependence of (a) effective magnetic moment and (b) specific heat of Er^{3+} : $LaCl_3$.

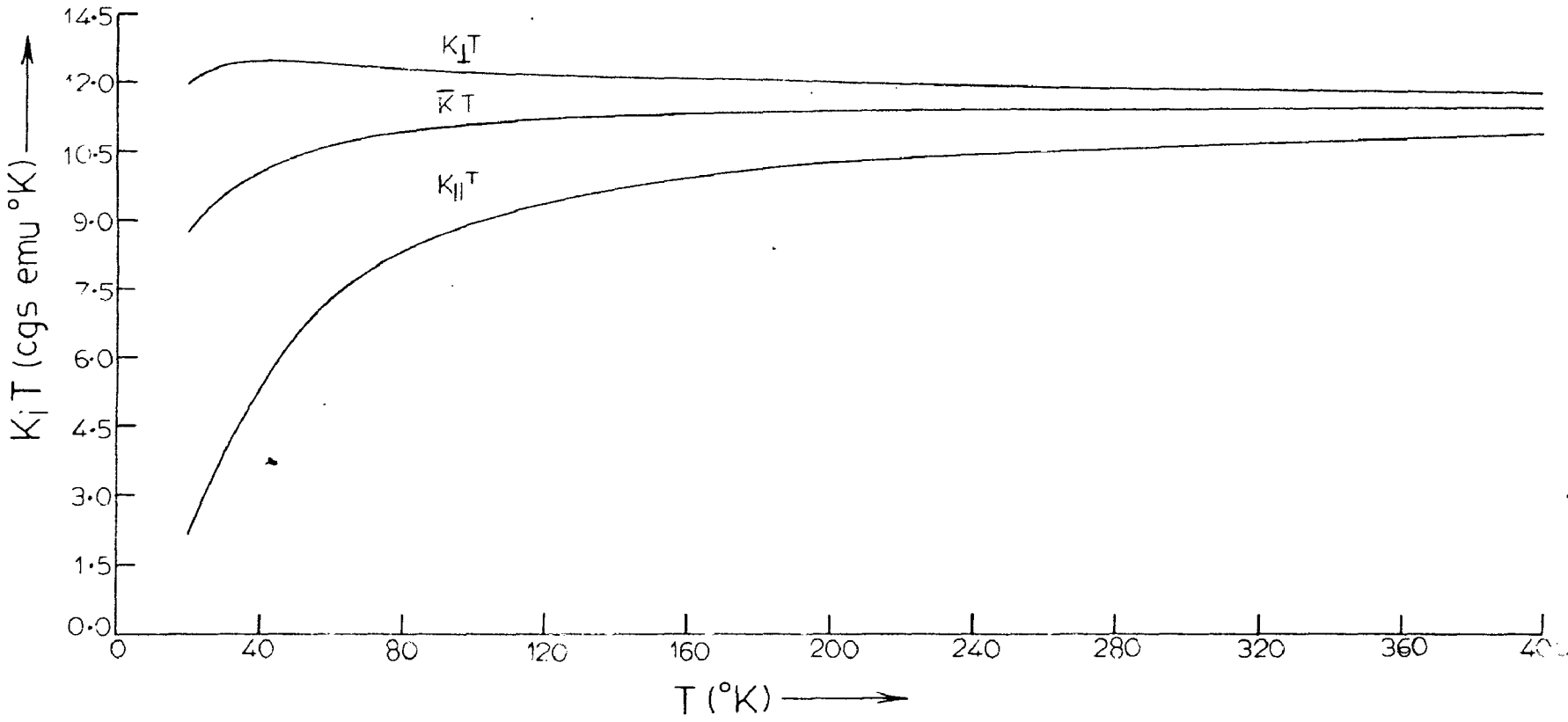

FIG. 2.11 Temperature dependence of $K_i T$ of Er^{3+}:$LaBr_3$

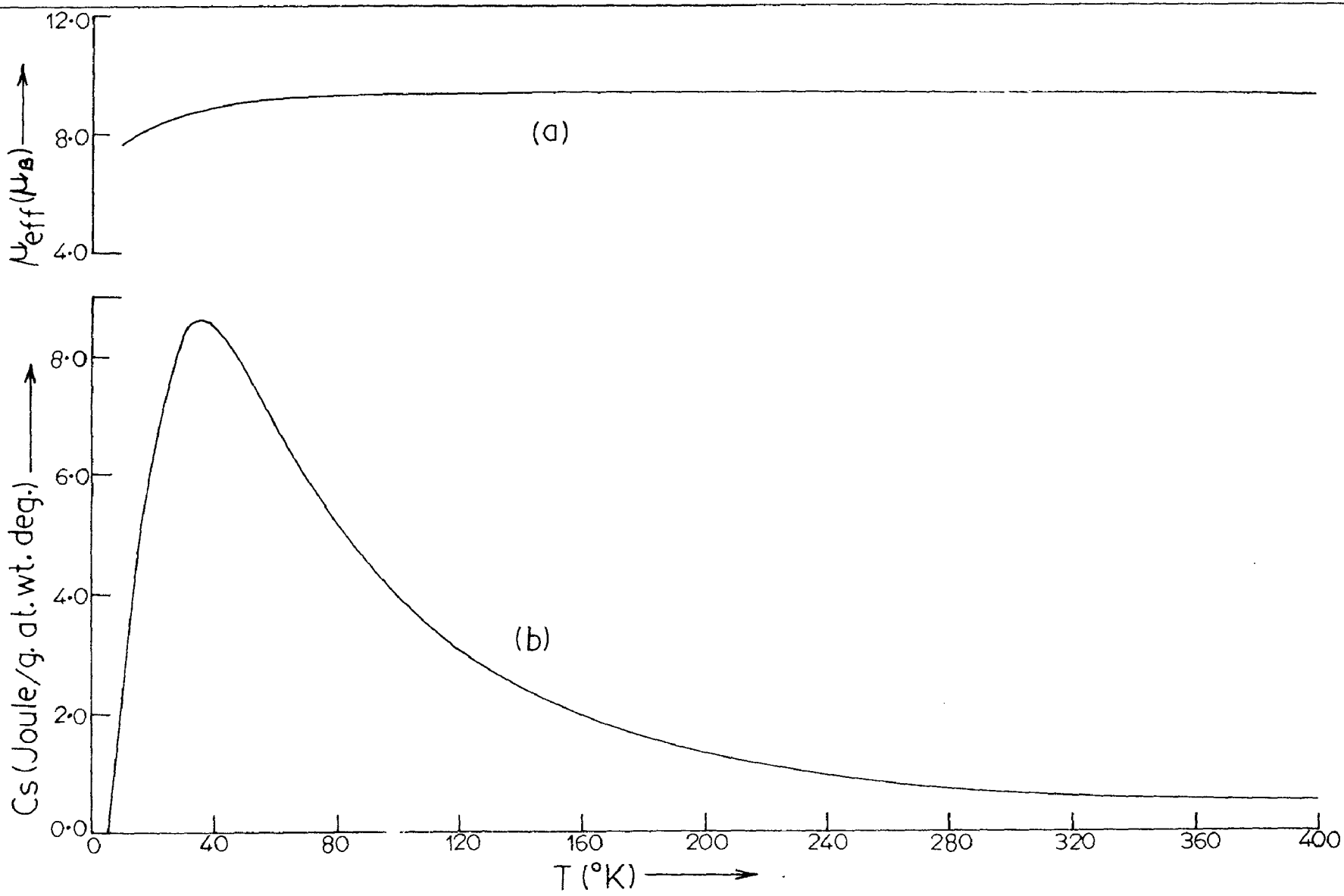

FIG. 2.12 Temperature dependence of (a) effective moment and (b) specific heat of Er^{3+}; $LaBr_3$.

two of which are designated by $\mu = 3$ and third by $\mu = 0$ and three non-Kramers doublets having $\mu = \pm 1$ for one of them and $\mu = \pm 2$ for the other two. The $^3H_5$ term lies 2086.7 cm^{-1} higher than $^3H_4$ in Pr^{3+}:$LaBr_3$ (29). The corresponding CEF parameters in the LS coupling approximation as obtained by Wong and Richman (29) are included in Table 2.1. The lowest level is found to be a doublet with $\mu = \pm 2$ and next is a singlet with $\mu = 3$. From the group theoretical considerations, the representation of the spherical rotation group with J = 4, under C_{3h} symmetry, decomposes into six irreducible representations $2\Gamma_1 + \Gamma_2 + 3\Gamma_3$. These can also be employed to designate the CEF levels. Using the reported CEF parameters and restricting to the ground J manifold, the Stark splittings and corresponding eigenfunctions are obtained:

E_i^o(cm^{-1})	μ	ψ_i^o
-97.26	± 2	$0.483\|\pm 4\rangle - 0.876\|\mp 2\rangle$
-62.63	3	$0.707\|+3\rangle - 0.707\|-3\rangle$
9.59	± 2	$0.876\|\pm 4\rangle + 0.483\|\mp 2\rangle$
34.29	± 1	$\|\pm 1\rangle$
56.86	3	$0.707\|+3\rangle + 0.707\|-3\rangle$
112.54	0	$\|0\rangle$.

The complete spectrum is

H || to z-axis		H $\perp$ to z-axis	
$E_{1\pm}^o$	0.603 G - 0.0602 G^2	E_1^o + 0	-0.0322 G^2
			-0.1818 G^2
E_2^o + 0	- 0.0753 G^2	E_2^o + 0	+ 0.1539 G^2

$E_3^o \pm 2.603\ G + 0.0602\ G^2$	$E_3^o + 0 \quad -0.0408\ G^2 \quad -0.1394\ G^2$
$E_4^o \pm 1.0\ G + 0\ G^2$	$E_{44}^o + 0 \quad +0.0686\ G^2 \quad -0.0591\ G^2$
$E_5^o + 0 + 0.0753\ G^2$	$E_5^o + 0 + 0.1029\ G^2$
$E_6^o + 0 + 0$	$E_6^o + 0 + 0.1278\ G^2$.

Once again this energy spectrum and the Stark splittings are used to calculate the principal magnetic susceptibilities, magnetic anisotropy, mean effective magnetic moment andthe specific heat at different temperatures; Table 2.7. The temperature dependence of $K_{\parallel} T$, $K_{\perp} T$ and $\bar{K}T$ is depicted in Fig.2.13. The extra entropy associated with the specific heat over a temperature range upto 400°K is given in Table 2.8.

2.4 Results and Discussion

In this section, the calculations reported above are discussed. Firstly, for Nd^{3+}:$LaCl_3$ the calculated spectroscopic splitting factors for the lowest Stark level; $g_{\parallel} = 4.075$ and $g_{\perp} = 1.864$, are in good agreement with the experimental values $g_{\parallel} = 3.996 \pm 0.001$ and $g_{\perp} = 1.763 \pm 0.001$ (24). For the next excited level, the values are $g_{\parallel} = 0.727$ and $g_{\perp} = 3.632$. From Table 2.2 it is observed that $K_{\parallel} > K_{\perp}$ and relative anisotropy ($\Delta K/\bar{K}$) increases from 0.103 at 300°K to 0.424 at 100°K and as the temperature is further lowered it increases more rapidly. The temperature dependence of magnetic susceptibilities is in accordance with the Curie-Weiss law, $K = C/(T+\theta)$, where θ is Curie temperature. The dependence can

TABLE 2.7: Temperature dependence of principal and mean magnetic susceptibilities, magnetic anisotropy, mean effective magnetic moment and Schottky specific heat of $Pr^{3+}:LaBr_3$.

T(^{o}K)	$K_{\parallel} \cdot 10^3$ (cgs emu)	$K_{\perp} \cdot 10^3$ (cgs emu)	$\bar{K} \cdot 10^3$ (cgs emu)	$\Delta K \cdot 10^3$ (cgs emu)	$\bar{\mu}_{eff}$ (μ_B)	C_S (J/gat.wt.deg.)
300	5.6	5.1	5.3	0.5	3.55	0.86
275	6.1	5.5	5.7	0.6	3.54	0.99
250	6.7	6.0	6.3	0.7	3.53	1.22
225	7.5	6.6	6.9	0.8	3.52	1.49
200	8.4	7.4	7.7	1.0	3.51	1.84
175	9.5	8.3	8.7	1.2	3.49	2.34
150	11.0	9.6	10.0	1.4	3.47	2.99
125	12.9	11.2	11.7	1.7	3.42	3.91
100	15.3	13.4	14.0	1.9	3.35	5.16
80	17.7	15.9	16.5	1.8	3.24	6.22
60	20.3	19.4	19.7	0.9	3.07	6.69
40	22.4	24.5	23.8	-2.2	2.76	5.14
20	24.5	32.2	29.7	-7.8	2.18	2.94
10	28.8	35.4	33.2	-6.6	1.63	0.70

TABLE 2.8: Comparison between extra entropy associated with Schottky specific heat upto 400°K and that obtained from the relation $S = R \log_e \left(\frac{2J+1}{p}\right)$

System	S e.u.	$R \log_e(2J+1/p)$ e.u.	degeneracy of lowest level (p)
$Nd^{3+}:LaCl_3$	12.8	13.4	2
$Ho^{3+}:LaCl_3$	17.4	17.8	2
$Er^{3+}:LaCl_3$	16.8	17.3	2
$Er^{3+}:LaBr_3$	17.1	17.3	2
$Pr^{3+}:LaBr_3$	12.3	12.5	2

be described with the following relations

$$K_{\parallel} = 1.70/(T - 0.3) \qquad T \gtrsim 60^{\circ}K ,$$

$$K_{\perp} = 1.79/(T + 47.7) \qquad T \gtrsim 140^{\circ}K ,$$

$$\bar{K} = 1.76/(T + 29.3) \qquad T \gtrsim 110^{\circ}K.$$

The difference in θ values along different directions is a consequence of the low symmetry of the crystal field at the Nd^{3+} ion. However, the Curie-Weiss constant C, related to μ_{eff} of the ions, is almost same for different directions in the crystal. The value 1.76 of this constant for mean susceptibility matches favourably with experimental 1.72 for metallic Neodymium over the temperature range 145-280°K(58). Furthermore, the room temperature value of $\mu_{eff} = 3.75\mu_B$ agrees well with the free ion value of $3.62\mu_B$ and $3.49\mu_B$ for Nd metal (59).

The C_S vs. T plot, Fig.2.6, shows that the contribution from Schottky specific heat will be maximum around 80°K (8.3 J/g.at.wt. deg.). Also the extra entropy 12.8 e.u. associated with it upto 400°K compares well with 13.4 e.u. obtained from the relation R ln(2J+1/2).

For $Dy^{3+}:LaCl_3$, Table 2.3 shows that $\bar{\mu}_{eff}$ remains almost constant over a wide range of temperature and changes only about 1% round 80°K. At 300°K, $\bar{\mu}_{eff} = 10.63\mu_B$ which is in good agreement with the free ion value $10.62\mu_B$ and also experimental value $10.67\mu_B$ for Dysprosium metal (60). The computed g-values for the lowest Stark level are $g_{\parallel} = 10.37$, $g_{\perp} = 0.0$; which have already been reported by Brower et al.(61)

and are in good agreement with those obtained by them from ESR measurements, $g_{\parallel} = 10.43$, $g_{\perp} < 0.1$. It is obvious from Table 2.3 that magnetic anisotropy $\Delta K/\bar{K}$ is positive and it increases from 0.18 at 300°K to 0.42 at 100°K. Also Fig.2.7 shows that principal magnetic susceptibilities increase with decreasing temperature. The variation of mean susceptibility follows the relation $\bar{K} = 14.38/(T+4.1)$; the calculated value 14.38 of Curie-Weiss constant is in nice agreement with the experimental value 14.07 for metallic Dy (62).

In the case of $Ho^{3+}:LaCl_3$, the computed g-values for the lowest CEF level are $g_{\parallel} = 16.12$, $g_{\perp} = 0.0$ which are in nice agreement with $g_{\parallel} = 16.01 \pm 0.18$, $g_{\perp} = 0.0$ obtained from PMR measurements (24). The variation of principal susceptibilities with temperature is found to be in comparison with that for experimental findings on isosymmetric compound Holmium ethylsulphate (63), as catalogued below

T(°K)	$K_{\parallel}T$	$K_{\perp}T$	$\bar{K}T$ a	$K_{\parallel}T$	$K_{\perp}T$	$\bar{K}T$ b
	(cm^3 °K/g.at.wt.)			(cm^3 °K/g.at.wt.)		
300	15.0	14.7	14.8	14.	15.5	-
100	17.0	13.6	14.7	-	-	14.
20	22.4	6.4	11.7	20.	6.	10.5

a) Present calculations for $HoCl_3$

b) Experimental results for $Ho(C_2H_5SO_4)_3 \cdot 9H_2O$ (Ref.63).

The temperature dependence of mean paramagnetic susceptibility follows the Curie-Weiss law $\bar{K} = C/(T+\theta)$ above 40°K with

$$C = 15.0 \quad \text{and} \quad \theta = 3.2^{\circ}K.$$

The calculated value of C is in good accordance with 14.5 obtained for Ho metal (64) over a wide range of temperature. Fig.2.8a shows the temperature dependence of $\bar{\mu}_{eff}$ and the departure from the room temperature value is 1% around 80°K. At room temperature $\bar{\mu}_{eff} = 10.87\,\mu_B$ which agrees well with the free ion value $10.6\,\mu_B$ and the experimental value $10.8\,\mu_B$ for metallic Holmium (64). The relative anisotropy $\Delta K/\bar{K}$ is 0.02 at 300°K and 0.24 at 100°K. Fig. 2.8b shows that the Schottky specific heat will be maximum 8.2 J/g.at.wt.deg. at 50°K. The additional entropy associated with this heat capacity 17.4 e.u. is in nice harmony with the expected value of 17.8 e.u.; Table 2.8.

In $Er^{3+}:LaCl_3$ and $Er^{3+}:LaBr_3$ the maxima in C_S versus T plots occur around 40°K (8.6 J/g.at.wt.deg) and 36°K (8.6 J/g.at.wt.deg), respectively. The peak positions and peak values are in good agreement with the corresponding experimental values of about 40--50°K and 8.0 J/g.at.wt.deg. for $Er(C_2H_5SO_4)_3.9H_2O$ (65). The extra entropy associated with the Schottky specific heat is listed in Table 2.8 and these values are in nice correspondence with the one obtained from R ln (2J+1/2).

The principal magnetic susceptibilities of two Er^{3+} systems vary with temperature according to the following relations:

$\underline{Er^{3+}:LaCl_3}$	$K_{\parallel} = 11.55/(T+1.9)$	$T \gtrsim 100°K$
	$K_{\perp} = 11.68/(T-0.9)$	$T \gtrsim 40°K$
	$\bar{K} = 11.71/(T+7.4)$	$T \gtrsim 20°K$

$\underline{Er^{3+}:LaBr_3}$ $K_{\parallel} = 11.61/(T+26.9)$ $T \gtrsim 120^{\circ}K$

$K_{\perp} = 11.52/(T- 6.3)$ $T \gtrsim 80^{\circ}K$

$\bar{K} = 11.51/(T+ 2.8)$ $T \gtrsim 80^{\circ}K$

The difference in θ values along different directions is a consequence of low symmetry at the Er^{3+} ion. Nonetheless, the Curie-Weiss constant which is connected with μ_{eff} of the ion, is nearly the same. At temperatures lower than the ones indicated above, deviations from these expressions are very little and the magnetic susceptibility follows Curie-Weiss law with slightly different parameters down to lower temperatures. As T tends to $0^{\circ}K$, $\bar{K}$ of these systems shows a temperature dependent behavior as anticipated for an ion with a doublet ground level.

In both these systems $K_{\perp} > K_{\parallel}$, which is contrary to the experimental findings in Erbium single crystal (66) but similar to the experimental and theoretical observations on isosymmetric $Er(C_2H_5SO_4)_3.9H_2O$ (63). The behaviour of K_i T vs. T plots of $Er^{3+}:LaCl_3$(Fig.2.9) and $Er^{3+}:LaBr_3$(Fig.2.11). systems is in accordance with that of $Er(C_2H_5SO_4)_3.9H_2O$. The magnitude of $\Delta K/\bar{K}$ rises from 0.084 to 1.107 for $Er^{3+}:LaCl_3$ and 0.091 to 1.134 for $Er^{3+}:LaBr_3$ as temperature is lowered from $300^{\circ}K$ to $20^{\circ}K$. For lack of any available measurements on these systems the calculations are compared with the experimental findings on Erbium ethylsulphate:

Comparison of magnetic anisotropy ΔK of Er^{3+} systems (milli cm^3/g.at.wt.deg).

T(^oK)	$Er^{3+}:LaCl_3$ [a]	$Er^{3+}:LaBr_3$ [a]	$Er(C_2H_5SO_4)_3.9H_2O$ [b]	
			Oscillation method	Direct measurement
290	-3.4	-4.	-4.	-4.
90.	-30.0	-39.4	-38.0	-44.0
20.4	-449.3	-484.4	-520.0	-500.0

a) Present work

b) Ref.63.

Evidently, the results are in fairly good agreement taking into consideration the host lattice effects. Further, the calculated values of C, 11.71 ($Er^{3+}:LaCl_3$) and 11.51 ($Er^{3+}:LaBr_3$), correspond well with that of 11.98 for Er metal (64).

It is observed from Figs.2.10a and 2.12a that $\overline{\mu}_{eff}$ of the two systems does not depart more than 3% from the room temperature value down to about 70^oK. The decrease at lower temperatures is due to gradual emptying of the higher energy levels; a similar trend is exhibited by $\bar{K}T$ vs T plots; Figs.2.9 and 2.11. The room temperature magnitudes of 9.45/μ_B ($Er^{3+}:LaCl_3$) and 9.55 μ_B($Er^{3+}:LaBr_3$) are in excellent agreement with 9.58 μ_B for the free ion and the experimental value 9.52/μ_B for Er metal (67).

The spectroscopic splitting factors for the lowest CEF levels of $Er^{3+}:LaCl_3$ and $Er^{3+}:LaBr_3$ are listed below along-with the experimental findings for the former (24).

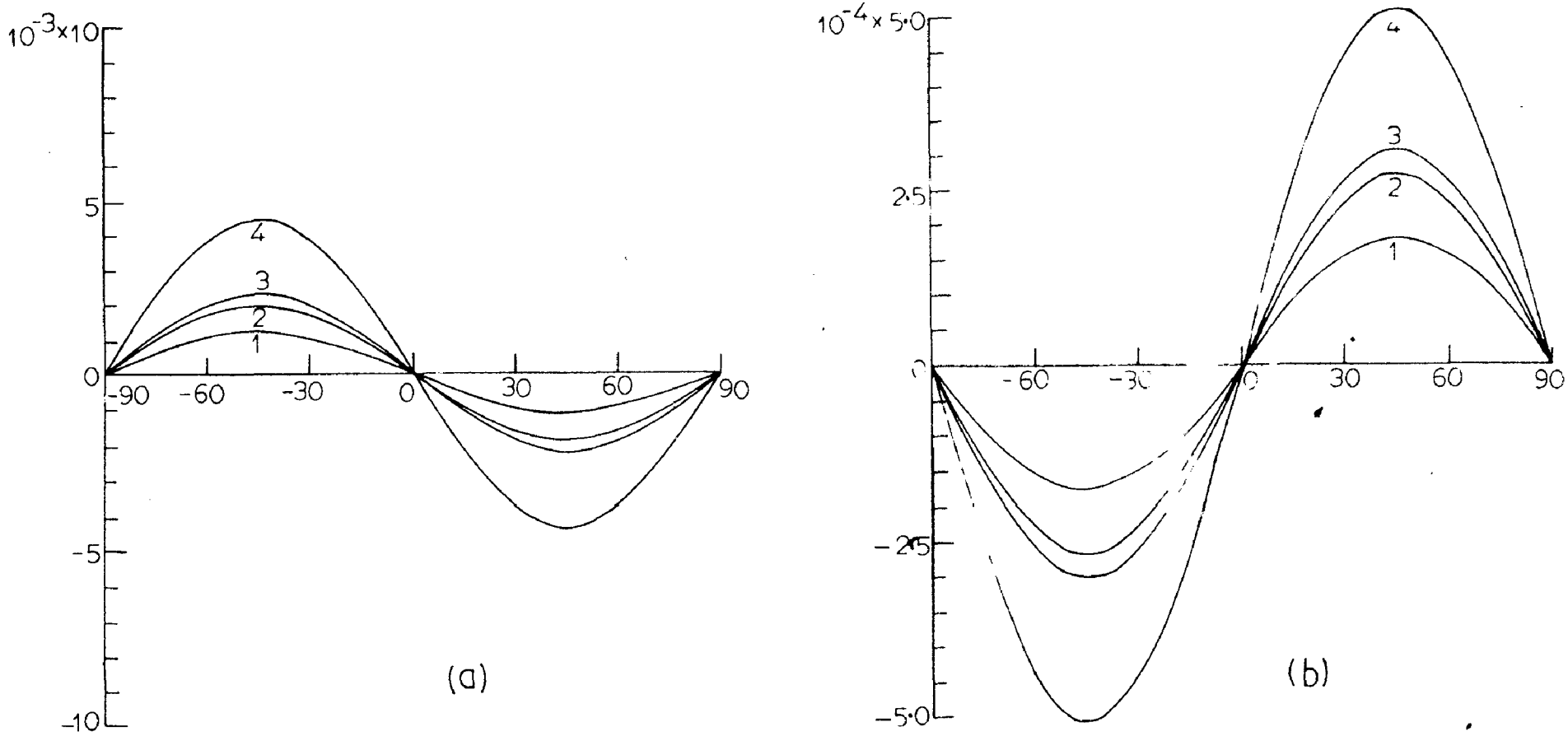

FIG. 2.14 Calculated torque on a crystal in unit magnetic field vs. angle between H and z-axis: (a) Er^{3+}: $LaBr_3$, (b) Pr^{3+}: $LaBr_3$ for temperatures (°K) (1) 90, (2) 195, (3) 273 and (4) 293.

System	$g_{\parallel}$	$g_{\perp}$
$Er^{3+}:LaCl_3$(Calc.)	2.12	8.82
(Expt.)	1.989±0.001	8.757±0.002
$Er^{3+}:LaBr_3$(Calc.)	1.54	8.89

Our calculations suggest that the ratio of the magnetic hyperfine interaction parameters A and B is 0.24 and 0.17 for $Er^{3+}:LaCl_3$ and $Er^{3+}:LaBr_3$ systems, respectively. This ratio for $LaCl_3$ host lattice has been found to be 0.217 from the PMR experiments (24).

Next the θ-dependence of torque experienced by a crystal, containing 1 g.at.wt. of Er^{3+} ion, in a unit magnetic field is calculated and displayed for $Er^{3+}:LaBr_3$ in Fig.2.14a as a typical case.

In the case of $Pr^{3+}:LaBr_3$, it is seen from Table 2.7 that the magnetic susceptibility along the symmetry axis (which coincides with the c-axis) is larger than that along a perpendicular direction and the anisotropy $\Delta K/\bar{K}$ increases from 0.098 to 0.145 with the decrease of temperature from 300°K to 125°K. With further fall in temperature, $\Delta K/\bar{K}$ decreases and changes sign at 52°K. The reversal of anisotropy is not surprising in light of the observations made by Rosenberg (19) and Schneider (68). Schneider found similar change in $Pr^{3+}:LaCl_3$ at 46°K. Comparison of temperature dependence of calculated principal magnetic susceptibilities of $Pr^{3+}:LaBr_3$ with the experimental observations on $Pr^{3+}:LaCl_3$(68) is given below:

T(°K)	Pr^{3+}:$LaBr_3$ $K_{\parallel}T$	Pr^{3+}:$LaBr_3$ $K_{\perp}T$	Pr^{3+}:$LaCl_3$ $K_{\parallel}T$	Pr^{3+}:$LaCl_3$ $K_{\perp}T$
300	1.68	1.52	1.65	1.44
52	1.10	1.10	1.03	0.98
46	1.00	1.04	0.95	0.95

The temperature dependence of principal susceptibilities can be described with the relations:

$$K_{\parallel} = 1.66/(T-2.2) \qquad T \geqslant 200^{\circ}K$$

$$K_{\perp} = 1.62/(T+8.1) \qquad T \geqslant 160^{\circ}K$$

$$\bar{K} = 1.63/(T+10.6) \qquad T \geqslant 190^{\circ}K$$

However, the variation is in accordance with Curie-Weiss law down to 60°K with slightly different parameters; appreciable departures are noted for temperatures lower than 60°K. The calculated value of C = 1.63 is in close agreement with the experimental 1.585 for Pr metal (69). Furthermore, the room temperature value $\bar{\mu}_{eff} = 3.55\mu_B$ agrees well with the free ion value $3.58\mu_B$ and experimental value of $3.56\mu_B$ for metallic Praseodymium (70).

The computed values of the components of spectroscopic splitting factor for the lowest Stark level are $g_{\parallel} = 0.965$, $g_{\perp} = 0.0$. No resonance data is available for this host lattice, but these values are in good agreement with PMR measurements on Pr^{3+}:$LaCl_3$; $g_{\parallel} = 1.035 \pm 0.005$, $g_{\perp} = 0.1 \pm 0.15$ (24). The maxima in the Schottky specific heat contribution occurs around 62°K with the peak value 6.7 J/g.at.wt.deg.. The extra entropy associated with it comes out to be 12.31 e.u. as compared with

12.51 e.u. obtained from R ln (2J+1/2).

2.5 Comments and Conclusions

The increase in magnitude of the relative anisotropy with decrease in temperature and its high value at low temperatures, is in conformity with the low symmetry of the CEF in the systems discussed in this chapter. The checking of Curie-Weiss constant with that of corresponding metals is justified by the fact that this parameter is determined by $\bar{\mu}_{eff}$ values of the ions and that the rare-earth metals can be regarded as collection of weakly interacting ions; the localized f-electrons being the main source of paramagnetic behaviour. The deviations from the predicted results can occur at low temperatures due to the following reasons:

(i) The CEF parameters $A_n^m \langle r^n \rangle$ are somewhat temperature dependent, while the values employed are at liquid air for some systems and He temperature for others.

(ii) The operator equivalent coefficients α_J, β_J and γ_J depend on the spin-orbit parameter ζ, which is always quenched by the host lattice interactions. Accordingly, these coefficients will be slightly different from the free ion values that have been used here.

(iii) The coupling of different J manifolds by the CEF is not completely negligible; for example, the upper limit for contribution from first excited term will be 3.2% for Er^{3+} and 9.8% for Pr^{3+} systems.

(iv) The exchange interactions become important at very low temperatures.

(v) The non-Kramers ground doublet of Pr^{3+}:$LaBr_3$ may have a small initial splitting caused by the Jahn-Teller effect or by random deviations from the ideal trigonal symmetry as is observed in Pr^{3+}:$LaCl_3$ (24,71). This will result into nonzero $g_\perp$ for the ground state.

However, the nice agreement discussed above for magnetic and thermal properties indicates clearly that the CEF parameters reported for these systems are reliably good.

CHAPTER III

THERMAL AND MAGNETIC PROPERTIES OF $Nd^{3+}:La_2(SO_4)_3.9H_2O$, $Tb(OH)_3$ AND $Tb^{3+}:Y(OH)_3$ SYSTEMS

3.1 $Nd^{3+}:La_2(SO_4)_3.9H_2O$

3.1.1 Introduction

Extensive studies on the rare-earth ions in various host lattices, viz. ethylsulphates, trichlorides, bromates etc. have been carried out by PMR, absorption and fluorescence measurements but fewer reports are available in Lanthanum hydrated sulphate lattice. The absorption spectra of Nd^{3+} in $La_2(SO_4)_3.9H_2O$ were reported by Dieke and Heroux (72). However, recently studies of the absorption spectra of Pr^{3+}, Nd^{3+} and Gd^{3+} in $La_2(SO_4)_3.9H_2O$ have been carried out (73,74) and in addition, EPR spectra of $Nd^{3+}:La_2(SO_4)_3.9H_2O$ system has been studied (74). The La^{3+} ion occupies two different sites with symmetries C_{3i} and C_{3h} in the crystal of $La_2(SO_4)_3.9H_2O$ (75). Like ethylsulphates and bromates the C_{3h} site has nine water molecules as the nearest neighbours. The rare-earth ions when present substitutionally experience the same symmetry. The similarity of EPR spectrum of $Nd^{3+}:La_2(SO_4)_3.9H_2O$ to that for ethylsulphate (76) indicates that the rare-earth ions in $La_2(SO_4)_3.9H_2O$ occupy principally the C_{3h} sites. It will be welcome attempt to tie up the magnetic properties of these salts with the symmetry and strength of the crystal field. In this section we give the detailed analysis of the

magnetic and thermal properties of Nd^{3+} substituted in $La_2(SO_4)_3.9H_2O$ assuming the point symmetry to be C_{3h}.

3.1.2 Calculations

The ground term of the free Nd^{3+} ion ($4f^3$) is $^4I_{9/2}$ and the nearest multiplet $^4I_{11/2}$ is higher by 1800 cm^{-1}. Both EPR and absorption spectra, indicate $\mu = 5/2$ as the ground level for Nd^{3+} in C_{3h} site symmetry. Under the influence of C_{3h} field, the double valued representation of the spherical rotation group for $J = 9/2$ decomposes into five irreducible representations $\Gamma_7 + {}^2\Gamma_8 + {}^2\Gamma_9$. Each of these levels possesses a two-fold Kramers degeneracy because of the time-reversal symmetry of the Hamiltonian which will be lifted only on the application of magnetic field. Viswanathan et.al. (73) have calculated the crystal field parameters by considering J-mixing from the ^4F_J levels obtained from the absorption spectra and EPR data of 1% Nd^{3+} doped in $La(SO_4)_3.9H_2O$. The CEF parameters are:

$A_2^0 \langle r^2 \rangle = 331.4\ cm^{-1}$, $A_4^0 \langle r^4 \rangle = -59.4\ cm^{-1}$,

$A_6^0 \langle r^6 \rangle = -45.35\ cm^{-1}$, $A_6^6 \langle r^6 \rangle = 487.7\ cm^{-1}$.

Employing these parameters the eigenvalues E_i^0 of the ground term and the corresponding eigenfunctions ψ_i^0 were calculated and are given below:

E_i^0 (cm^{-1})	μ	ψ_i^0
-186.34	$\pm 5/2$	$0.942\|\pm 7/2\rangle + 0.336\|\mp 5/2\rangle$
- 50.24	$\pm 3/2$	$0.922\|\pm 9/2\rangle + 0.388\|\mp 3/2\rangle$

7.84	$\pm 1/2$	$\lvert\pm 1/2\rangle$
108.24	$\pm 5/2$	$0.336\lvert\pm 7/2\rangle - 0.942\lvert\mp 5/2\rangle$
120.52	$\pm 3/2$	$0.388\lvert\pm 9/2\rangle - 0.922\lvert\mp 3/2\rangle$

On the application of the external magnetic field degeneracy of all Kramers doublets is lifted; the final energies upto second order in $\vec{H}$ are given below:

$H \parallel$ to z-axis	$H \perp$ to z-axis
$E_1^o \pm 2.821\ G - 0.0122\ G^2$	$E_1^o \pm 1.277\ G - 0.0270\ G^2$
$E_2^o \pm 3.596\ G - 0.0269\ G$	$E_2^o \pm 0 + 0.0023\ G^2$
$E_3^o \pm 0.5\ G + 0$	$E_3^o \pm 2.500\ G - 0.0296\ G^2$
$E_4^o \pm 1.820\ G + 0.0122\ G^2$	$E_4^o \pm 1.267\ G - 0.3795\ G^2$
$E_5^o \pm 0.595\ G + 0.0269\ G^2$	$E_5^o \pm 0 + 0.4338\ G^2$

The ionic susceptibilities for directions $\parallel$ and $\perp$ to symmetry axis are computed as a function of temperature; Table 3.1. These, in turn, are used to generate magnetic anisotropy and mean effective moment. These are also listed in Table 3.1. Furthermore, calculations are presented for specific heat and results displayed in Fig.3.1.

3.1.3 Discussion

The g-values calculated from the Zeeman splitting of the lowest Stark level are $g_{\parallel} = 4.103$, $g_{\perp} = 1.842$, which are in reasonable agreement with $g_{\parallel} = 3.963 \pm 0.003$ and $g_{\perp} = 1.743 \pm 0.001$ obtained from EPR measurements (74). The magnetic anisotropy $\Delta K/\bar{K}$ is 0.30 at 300°K and 0.75 at 100°K

TABLE 3.1: Variation of principal susceptibilities, magnetic anisotropy and $\bar{\mu}_{eff}$ with temperature of $Nd^{3+}:La_2(SO_4)_3.9H_2O$.

T(°K)	$K_{\parallel} .10^3$ cgs emu	$K_{\perp} .10^3$ cgs emu	$\bar{K}.10^3$ cgs emu	$\Delta K.10^3$ cgs emu	$\bar{\mu}_{eff}$ (μ_B)
300	6.3	4.7	5.3	1.6	3.55
280	6.8	5.0	5.6	1.8	3.54
260	7.4	5.3	6.0	2.1	3.53
240	8.0	5.6	6.4	2.4	3.52
220	8.8	6.0	7.0	2.8	3.50
200	9.8	6.5	7.6	3.3	3.48
180	10.9	6.9	8.3	4.0	3.45
160	12.4	7.5	9.1	4.9	3.41
140	14.1	8.1	10.1	6.0	3.36
120	16.4	8.8	11.4	7.6	3.30
100	19.4	9.7	12.9	9.7	3.21
80	23.6	10.8	15.1	12.8	3.10
60	30.1	12.4	18.3	17.7	2.96
40	43.0	15.3	24.6	27.7	2.80
20	82.4	23.4	43.0	59.0	2.62

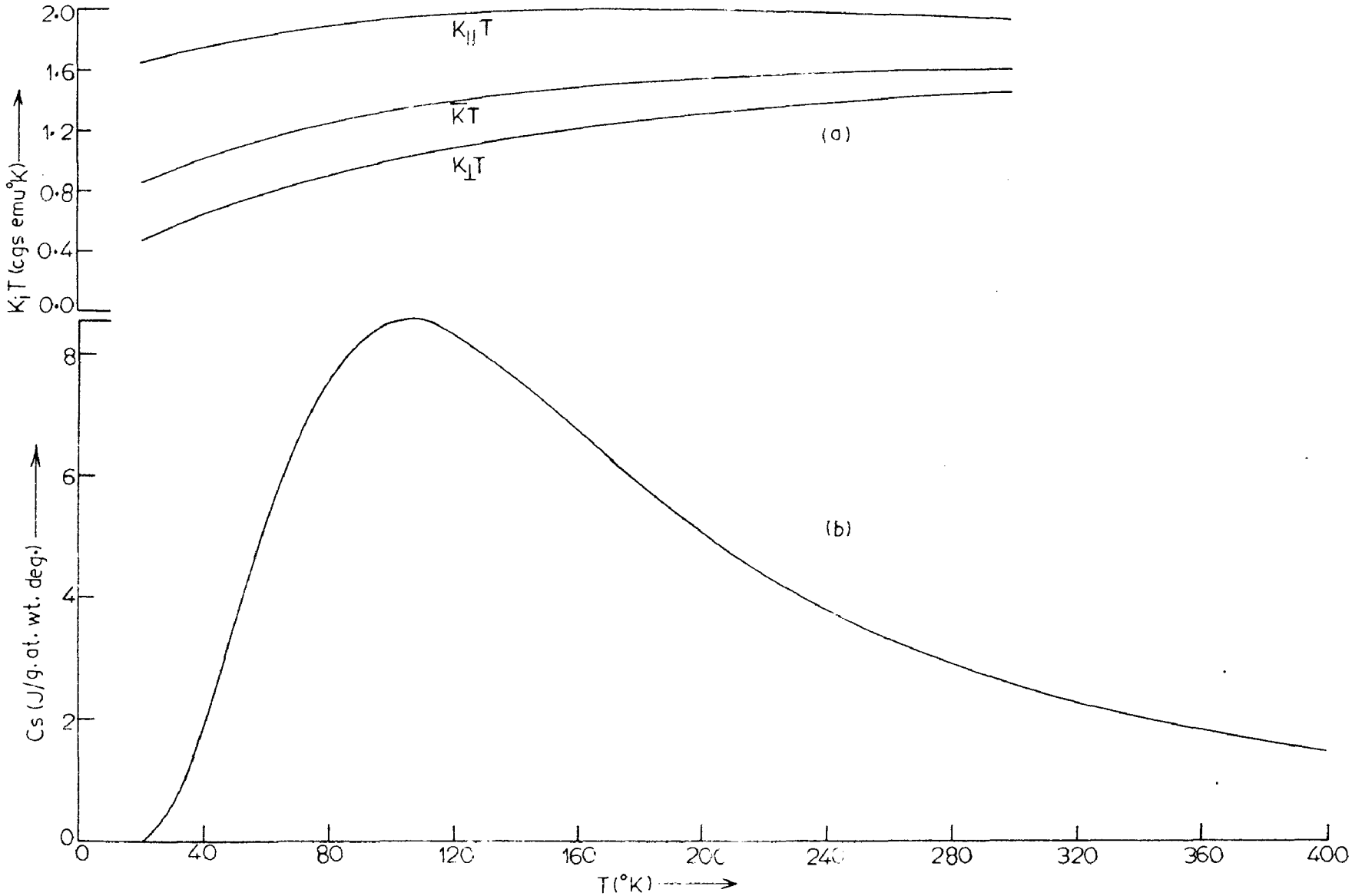

FIG.3.1 _ Temperature dependence of (a) $K_i T$ and (b) schottky specific heat of Nd^{3+}: $La_2(SO_4)_3 \cdot 9H_2O$

and increases further as the temperature is lowered which conforms with the presence of lower symmetry. The temperature dependence of magnetic susceptibility is comparable with our observations on isosymmetric $Nd^{3+}:LaCl_3$. However, the anisotropy is relatively larger in $Nd^{3+}:La_2(SO_4)_3.9H_2O$, which is not unexpected because of large splitting. The maximum in Schottky specific heat vs. T. curve occurs around 108°K (8.5J/g.at.wt.deg.) andthe entropy associated with it upto 400°K is S = 12.65 e.u. ; the latter compares favourably with 13.38 e.u. computed from Nk ln (2J+1/2) for the lowest ground state doublet. The room temperature magnitude of μ_{eff}, 3.55 μ_B matches well with the free ion value 3.62 μ_B, and 3.49 μ_B for Nd metal (59). The departure of the $\bar{\mu}_{eff}$ from the room temperature value is less than 3% down to about 150°K. This temperature range differs from that in $Nd^{3+}:LaCl_3$ system because of large CEF in sulphate lattice. It is clear from Table 3.1 that the magnetic susceptibility increases with decreasing temperature in accordance with the Curie-Weiss law $K_i = C_i/(T+\theta_i)$. The linearity holds for $\bar{K}$ above 60°K with C = 1.78 and θ = 36.7°K. The calculated value of C is in good accord with the experimental value of 1.72 for Nd metal in the temperature range 145 -280°K(58).

3.2 $Tb(OH)_3$ and $Tb^{3+}:Y(OH)_3$.

3.2.1 Introduction

Although the rare-earth hydroxides have been known for more than two decades (77) but their optical and magnetic

properties did not receive much attention. Recently, Wolf and co-workers (78-81) observed the optical and magnetic properties of some of the single crystals of hydroxides and Scott et.al.(82) studied the crystal fields for Tb^{3+} in hydroxides. The hydroxides of La - Yb and Y have general formula $R(OH)_3$ and form a series of simple magnetic crystals isostructural to the corresponding anhydrous trichlorides.

3.2.2 Crystal Structure

The rare-earth hydroxides have two rare-earth ions per unit cell, but both the sites are magnetically equivalent. These have $Y(OH)_3$ type structure (77,83), which is hexagonal with $a_o = 6.24\text{Å}$ and $c_o = 3.53\text{Å}$. The space group of the crystal is C^2_{6h} ($C6_3/m$) and the metal ion occupies C_{3h} sites. The arrangement of atoms is shown in Fig.3.2. Each metal atom is surrounded by nine OH^- groups, six of these are at a distance of 2.42Å and the remaining three at 2.54Å. The nearest approach of two OH^- is 2.78Å.

3.2.3 Crystal Field Calculations

In a number of paramagnetic salts, where the angular momentum of the paramagnetic ion has an integral quantum number, the degeneracy ofthe energy levels is not completely lifted. This occurs when the surroundings ofthe paramagnetic ion have higher than two-fold point symmetry. The doublets obtained in such systems are referred to as accidentally degenerate or non-Kramers doublets. It is the characteristic

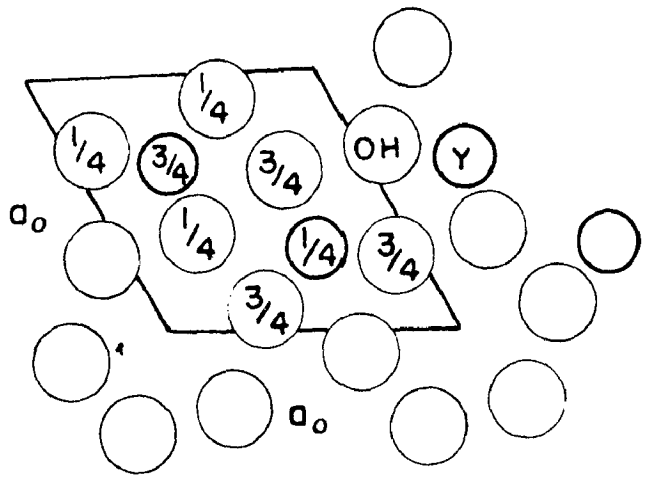

FIG. 3-2 A BASAL PROJECTION OF THE HEXAGONAL UNIT OF $Y(OH)_3$

of such doublets that first order Zeeman effect is obtained if a magnetic field is applied parallel to the axis of symmetry, but only a second order effect if the field is perpendicular to this axis. This applies to the rare-earth ions with an even number of 4f electrons excluding f^6 and f^{14} configurations which have J = 0 for their ground term. The trivalent ions to which these considerations apply are Pr^{3+}, Pm^{3+}, Tb^{3+}, Ho^{3+} and Tm^{3+} with 2,4,8,10 and 12 electrons, respectively. The properties of such ions have been investigated in the isomorphic series of salts such as ethylsulphates, chlorides etc. Here we consider the cases of $Tb(OH)_3$ and Tb^{3+}:$Y(OH)_3$ systems isostructural to anhydrous chlorides.

The ground term of $Tb^{3+}(4f^8)$ is $^7F_6$ and the Landé g-factor is 3/2. The first excited term $^7F_5$ is separated from the ground term by 2020 cm^{-1}(84). When Tb^{3+} is present in C_{3h} sites, the representation D_6 of R_3 is reduced to the irreducible representations $2\,^1\Gamma_1 + {}^1\Gamma_2 + {}^1\Gamma_3 + {}^1\Gamma_4 + {}^2\Gamma_5 + {}^2\Gamma_6$. The CEF levels thus obtained can alternatively be designated by the crystal quantum numbers $\mu = 0$ ($^1\Gamma_1$ and $^1\Gamma_2$), $\mu = \pm 1$($^2\Gamma_5$), $\mu = \pm 2$($^2\Gamma_6$) and $\mu = 3$($^1\Gamma_3$ and $^1\Gamma_4$). Scott et al. (82) found that the $^7F_5$ lies 2082 and 2061 cm^{-1} above the $^7F_6$ term in $Tb(OH)_3$ and Tb^{3+}:$Y(OH)_3$, respectively. They interpreted the observed optical spectra with the following CEF parameters (in cm^{-1}):

$Tb(OH)_3$: $A_2^0\langle r^2\rangle = 208\pm3$, $A_4^0\langle r^4\rangle = -69\pm2$,
$A_6^0\langle r^6\rangle = -45\pm1$, $A_6^6\langle r^6\rangle = 585\pm2$;

$Tb^{3+}:Y(OH)_3$: $A_2^0\langle r^2\rangle = 189 \pm 3$, $A_4^0\langle r^4\rangle = -69\pm 2$,

$A_6^0\langle r^6\rangle = -46\pm 1$, $A_6^6\langle r^6\rangle = 606\pm 3$.

Keeping in view the accuracy and assumptions made for the determination of the CEF parameters and the fact that the breakdown of Russell-Saunders coupling changes the g_J value of $^7F_6$ term by only 0.5% and our main interest being to calculate the bulk thermal and magnetic properties, we carried out the calculations within the ground J manifold. Using the operator equivalent method the positions of the Stark levels E_i^o and corresponding wavefunctions are determined. In both the systems $\mu = 0^+$ and 0^- levels are found to lie the lowest and separated by about 0.4 cm^{-1}.

If the Stark levels $\mu = 0^+$ and 0^- are taken as resolved, i.e. the lowest CEF level $\mu = 0^+$ as a singlet, then $g_{\parallel}$ and $g_{\perp}$ as obtained by a frist order perturbation will be identically equal to zero and the second order effect of magnetic interaction will be very large; it is $-73.6762\ G^2$ and $+73.6758\ G^2$ for 0^+ and 0^- levels, respectively, when $\underline{H}$ is $\parallel$ to the z-axis in $Tb(OH)_3$ and corresponding values for $Tb^{3+}Y(OH)_3$ are $-61.7202\ G^2$ and $+61.7196\ G^2$. But Zeeman effect measurements for $Tb(OH)_3$ give $g_{\parallel} = 17.7\pm 0.2$ (79). To reconcile with this, the lowest two levels 0^+ and 0^- should be taken as accidentally degenerate. Under these conditions the calculated g-values in the first-order approximation become

	$g_{\parallel}$	$g_{\perp}$
$Tb(OH)_3$	17.98	0.0
$Tb^{3+}:Y(OH)_3$	17.97	0.0.

These are obviously in good agreement with the experimental data. The second order splitting for $\underline{H}$ || z-axis also becomes very small; it is $-0.0002\ G^2$ for $Tb(OH)_3$ and $-0.0003\ G^2$ for $Tb^{3+}:Y(OH)_3$. The first and second order Zeeman splittings E_i^1 and E_i^2 (corresponding to $\underline{H}$ || and $\perp$ to z-axis) for each CEF level are obtained separately by first taking the ground level to be nondegenerate and secondly by assuming it to be accidentally degenerate. These in turn are employed to generate the principal magnetic susceptibilities in the temperature range 10-300°K from the Van Vleck formula. The results for the nondegenerate and degenerate ground levels are found to be the same; the maximum difference being 0.02% (10°K). The results are given in Table 3.2 and Fig.3.3. Furthermore, the CEF energies E_i^o are employed to calculate the Schottky specific heat for both the systems; Table 3.2. The results with degenerate and non-degenerate O^+ and O^- ground levels differ at all only at low temperatures (the calculations for nondegenerate cases are given in brackets).

3.2.4 Discussion

It is found that $K_{||} > K_{\perp}$ and the relative anisotropy rises from 0.615 and 0.556 at 300°K to 2.916 and 2.910 at 10°K for $Tb(OH)_3$ and $Tb^{3+}:Y(OH)_3$ systems respectively. Furthermore, the calculated value of $K_{||}$ (300°K) = 55.3×10^{-3} cgs emu for $Tb(OH)_3$ is in fair agreement with the experimental value of 54.7×10^{-3} cgs emu obtained by Wolf et al (78). $K_{\perp}$ increases with decreasing temperature down to 130° and 125°K for $Tb(OH)_3$

TABLE 3.2: Calculated thermal and magnetic parameters for $Tb(OH)_3$ and $Tb^{3+}:Y(OH)_3$.

T(°K)	$K_{\parallel}$ 10^3 cgs emu	$K_{\perp}$ 10^3 cgs emu	$\bar{K}.10^3$ cgs emu	$\Delta K.10^3$ cgs emu	μ_{eff} (μ_B)	C_S J/g.at.wt.deg.
			$Tb(OH)_3$			
300	55.3	31.2	39.2	24.1	9.70	2.07
200	96.7	39.4	58.5	57.3	9.68	4.72
100	260.7	41.2	114.4	219.6	9.56	11.01
50	597.9	30.6	219.7	567.3	9.37	4.91
20	1516.1	28.9	524.6	1487.1	9.16	0.10
10	3032.1	28.9	1030.0	3003.1	9.08	0.00 (0.01)
			$Tb^{3+}:Y(OH)_3$			
300	53.8	32.0	39.2	21.8	9.70	1.75
200	93.3	41.2	58.6	52.1	9.68	4.06
100	252.7	45.6	114.6	207.0	9.58	10.72
50	594.1	33.5	220.4	560.6	9.39	5.86 (5.92)
20	1515.0	30.8	525.5	1484.2	9.17	0.15 (0.16)
10	3029.9	30.8	1030.5	2999.1	9.08	0.00 (0.01)

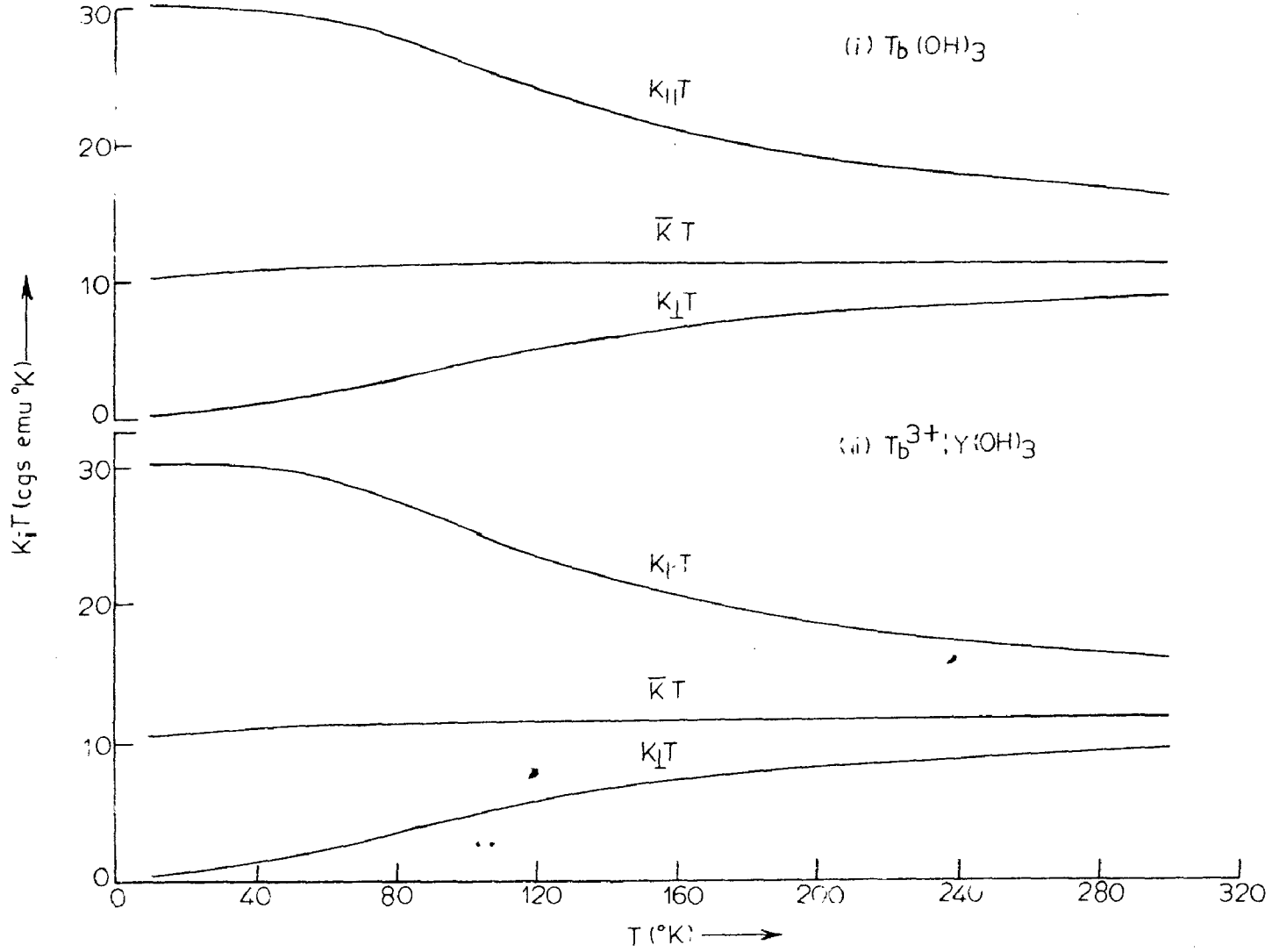

FIG. 3.3 Temperature variation of K_iT for (i) $Tb(OH)_3$ and (ii) $Tb^{3+}; Y(OH)_3$.

and $Tb^{3+}:Y(OH)_3$, but it shows a decreasing trend at lower temperatures. The mean paramagnetic susceptibility follows the Curie-Weiss law $\bar{K} = C/(T+\theta)$ down to 40°K for both the systems with the following parameters:

	C	θ
$Tb(OH)_3$	11.93	4.10
$Tb^{3+}:Y(OH)_3$	11.92	3.85.

However, $\bar{K}$ follows Curie-Weiss law with slightly different C and θ values down to 10°K. The values of C compare well with 11.6 obtained by Thoburn et al. for Tb metal (85).

The present calculations show that $\bar{\mu}_{eff}$, derived from the relationship $\bar{\mu}_{eff} = 2.83\sqrt{\bar{K}T}$ and listed in Table 3.2, does not change more than 3% from the room temperature value $9.70\mu_B$ (for both the systems) down to 60°K in $Tb(OH)_3$ and 55°K in $Tb^{3+}:Y(OH)_3$. The room temperature value is in nice agreement with the free ion value of $9.72\mu_B$ and experimental value of $9.7\mu_B$ for metallic terbium (85).

As pointed out earlier, the Schottky specific heat values are slightly different for the case with degenerate O^+ and O^- levels from that with non-degenerate levels, but the maximum difference is of the order of experimental accuracy. However, it is found that C_S will be prominent at low temperatures and the maxima occur at 94°K for $Tb(OH)_3$ (11.1J/g.at.wt.deg) and 86°K for $Tb^{3+}:Y(OH)_3$ (11.1J/g.at.wt.deg.). The extra entropy associated with the Schottky anomaly comes to be 15. e.u., which matches well with 15.6 e.u. obtained from the relation R ln (2J+1/2).

Since the interpretation of g-factors demands the ground levels to be degenerate and the bulk thermal and magnetic properties are found to be insensitive of the degeneracy of the ground level, we may safely conclude that the lowest CEF levels of Tb^{3+} in both the hydroxides behave as accidentally degenerate. Moreover, the fair agreement of present calculations with available measurements lends support to such calculations being carried out in the ground J manifold.

CHAPTER IV

THERMAL AND MAGNETIC STUDIES OF DYSPROSIUM AND YTTERBIUM ETHYLSULPHATES

4.1 Introduction

The magnetic properties of rare-earth ethylsulphates have been of considerable interest since the first reports of their magnetic susceptibility (86) and Faraday rotation (87). The rare-earth ethylsulphates form an isomorphous series of salts of the general formula, $R(C_2H_5SO_4)_3.9\,H_2O$, where R is the trivalent rare-earth ion. These crystallize readily throughout the series as crystals of hexagonal symmetry. Ketelaar (88) showed that all the rare-earth ions in an ethylsulphate lattice are magnetically equivalent, so that the bulk magnetic properties are closely related to the properties of the individual ions. Moreover, since the interactions between the rare-earth ions are important only at very low temperatures $1^{o}K$ (for magnetically dilute crystals), the magnetic properties of the salts are completely determined by the CEF seen by the paramagnetic ion. In a series of papers Stevens (12), Elliot and Stevens (13,14) and Elliot et al. (89) developed a theory of the crystal field appropriate to the ethylsulphate series. They proposed a CEF of predominantly C_{3h} symmetry in rare-earth ethylsulphates and were successful in explaining the observed EPR and magnetic susceptibility results in a number of salts. The crystal field splitting under a field of C_{3h} symmetry can be described in terms of four parameters $A_2^o\langle r^2\rangle$, $A_4^o\langle r^4\rangle$, $A_6^o\langle r^6\rangle$ and $A_6^6\langle r^6\rangle$. Elliot

and Stevens assumed that $A_n^m \langle r^n \rangle$ varies as $(Z-55)^{-n/4}$, where Z is the atomic number of the rare-earth atom. This followed from the observed empirical variation of the spin-orbit coupling constant (proportional to $\langle r^{-3} \rangle$, where r is the radius of 4f-orbital) with Z in the rare-earth series and assuming the 4f-wavefunctions to be hydrogenic. This extrapolation gave good agreement with the then available experimental results. Later on Baker et al.(90) and Judd(26,40) pointed out, while determining the CEF parameters for Praseodymium and Terbium ethylsulphate and Neodymium chloride, that the extrapolation procedure of Elliot and Stevens was not correct. They suggested the empirical determination of the CEF parameters by fitting the absorption and fluorescence spectra. This procedure was further developed by a number of workers (91-96), who employed this technique for interpretation of the optical spectra of various rare-earth ethylsulphates. Thermal and magnetic properties of Praseodymium, Neodymium, Holmium, Erbium and Thulium ethylsulphates have been studied both experimentally and on the basis of the crystal field effects (63,97-99). Similar experimental studies for Dysprosium and Ytterbium ethylsulphates have been reported (100,101) at low temperatures (1-20°K), but no crystal field analysis has been done. In the present section, we report the crystal field studies of thermal and magnetic properties of these two compounds. The CEF parameters obtained by Hüfner (92) for $Dy(C_2H_5SO_4)_3.9H_2O$ and for $Yb(C_2H_5SO_4)_3.9H_2O$ by Wheeler et al. (102) have been used in the present calculations.

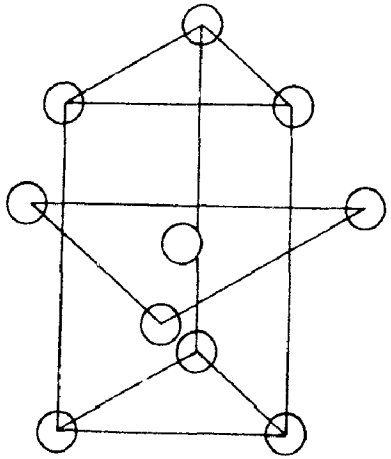

FIG. 4.1 Probable positions of the nine watermolecules round the metal ion in ethyl sulphates.

4.2 Crystal Structure

The ethylsulphates of rare-earths and Y form a hexagonal isostructural series with the point symmetry at the metal ion as trigonal-dipyramidal (C_{3h}). These have two molecular units in a unit cell and belong to the space group C^2_{6h} ($C6_3/m$). The metal ion has nine water molecules as the nearest neighbours; six forming a trigonal prism above and below the mirror plane containing the other three H_2O molecules and metal ion; Fig.4.1(88)

4.3 Crystal Field Analysis

(a) Dysprosium Ethylsulphate

The ground multiplet of $Dy^{3+}(4f^9)$ is $^6H_{15/2}$ state, which splits under a crystal field of axial symmetry (C_{3h}) into eight Kramers doublets. These doublets can be represented by crystal quantum numbers $\mu = \pm 1/2, \pm 3/2$ and $\pm 5/2$. The nearest multiplet level $^6H_{13/2}$ is about 3,300 cm^{-1} above the ground multiplet and as such the effect of higher J-levels on the ground term is negligible. The CEF parameters obtained by Hüfner (92) are:

$$A^0_2\langle r^2\rangle = 124.\ cm^{-1}, \qquad A^0_4\langle r^4\rangle = -79.\ cm^{-1},$$

$$A^0_6\langle r^6\rangle = -31.\ cm^{-1}, \qquad A^6_6\langle r^6\rangle = 492.\ cm^{-1}.$$

The various Stark levels and their wavefunctions are calculated through these parameters and the results are listed below

$E_i^o(cm^{-1})$	μ	ψ_i^o
-94.46	$\pm 3/2$	$0.058\|\pm 15/2\rangle - 0.267\|\pm 3/2\rangle + 0.962\|\mp 9/2\rangle$
-78.31	$\pm 5/2$	$0.869\|\pm 7/2\rangle - 0.495\|\mp 5/2\rangle$
-74.15	$\pm 1/2$	$0.102\|\pm 13/2\rangle - 0.196\|\pm 1/2\rangle + 0.975\|\mp 11/2\rangle$
-35.86	$\pm 3/2$	$0.994\|\pm 15/2\rangle - 0.069\|\pm 3/2\rangle - 0.080\|\mp 9/2\rangle$
-26.57	$\pm 1/2$	$0.983\|\pm 13/2\rangle - 0.128\|\pm 1/2\rangle - 0.131\|\mp 11/2\rangle$
54.41	$\pm 5/2$	$0.495\|\pm 7/2\rangle + 0.869\|\mp 5/2\rangle$
107.27	$\pm 3/2$	$0.087\|\pm 15/2\rangle + 0.959\|\pm 3/2\rangle + 0.269\|\mp 9/2\rangle$
147.68	$\pm 1/2$	$0.151\|\pm 13/2\rangle + 0.971\|\pm 1/2\rangle + 0.183\|\mp 11/2\rangle$

Further considering the effect of the magnetic field as a small perturbation on the crystal field, the Zeeman splittings of various levels are computed; for directions parallel and perpendicular to the symmetry axis. The complete energy expressions are:

H $\parallel$ to z-axis	H $\perp$ to z-axis
$E_1^o \pm 4.031\ G - 0.0224\ G^2$	$E_1^o + 0 \quad -1.2117\ G^2$
$E_2^o \pm 2.029\ G - 0.0502\ G^2$	$E_2^o \pm 3.215\ G + 0.7127\ G^2$
$E_3^o \pm 5.146\ G - 0.0433\ G^2$	$E_3^o \pm 0.678\ G + 0.3451\ G^2$
$E_4^o \pm 7.396\ G + 0.0081\ G^2$	$E_4^o + 0 \quad -0.4149\ G^2$
$E_5^o \pm 6.196\ G + 0.0329\ G^2$	$E_5^o \pm 0.613\ G + 0.5549\ G^2$
$E_6^o \pm 1.0288\ G + 0.0502\ G^2$	$E_6^o \pm 3.190\ G - 0.2520\ G^2$
$E_7^o \pm 1.113\ G + 0.0142\ G^2$	$E_7^o + 0 \quad -0.1086\ G^2$
$E_8^o \pm 0.436\ G + 0.0104\ G^2$	$E_8^o \pm 3.921\ G + 0.3733\ G^2$.

Likewise the calculations are reported for the principal magnetic susceptibilities $K_{\parallel}$ and $K_{\perp}$; magnetic anisotropy ΔK, effective magnetic moment μ_{eff} and the Schottky specific heat C_S; Table 4.1 and Fig.4.2.

(b) Ytterbium Ethylsulphate:

The ground term of free Yb^{3+} ion is $4f^{13}$, $^2F_{7/2}$ and the entire energy level scheme consists of only two groups $^2F_{7/2}$ and $^2F_{5/2}$ separated by about 10,300 cm^{-1}. Under the influence of a crystalline field of C_{3h} symmetry, the $^2F_{7/2}$ term splits into four Kramers doublets; two being pure states $|\pm 1/2\rangle$ and $|\pm 3/2\rangle$, and the other two are admixture between $|\pm 5/2\rangle$ and $|\mp 7/2\rangle$ states. However, when a magnetic field is applied the degeneracy of all the doublets is completely lifted. Since the separation of the two terms is 10,300 cm^{-1}, the influence of higher term $^4F_{5/2}$ on the ground term $^4F_{7/2}$ may be neglected. Wheeler et al.(102) explained their optical spectra of $Yb(C_2H_5SO_4)_3.9H_2O$ with the following CEF parameters:

$A_2^0 \langle r^2 \rangle = 155.4\ cm^{-1}$, $A_4^0 \langle r^4 \rangle = -57.7\ cm^{-1}$,

$A_6^0 \langle r^6 \rangle = -25.6\ cm^{-1}$, $A_6^6 \langle r^6 \rangle = 472.9\ cm^{-1}$.

Employing these parameters the eigenvalues and eigenfunctions of various Stark levels are found to be

E_i^0 (cm^{-1})	μ	ψ_i^0
-105.34	$\pm 3/2$	$\lvert\pm 3/2\rangle$
- 61.23	$\pm 5/2$	$0.313\lvert\pm 7/2\rangle - 0.950\lvert\mp 5/2\rangle$

TABLE 4.1 Variation of principal magnetic susceptibilities, magnetic anisotropy and mean effective magnetic moment with temperature of Dy $(C_2H_5SO_4)_3 9H_2O$.

T(°K)	$K_{\parallel} .10^3$ cgs emu	$K_{\perp} .10^3$ cgs emu	$\bar{K} .10^3$ cgs emu	$\Delta K.10^3$ cgs emu	$\bar{\mu}_{eff}$ (μ_B)
300	53.8	41.8	45.8	12.0	10.48
260	62.7	47.8	52.8	15.0	10.47
220	75.0	55.9	62.2	19.1	10.46
200	82.9	61.1	68.4	21.8	10.45
180	92.5	67.5	75.8	23.0	10.45
160	104.4	75.4	85.1	29.0	10.43
140	119.4	85.8	97.0	33.7	10.41
120	138.8	99.6	112.7	39.1	10.39
100	164.4	119.5	134.4	44.9	10.36
80	199.5	150.1	166.6	49.3	10.32
60	250.2	203.2	218.8	47.0	10.24
50	285.5	246.7	259.6	38.7	10.18
40	333.1	312.4	319.3	20.7	10.10
20	555.7	610.0	591.9	-54.3	9.74

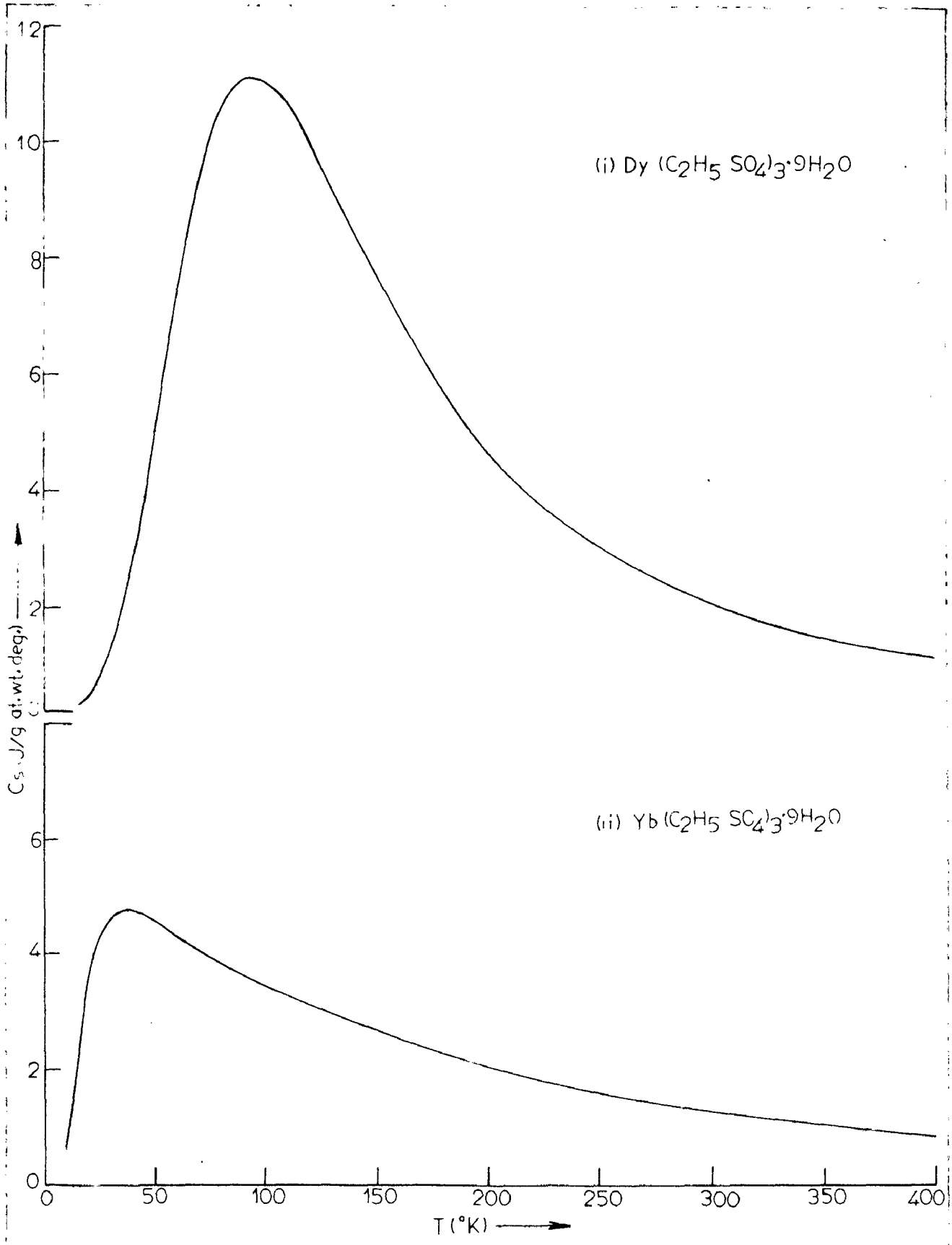

FIG.4.2 Temperature dependence of schotty specific heat of (i) Dy $(C_2H_5\ SO_4)_3 \cdot 9H_2O$ and (ii) Yb $(C_2H_5\ SO_4)_3 \cdot 9H_2O$.

3.82	$\pm 1/2$	$\|\pm 1/2\rangle$
162.75	$\pm 3/2$	$0.950\|\pm 7/2\rangle + 0.313\|\mp 5/2\rangle$.

The complete energy spectrum including the Zeeman splittings is

H $\|\|$ to z-axis	H $\perp$ to z-axis
$E_1^o \pm 1.5$ G + 0	E_1^o + 0 -0.1383 G^2
$E_2^o \pm 1.911$ G $- 0.0142$G^2	$E_2^o \pm 0.787$ G$+0.0980$ G^2
$E_3^o \pm 0.5$ G + 0	$E_3^o \pm 2.0$ G + 0.0291 G^2
$E_4^o \pm 2.911$ G + 0.0142 G^2	$E_4^o \pm 0.787$ G + 0.0112 G^2.

Using this energy spectrum the calculations are carried out for principal magnetic susceptibilities $K_{\parallel}$ and $K_{\perp}$, the magnetic anisotropy ΔK, and mean effective moment $\bar{\mu}_{eff}$; Table 4.2. In addition, the temperature dependence of Schottky specific heat is derived and displayed in Fig.4.2.

4.4 Discussion

In the case of $Dy(C_2H_5SO_4)_3.9H_2O$, $g_{\parallel} = 10.75$, $g_{\perp} = 0.0$ for the lowest Stark level and $g_{\parallel} = 5.42$, $g_{\perp} = 8.57$ for the next excited energy level, which are in good agreement with the corresponding experimental values of $g_{\parallel} = 10.76 \pm 0.1$, $g_{\perp} \simeq 0.0$ and $g_{\parallel} = 5.6 \pm 0.2$, $g_{\perp} = 7.28 \pm 0.6$, respectively (103). Cooke et al.(101) determined the magnetic susceptibility of this compound over the temperature range 1-20°K. The calculated values of $K_{\parallel} = 0.56$ cgs emu and $K_{\perp} = 0.61$ cgs emu at 20°K compare well with the experimental $K_{\parallel} = 0.57$cgs emu

TABLE 4.2: Temperature dependence of paramagnetic susceptibility parameters (in cgs emu) and $\bar{\mu}_{eff}$ (in μ_B) of $Yb(C_2H_5SO_4)_3.9H_2O$.

T(^oK)	$K_{\parallel} .10^3$	$K_{\perp} .10^3$	$\Delta K.10^3$	$\bar{K}.10^3$	$\bar{\mu}_{eff}$
300	6.6	11.7	-5.1	10.0	4.89
280	7.0	12.6	-5.6	10.7	4.89
260	7.4	13.6	-6.2	11.5	4.89
240	7.8	14.7	-6.9	12.4	4.88
220	8.4	16.1	-7.7	13.5	4.87
200	9.0	17.7	-8.7	14.8	4.86
180	9.7	19.7	-10.0	16.4	4.85
160	10.6	22.1	-11.5	18.3	4.83
140	11.7	25.2	-13.5	20.7	4.81
120	13.1	29.1	-16.0	23.8	4.77
100	15.1	34.3	-19.2	27.9	4.72
80	18.0	41.5	-23.5	33.7	4.64
60	22.7	51.9	-29.1	42.2	4.49
40	31.7	67.6	-35.9	55.6	4.21
20	56.9	88.4	-31.5	77.9	3.52

and $K_\perp$ = 0.59 cgs emu. The relative anisotropy values are 0.262 and 0.347 at 300°K and 140°K, respectively. It decreases below 140°K and finally changes sign at about 34°K. The mean magnetic susceptibility increases with decreasing temperature according to the relation $\bar{K} = 13.90/(T+3.41)$. The value 13.90 of C compares favorably with the experimental value of 14.07 for Dysprosium metal (62). Furthermore, the room temperature value of $\bar{\mu}_{eff}$ is found to be 10.48 μ_B and this is in good agreement with the free ion value 10.62 μ_B and 10.67 μ_B for Dy metal (60).

From Fig.4.2 it is observed that C_S will be maximum at 95°K and the peak value will be 11.1 J/g.at.wt.deg. The extra entropy associated with the Schottky specific heat upto 400°K comes out to be 15.05 J/g.at.wt.deg. as compared with 17.29 e.u. obtained from the formula R ln (2J+1/2).

For $Yb(C_2H_5SO_4)_3 . 9H_2O$, $g_{\parallel} = 3.43$, $g_\perp = 0.0$ for the lowest level which compares well with values from susceptibility data $g_{\parallel} = 3.40 \pm 0.07$, $g_\perp = 0.0 \pm 0.05$ (100). The corresponding values for the first excited level are $g_{\parallel} = 4.37$, $g_\perp = 1.80$. Cooke et al. (100) found that magnetic anisotropy changes sign at 18°K and the present calculations give this temperature as 12°K. Also our low temperature value of $K_{\parallel} T$ = 1.1 cgs emu °K/g.at.wt. matches fairly with 1.08 cgs emu °K/g.at.wt. obtained by Cooke et al. in the temperature range 1-20°K. The variation of mean magnetic susceptibility with temperature follows the relation $\bar{K} = 3.12/(T+11.9)$ for temperatures higher than 80°K. Furthermore, the calculated room

temperature value of $\overline{\mu}_{eff} = 4.89\,\mu_B$ compares fairly with the free ion value $4.54\,\mu_B$. The C_S vs. T plot exhibits a maximum of 4.72 J/g.at.wt.deg. at 38°K and the extra entropy associated with it upto 400°K is found to be 11.0 e.u. The latter is to be compared with 11.5 e.u. calculated from the relation R ln (2J+1/2).

CHAPTER V

STUDY OF Er^{3+} ION IN CRYSTAL FIELDS WITH D_{2d} AND O_h SITE SYMMETRIES

5.1 Thermal and Magnetic Properties of Er^{3+}:YAlG

5.1.1 Introduction

The magnetic properties of the rare-earth iron garnets $[3(RE)_2O_3.5Fe_2O_3]$ have been a subject of intensive interest ever since their first detailed investigation by Pauthenet(104). The rare-earth Gallium and rare-earth Aluminium garnets of the general formula $R_3Ga_5O_{12}$ or $R_3Al_5O_{12}$ were studied next because of their relation to the ferrimagnetic rare-earth iron garnets. The interest in these systems arose primarily from large anisotropic exchange interaction (105,106). The main interaction in the iron garnets is among Fe^{3+} ions, and it seemed interesting to study CEF effects and exchange interactions in the paramagnetic garnets, i.e. the ones in which Fe ions are replaced by Ga or Al. These present a relatively simple problem than ferrimagnetic iron garnets. It was observed that these garnets themselves form an interesting series of compounds and observations have been reported on magnetic resonance (106-08), magnetic susceptibility (109), specific heat (109-11) and optical spectra (112). It was thought expectedly that the rare-earth ions, on substitution in either of the Al or Ga garnets, would have similar properties and this was confirmed experimentally(107,109).

Further, the lattice constant of YAlG although slightly smaller than that of $Y_3Ga_5O_{12}$ (Al:Ga = 12.003: 12.273), this does not reflect in the above measurements. Trivalent rare-earth ions replace Y^{3+} substitutionally and since the site symmetry at Y^{3+} is orthorhombic, the rare-earth ions experience a CEF of low symmetry.

The only rare-earth ion for which a complete and satisfactory treatment of the crystal field interaction exists is Yb^{3+} ion with $4f^{13}$ electron configuration. Hutching and Wolf (113) derived an appropriate set of CEF parameters for Yb^{3+} in Yttrium gallium garnet by using the available experimental data. Later Buchanan and co-workers (114,115) determined the CEF levels and improved the calculations of Hutchings and Wolf by incorporating more experimental data. These efforts showed that at least in the case of Yb^{3+}, the properties in the garnet lattice could be described adequately by using the phenomenological Hamiltonian first introduced by Stevens.

The absorption bands and fluorescence lines of rare-earth doped garnets in the infrared and visible spectral regions are nearly all due to transitions between LSJ states which arise from the $(4f)^n$ electronic configurations of the lanthanide ions. The LSJ manifolds of the free rare-earth ions are (2J+1)-fold degenerate. If the ions experience a crystal field of orthorhombic symmetry, this degeneracy is

completely removed for integral value of J, and J+ $\frac{1}{2}$ Kramers pairs are left for helf-integral J. Koningstein et.al. (116, 117) studied the absorption and fluorescence spectra of Nd^{3+} and Er^{3+} in YAlG and noted the complete removal of $(J+\frac{1}{2})$-fold degeneracy, which suggests that the symmetry of the crystal field for these ions in YAlG is lower than or equal to tetragonal. This has also been observed in case of Dy^{3+}:YAlG that g-values have nearly axial symmetry w.r.t. the z-axis (118). Though in the garnets, the point symmetry at the rare-earth ion site is accepted to be D_2 yet in YAlG the tetragonal symmetry is a good approximation (119).

In this section we report the calculations of thermal and magnetic properties of Er^{3+}:YAlG system considering the nearly tetragonal symmetry and employing the CEF parameters determined by Koningstein and Geusic (117).

5.1.2 Crystal Structure

The crystal structure of garnets is relatively complicated, and the general formula is $A_3B_5O_{12}$, where A is a trivalent ion such as Y^{3+} or Lu^{3+}; B can be a trivalent ion like Fe^{3+}, Al^{3+} or Ga^{3+}. The crystallographic studies (120) show that the garnets crystallize in the cubic group with space symmetry O_h^{10} (Ia 3d) and that there are eight molecular units per unit cell. In the unit cell of a typical garnet such as YAlG, the 24 Y^{3+} ions occupy the dodecahedral {c} sites, while the 40 Al^{3+} ions are distributed in 24 tetrahedral (d) and 16 octahedral (a) positions. The Y^{3+} ions are surrounded by

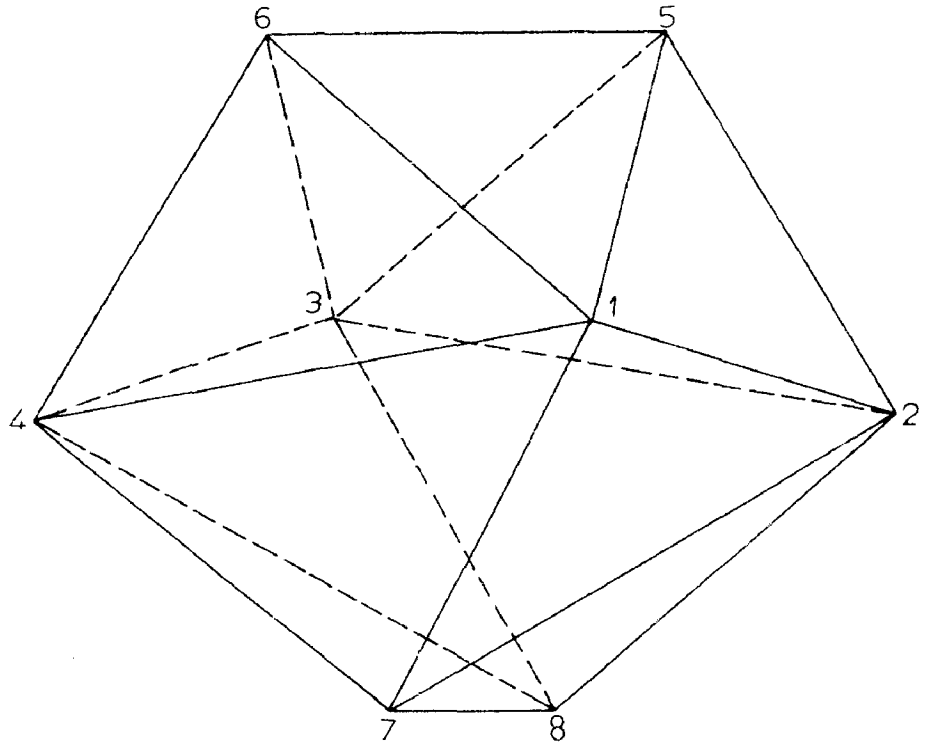

FIG. 5.1 Coordination of the dodecahedron of oxygen ions about the central y^{3+} ion in YAlG.

eight O^{2-} ions situated roughly at the corners of a distorted cube such that there are two distinct distances from the central Y^{3+} ion, Fig.5.1. The rare-earth ions replace Y^{3+} substitutionally and thus occupy 8-coordinated sites with D_2 symmetry. However, as discussed in section 5.1.1, the CEF at the rare-earth site may be taken as tetragonal.

5.1.3 Crystal Field Analysis

The ground term of Er^{3+} ion ($4f^{11}$) is $^4I_{15/2}$ and since the first excited term $^4I_{13/2}$ lies 6770 cm^{-1} higher, J can be taken as a good quantum number. Now, the crystal electric field in tetragonal symmetry can be expressed as

$$\begin{aligned} V_c = {} & A_2^0\langle r^2\rangle\, \alpha_J\left[3J_z^2 - J(J+1)\right] + A_4^0\langle r^4\rangle \beta_J\left[35J_z^4 - \{30J(J+1)-25\}J_z^2\right. \\ & \left. - 6J(J+1) + 3J^2(J+1)^2\right] \\ & + A_4^4\langle r^4\rangle\, \beta_J\left[0.5\,(J_+^4 + J_-^4)\right] \\ & + A_6^0\langle r^6\rangle\, \gamma_J\left[231J_z^6 - 105\{3J(J+1)-7\}J_z^4 + 21\{5J^2(J+1)^2 - 25J(J+1)\right. \\ & \left. +14\}J_z^2 - 5J^3(J+1)^3 + 40J^2(J+1)^2 - 60J\,(J+1)\right] \\ & + A_6^4\langle r^6\rangle\, \gamma_J\, \tfrac{1}{4}\left[\{11J_z^2 - J(J+1) - 38\}\,(J_+^4 + J_-^4)\right. \\ & \left. + (J_+^4 + J_-^4)\,\{11J_z^2 - J(J+1) - 38\}\right]. \qquad (5.1) \end{aligned}$$

Under the influence of such a field, the spherical rotation group $D_{15/2}$ corresponding to the ground multiplet $^4I_{15/2}$ is transformed according to the reduction

$$D_{15/2} \rightarrow 4(^2\Gamma_6 + {}^2\Gamma_7)$$

and thus the ground term splits into eight Kramers doublets. These doublets can also be designated by the crystal quantum numbers $\mu = \pm 3/2(^2\Gamma_6)$ and $\mu = \pm 1/2(^2\Gamma_7)$. Koningstein and Geusic (117) found that the first excited term $^4I_{13/2}$ lies at 6766 cm^{-1} w.r.t. $^4I_{15/2}$ in Er^{3+}:YAlG. They interpreted the optical spectra assuming a tetragonal field and employing the effective operator equivalent factors α_J, β_J, γ_J within the ground J manifold as obtained by Erath (121). The CEF parameters reported by Koningstein and Geusic are:

$$A_2^0\langle r^2\rangle = 260.\ ,\ A_4^0\langle r^4\rangle = -160.\ ,\ A_4^4\langle r^4\rangle = -800,$$
$$A_6^0\langle r^6\rangle = 45.\ ,\ \text{and}\ A_6^4\langle r^6\rangle = -710.\ cm^{-1}$$

The Stark splittings and corresponding zeroth order wavefunctions obtained from these parameters are listed below:

$E_i^0(cm^{-1})$	μ	ψ_i^0
-295.97	±1/2	$0.539\|\pm13/2\rangle+0.549\|\pm5/2\rangle-0.571\|\mp3/2\rangle$ $-0.285\|\mp11/2\rangle$
-238.08	±3/2	$0.054\|\pm15/2\rangle+0.079\|\pm7/2\rangle-0.975\|\mp1/2\rangle$ $-0.201\|\mp9/2\rangle$
-204.11	±1/2	$0.550\|\pm13/2\rangle+0.340\|\pm5/2\rangle+0.634\|\mp3/2\rangle$ $+0.424\|\mp11/2\rangle$
-109.40	±3/2	$0.789\|\pm15/2\rangle+0.608\|\pm7/2\rangle+0.088\|\mp1/2\rangle$ $+0.027\|\mp9/2\rangle$
158.12	±1/2	$0.353\|\pm13/2\rangle-0.339\|\pm5/2\rangle+0.396\|\mp3/2\rangle$ $-0.777\|\mp11/2\rangle$
175.50	±3/2	$0.025\|\pm15/2\rangle-0.018\|\pm7/2\rangle+0.202\|\mp1/2\rangle$ $-0.979\|\mp9/2\rangle$

233.37 $\pm 1/2$ $0.531|\pm 13/2\rangle - 0.684|\pm 5/2\rangle - 0.339|\mp 3/2\rangle + 0.367|\mp 11/2$

280.56 $\pm 3/2$ $0.611|\pm 15/2\rangle - 0.790|\pm 7/2\rangle - 0.035|\mp 1/2\rangle + 0.023|\mp 9/2\rangle$

Further the Zeeman splittings of these doublets are as follows:

H $\parallel$ to z-axis	H $\perp$ to z-axis
$E_1^o \pm 1.708\ G - 0.1442\ G^2$	$E_1^o \pm 3.243\ G - 0.1457\ G^2$
$E_2^o \pm 0.613\ G - 0.0039\ G^2$	$E_2^o \pm 3.692\ G - 0.0890\ G^2$
$E_3^o \pm 0.662\ G + 0.1239\ G^2$	$E_3^o \pm 2.905\ G + 0.1562\ G^2$
$E_4^o \pm 5.954\ G - 0.0074\ G^2$	$E_4^o \pm 0.143\ G + 0.0432\ G^2$
$E_5^o \pm 2.462\ G - 0.1530\ G^2$	$E_5^o \pm 2.489\ G - 0.4614\ G^2$
$E_6^o \pm 4.327\ G + 0.0009\ G^2$	$E_6^o \pm 0.287\ G + 0.3511\ G^2$
$E_7^o \pm 2.092\ G + 0.1732\ G^2$	$E_7^o \pm 2.829\ G - 0.0932\ G^2$
$E_8^o \pm 4.986\ G + 0.0103\ G^2$	$E_8^o \pm 0.122\ G + 0.2387\ G^2$.

The Stark splittings are used to get the temperature dependence of Schottky spcific heat; Fig.5.2. Next, the principal susceptibilities $K_{\parallel}$ and $K_{\perp}$, anisotropy ΔK, and $\overline{\mu}_{eff}$ are generated and their values for some typical temperatures are catalogued in Table 5.1.

5.1.4 Discussion

The Schottky specific heat exhibits two peaks at 44^oK (6.26 J/g.at.wt.deg) and 210^oK (4.83 J/g.at.wt.deg.). The second peak is not as sharp as the first and it appears because the fifth CEF level ($\mu = \pm 1/2$) is separated from the fourth ($\mu = \pm 3/2$) by 267.5 cm^{-1}, while the crystal field splittings of

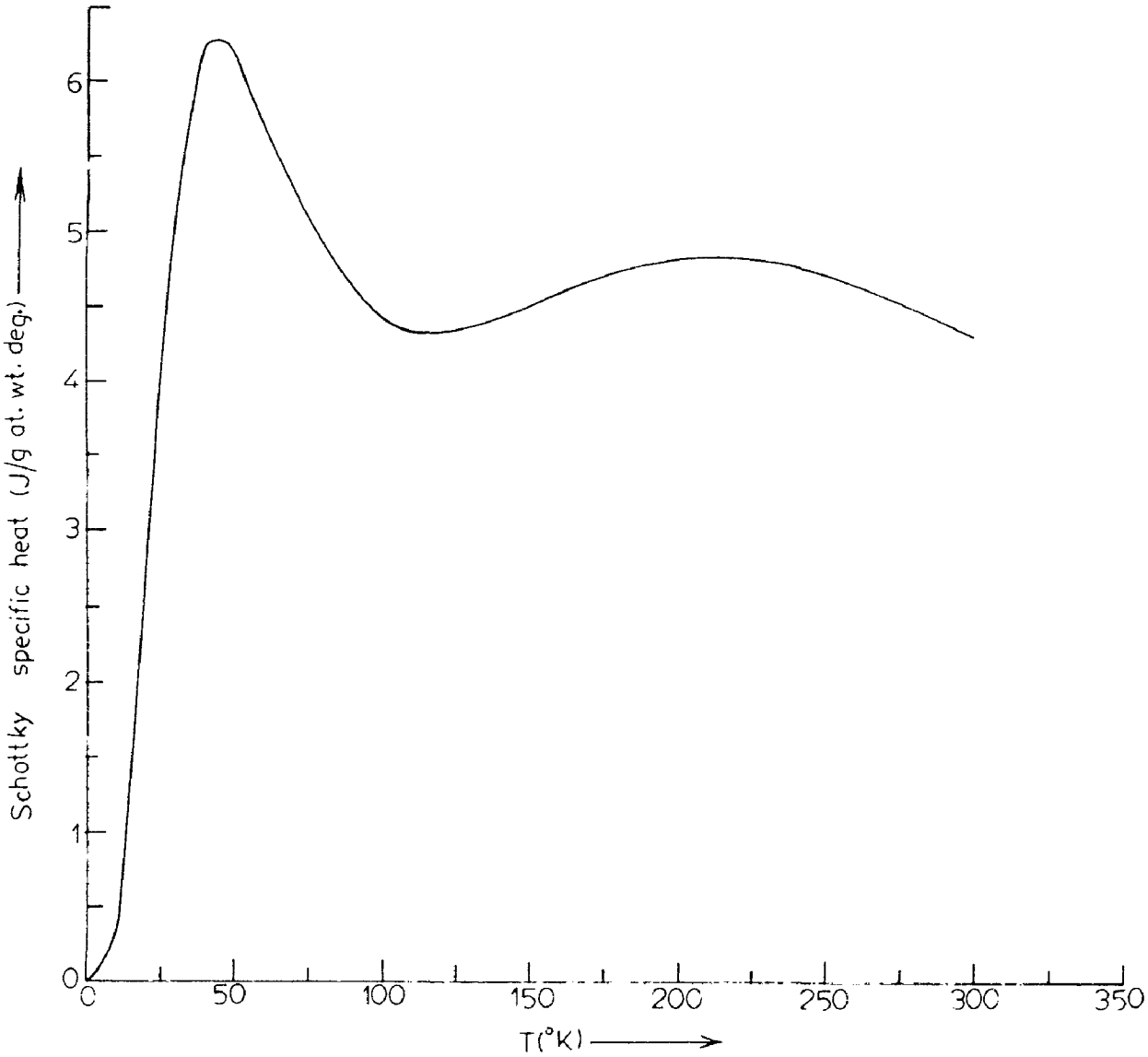

FIG. 5.2 Temperature variation of schottky specific heat of Er^{3+}: YAlG.

TABLE 5.1 : Temperature dependence of theoretical gram-atomic magnetic susceptibility parameters (in milli cgs emu) and μ_{eff} (in μ_B) of Er^{3+}:YAlG.

T(^{o}K)	$K_{\parallel}$	$K_{\perp}$	$\bar{K}$	ΔK	$\bar{\mu}_{eff}$
300	30.0	39.8	36.5	-9.8	9.36
256	34.2	47.8	43.3	-13.6	9.30
200	40.1	59.7	53.1	-19.6	9.22
175	43.9	68.0	60.0	-24.1	9.16
150	48.8	79.0	69.0	-30.2	9.09
125	55.4	94.0	81.1	-38.6	9.00
100	64.8	115.5	98.6	-50.7	8.88
75	79.9	148.7	125.8	-68.8	8.68
60	94.1	178.5	150.4	-84.4	8.49
50	107.3	205.4	172.7	-98.1	8.31
40	124.7	241.4	202.5	-116.7	8.05
30	148.3	294.6	245.3	-146.3	7.68
20	182.8	391.2	321.7	-208.4	7.17
10	264.0	673.2	536.8	-409.2	6.55

levels with i = 1 → 4 and i = 5 → 8 are 186.6 and 122.5 cm^{-1}, respectively. For lack of experimental measurements for Er^{3+}:YAlG or Er^{3+}:YGaG, no comparison is possible. Nonetheless, the extra entropy S = 15.1 e.u. associated with the Schottky specific heat upto 400°K shows a fair agreement with 17.3 e.u. derived from the relation, S = R ln(2J+1/2). The closer agreement obtained in the case of other Er^{3+} systems (Chapter 2), is not tenable due to larger CEF splitting (576.5 cm^{-1}) in the garnet system.

The g-values for the lowest CEF level are: $g_{\parallel}$ = 4.09 and $g_{\perp}$ = 7.76, which give $\bar{g}$ = 6.53 in good agreement with the experimental value of 6.27 (109). Also the result $g_{\perp} > g_{\parallel}$ is in harmony with the observation made by Ball et al. (109). From Table 5.1, it is clear that $K_{\parallel} < K_{\perp}$ and that the magnetic susceptibilities increase with decreasing temperature. The variation with temperature is in accordance with the following relations:

$$K_{\parallel} = 11.62/(T + 87.4) \qquad T \gtrsim 120^{\circ}K,$$

$$K_{\perp} = 12.02/(T + 2.7) \qquad T \gtrsim 100^{\circ}K,$$

$$\bar{K} = 11.57/(T + 17.1) \qquad T \gtrsim 20^{\circ}K.$$

The difference in θ_p values along different directions, is a consequence of the low symmetry of the CEF at the Er^{3+} ion. The computed value of Curie constant, C = 11.57, for the mean susceptibility corresponds well with 11.98 measured for Erbium metal (64). Furthermore, the relative anisotropy changes from -0.270 to -0.762 as temperature is varied from

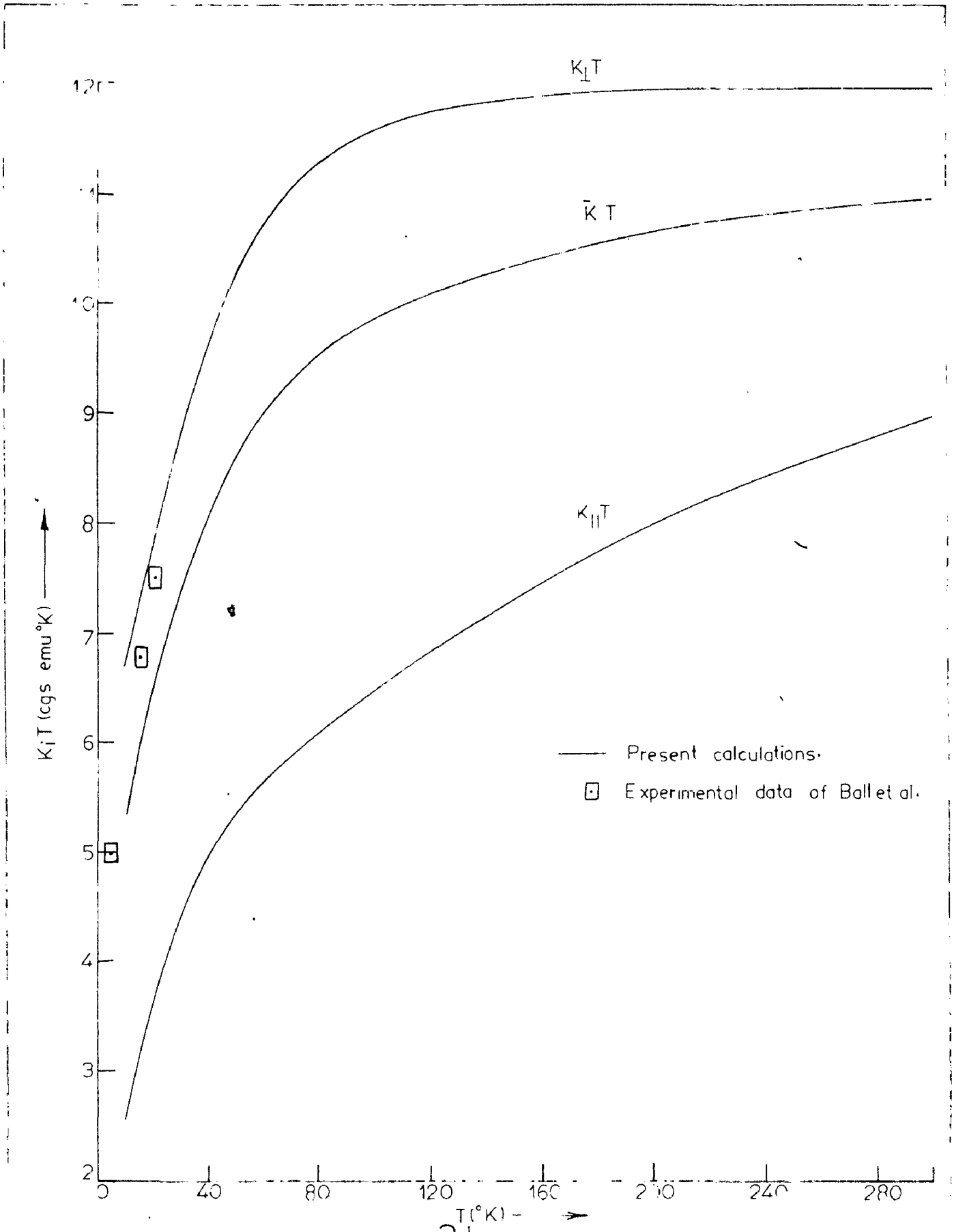

FIG. 5.3 $\bar{K}T$ vs T plot for Er^{3+}:YAlG.

300°K to 10°K. The calculated $K_i T$ are plotted as function of temperature in Fig.5.3 and the results for $\bar{K}T$ compared with the experimental data upto 20°K. The not so good agreement is not unexpected because at low temperatures for which the measurements are available, other interactions not accounted for in our work become significant. It may be remarked that appreciable deviation of calculations from measurements at low temperatures have been reported in the case of Dy^{3+}:YAlG (118).

It is found that $\bar{\mu}_{eff}$ of Er^{3+}:YAlG does not depart more than 3% from the room temperature value down to 145°K. The calculated room temperature value of $9.36\mu_B$ is in nice agreement with the free ion value $9.55\mu_B$ and $9.52\mu_B$ for metallic Er (67). The difference in the room temperature magnitude and the temperature down to which departure is less than 3%, from the corresponding quantities for other Er^{3+} systems (Chapter II and Sections 5.2 and 5.3) is due to comparatively larger crystal fields in YAlG host lattice. The extrapolated value of $\bar{\mu}_{eff}$ at 0°K = $5.88\mu_B$ is in good agreement with $5.9\mu_B$ obtained by neutron diffraction from isosymmetric ErGaG (122).

5.2 Thermal and Magnetic Properties of Er^{3+};YVO_4 and Er^{3+}:YPO_4

5.2.1 Introduction

The optical and EPR measurements of rare-earth substituted Yttrium orthovanadate (YVO_4) and Yttrium orthophosphate (YPO_4) have been of recent interest to a number of workers (123-127). Brecher et al. (123) investigated the nature of crystal field in orthovanadate from the analysis of the polarized

tra of Eu^{3+} in YVO_4. They found that the site symmetry he rare-earth ion in this lattice is D_{2d}. The optical EPR spectra of Eu^{3+}, Gd^{3+}, Er^{3+} etc. in YVO_4 and YPO_4 lattices have been analysed by Brecher et al.(123), Rosenthall et al. (124) and Kuse (125) with D_{2d} site symmetry. In the present section we studied the thermal and magnetic properties of Er^{3+}:YVO_4 and Er^{3+}:YPO_4 systems.

5.2.2 Crystal Structure:

The vanadates and phosphates of scandium, Yttrium and rare-earths crystallize with zircon structure (128,129) and can be described by the general formula $P^{+m}\ Q^{+(8-m)}\ O_4$, where P and Q are metal ions having coordination numbers of 8and 4, respectively. This tetragonal structure belongs to the space group D_{4h}^{19} - I_4/amd. There are four molecules in the unit cell and the rare-earth ions enter the lattice substitutionally in the 8-coordinated trivalent ion sites. Thus the rare-earth ions experience a D_{2d} crystal field, whose S_4 axis coincides with the crystalline four-fold axis.

5.2.3 Calculations

The ground term $^4I_{15/2}$ of Er^{3+} splits into eight Kramers doublets under the crystal field with D_{2d} symmetry. Kuse (125) studied the optical spectra of Er^{3+}:YVO_4 and Er^{3+} YPO_4 systems and interpreted the results through the crystal field given by Eq.5.1. The relevant CEF parameters are transformed to the present notation using the relations given independently by Kuse (125) and Kassmann (130). These parameters are (in cm^{-1}):

$Er^{3+}:YVO_4$ $\quad A_2^0\langle r^2\rangle = -102.8,\ A_4^0\langle r^4\rangle = 45.5,\ A_6^0\langle r^6\rangle = -43.0,$

$A_4^4\langle r^4\rangle = \pm 968.2,\ A_6^4\langle r^6\rangle = \pm 22.1;$

$Er^{3+}:YPO_4$ $\quad A_2^0\langle r^2\rangle = -141.4,\ A_4^0\langle r^4\rangle = 18.1,\ A_6^0\langle r^6\rangle = .40.4,$

$A_4^4\langle r^4\rangle = \pm 837.2,\ A_6^4\langle r^6\rangle = \pm 88.5.$

The Stark splittings and corresponding wavefunctions for the two systems are obtained through these CEF parameters and these, in turn, are employed to find the Zeeman splittings for each Stark level. The results are listed below:

(i) $Er^{3+}:YVO_4$

(a) E_i^0 (cm^{-1})	ψ_i^0
-150.05	$0.266\|\pm 15/2\rangle - 0.814\|\pm 7/2\rangle + 0.318\|\mp 1/2\rangle - 0.406\|\mp 9/2\rangle$
-106.47	$0.296\|\pm 15/2\rangle - 0.384\|\pm 7/2 - 0.127\|\mp_1/2\rangle + 0.865\|\mp 9/2\rangle$
- 97.80	$0.162\|\pm 13/2\rangle - 0.813\|\pm 5/2\rangle + 0.497\|\mp 3/2\rangle - 0.256\|\mp 11/2\rangle$
- 65.02	$0.917\|\pm 15/2\rangle + 0.353\|\pm 7/2\rangle - 0.077\|\mp 1/2\rangle - 0.168\|\mp 9/2\rangle$
- 3.85	$0.145\|\pm 13/2\rangle - 0.407\|\pm 5/2\rangle - 0.270\|\mp 3/2\rangle + 0.861\|\mp 11/2\rangle$
110.41	$0.714\|\pm 13/2\rangle - 0.107\|\pm 5/2\rangle - 0.593\|\mp 3/2\rangle - 0.357\|\mp 11/2\rangle$
142.76	$0.666\|\pm 13/2\rangle + 0.402\|\pm 5/2\rangle + 0.573\|\mp 3/2\rangle + 0.258\|\mp 11/2\rangle$
170.03	$0.026\|\pm 15/2\rangle + 0.253\|\pm 7/2\rangle + 0.936\|\mp 1/2\rangle + 0.242\|\mp 4/5\rangle$

(b)

H || to z-axis	H $\perp$ to z-axis
E_1^o ±2.058 G - 0.2518 G^2	E_1^o ±2.697 G - 0.3324 G^2
E_2^o ±2.199 G + 0.1250 G^2	E_2^o ±2.239 G - 0.0511 G^2
E_3^o ±1.094 G - 0.0651 G^2	E_3^o ±3.349 G + 0.2080 G^2
E_4^o ±6.613 G + 0.1194 G^2	E_4^o ±0.389 G + 0.0324 G^2
E_5^o ±3.633 G + 0.0134 G^2	E_5^o ±1.509 G + 0.0434 G^2
E_6^o ±2.112 G - 0.4463 G^3	E_6^o ±0.8538 G - 0.0859 G^2
E_7^o ±2.427 G + 0.4980 G^2	E_7^o ±2.693 G - 0.2030 G^2
E_8^o ±0.472 G - 0.0075 G^2	E_8^o ±3.931 G + 0.3886 G^2

(ii) $Er^{3+}:YPO_4$

(a)

E_i^o (cm^{-1})	ψ_i^o
-147.27	$0.275\|\pm15/2\rangle - 0.871\|\pm7/2\rangle + 0.301\|\mp1/2\rangle - 0.273\|\mp9/2\rangle$
-108.60	$0.184\|\pm13/2\rangle - 0.846\|\pm5/2\rangle + 0.462\|\mp3/2\rangle - 0.193\|\mp11/2\rangle$
- 94.80	$0.171\|\pm15/2\rangle - 0.310\|\pm7/2\rangle - 0.229\|\mp1/2\rangle + 0.907\|\mp9/2\rangle$
- 14.91	$0.150\|\pm13/2\rangle - 0.443\|\pm5/2\rangle - 0.601\|\mp3/2\rangle + 0.648\|\mp11/2\rangle$
- 12.46	$0.943\|\pm15/2\rangle + 0.292\|\pm7/2\rangle - 0.116\|\mp1/2\rangle - 0.107\|\mp9/2\rangle$
99.93	$0.158\|\pm13/2\rangle - 0.149\|\pm5/2\rangle - 0.642\|\mp3/2\rangle - 0.735\|\mp11/2\rangle$
108.92	$0.071\|\pm15/2\rangle + 0.245\|\pm7/2\rangle + 0.918\|\mp1/2\rangle + 0.302\|\mp9/2\rangle$
169.18	$0.958\|\pm13/2\rangle + 0.257\|\pm5/2\rangle + 0.111\|\mp3/2\rangle + 0.057\|\mp11/2\rangle$

(b)

H || to z-axis	H $\perp$ to z-axis
E_1^o ±2.844 G - 0.1212 G^2	E_1^o ±2.011 G - 0.4676 G^2
E_2^o ±1.484 G - 0.0540 G^2	E_2^o ±3.216 G +0.2856 G^2
E_3^o ±3.173 G + 0.0847 G^2	E_3^o ±1.735 G + 0.0082 G^2
E_4^o ±2.210 G + 0.0026 G^2	E_4^o ±2.580 G + 0.0582 G^2
E_5^o ±6.914 G + 0.0202 G^2	E_5^o ±0.164 G + 0.0046 G^2

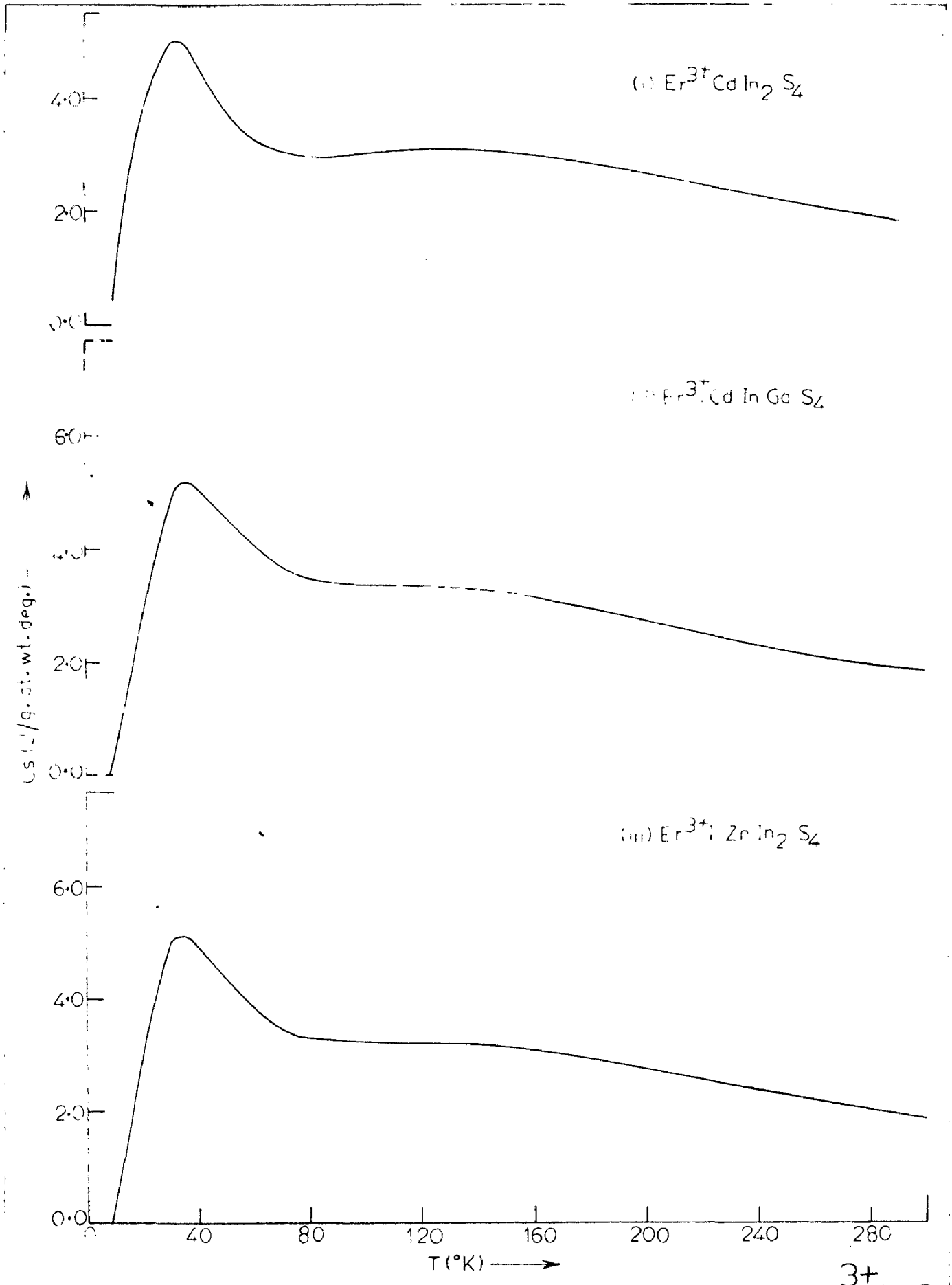

FIG. 5.5 Temperature dependence of schottky specfic heat of $Er^{3+}:CdIn_2S_4$, $Er^{3+}:Cd In Ga S_4$ and $Er^{3+}:Zn In_2 S_4$.

$E_6^o \pm 3.372\ G + 0.0268\ G^2$ $\qquad$ $E_6^o \pm 0.126\ G - 1.1560\ G^2$

$E_7^o \pm 0.585\ G + 0.0163\ G^2$ $\qquad$ $E_7^o \pm 3.887\ G + 1.126\ G^2$

$E_8^o \pm 6.098\ G + 0.0246\ G^2$ $\qquad$ $E_8^o \pm 0.510\ G + 0.131\ G^2$

These values are used to calculate the principal and mean magnetic susceptibilities, magnetic anisotropy, $\bar{\mu}_{eff}$ and Schottky specific heat for both the systems. The results are displayed in Table 5.2 and Fig.5.4.

5.2.4 Discussion

From Fig.5.4 it is observed that the Schottky specific heat exhibits maxima at 28°K (7.85 J/g.at.wt.deg.) and 23°K (6.78 J/g.at.wt. deg.) for Er^{3+}: YVO_4 and Er^{3+}:YPO_4 systems, respectively. The additional entropy associated with the Schottky specific heat upto 400°K comes out to be 16.0 and 16.6 e.u. in the two systems; these numbers compare fairly well with the value 17.3 J/g.at.wt. deg. obtained from the relation, $S = R \ln \frac{2J+1}{2}$

The computed g-values for the ground Stark level are

	$g_{\parallel}$	$g_{\perp}$
Er^{3+}:YVO_4	4.94	6.47
Er^{3+}:YPO_4	6.83	4.83

These have very poor correspondence with the experimental g-values for YVO_4 host lattice : $g_{\parallel} = 3.544 \pm 0.005$, $g_{\perp} = 7.085 \pm 0.005$. This has already been pointed out by Ranon (126). Nonetheless, the mean value of spectroscopic splitting factor for Er^{3+}:YVO_4 as calculated($\bar{g} = 5.96$) and obtained from EPR data($\bar{g} = 5.90$) show a good agreement.

TABLE 5.2: Temperature dependence of Calculated susceptibility parameters and μ_{eff} of $Er^{3+}:YVO_4$ and $Er^{3+}: YPO_4$ systems.

T(^{o}K)	$K_{\parallel}$	$K_{\perp}$	$\bar{K}$	ΔK	$(\frac{\mu}{\mu_B})_{eff}$
	(milli cgs. emu/g.at.wt.)				
	(i) $Er^{3+}:YVO_4$				
300	38.9	37.3	37.8	1.6	9.53
250	46.4	44.6	45.2	1.8	9.51
200	57.2	55.6	56.1	1.7	9.47
150	74.1	73.7	73.9	0.4	9.41
100	103.6	110.0	107.9	-6.4	9.29
75	128.4	145.9	140.1	-17.5	9.17
50	168.9	214.2	199.1	-45.2	8.92
40	194.3	260.5	238.4	-66.2	8.73
30	230.8	326.9	294.9	-96.1	8.41
20	289.4	427.5	381.4	-138.1	7.81
10	417.2	641.7	566.9	-224.5	6.73
	(ii) $Er^{3+}:YPO_4$				
300	34.7	39.5	37.9	-4.8	9.53
250	40.7	47.6	45.3	-6.8	9.51
200	49.2	59.7	53.2	-10.5	9.48
150	62.1	80.0	74.1	-17.9	9.42
100	84.1	120.3	108.2	-36.2	9.30
75	103.2	159.2	140.6	-56.0	9.18
50	138.7	230.6	200.0	-91.9	8.94

40	165.3	277.2	239.9	-111.9	8.76
30	209.7	341.5	297.6	-131.7	8.45
20	295.4	429.7	384.9	-134.2	7.84
10	526.5	568.6	554.6	- 42.1	6.66

In both the systems, the principal and mean magnetic susceptibilities increase with decreasing temperature in accordance with the Curie-Weiss law, $K = C/(T + \theta_p)$; the temperature above which linear trend is observed depends on the direction of study and the nature of the host lattice and likewise the θ_p values. This behaviour of susceptibilities can be described with the following relations:

$Er^{3+}:YVO_4$

$$K_{\parallel} = 12.08/(T+11.4) \qquad T \geq 160^{\circ}K,$$

$$K_{\perp} = 11.32/(T+3.2) \qquad T \geq 80^{\circ}K,$$

$$\bar{K} = 11.70/(T+9.2) \qquad T \geq 10^{\circ}K;$$

$Er^{3+}:YPO_4$

$$K_{\parallel} = 11.71/(T+38.2) \qquad T \geq 60^{\circ}K,$$

$$K_{\perp} = 11.64/(T-51) \qquad T \geq 160^{\circ}K,$$

$$\bar{K} = 11.66/(T+7.9) \qquad T \geq 40^{\circ}K.$$

The difference in θ_p values along different directions is a consequence of low symmetry of CEF at the Er^{3+} site. The computed values of C compare favourably with experimental 11.98 for Er metal (64). In case of $Er^{3+}:YVO_4$ the relative anisotropy $\Delta K/\bar{K}$ decreases from 0.042 at 300°K to -0.396 at 10°K, changing sign at about 144°K. However $\Delta K/\bar{K}$ for $Er^{3+}:YPO_4$ decreases from -0.127 at 300°K to -0.466 at 40°K and then increases to -0.08 at 10°K.

The effective magnetic moments are also derived for the two systems and included in Table 5.2. The room temperature value of 9.53μ_B matches well with the Hund's value of 9.58μ_B for the free ion and 9.52μ_B for metallic erbium (67). The $\bar{\mu}_{eff}$ values are found not to fall more than 3% from the room temperature value down to 90 and 85°K in YVO_4 and YPO_4 host lattices.

5.3 Thermal and Magnetic Properties of Er^{3+}: $CdIn_2S_4$, Er^{3+}:$CdInGaS_4$ and Er^{3+} $ZnIn_2S_4$ Systems

5.3.1 Introduction

The efforts to understand the behaviour of the trivalent rare-earth ions in crystals have long been plagued by the difficulty of low point symmetry at the ion site, as the number of parameters to be determined becomes large and the arbitrariness involved in their evaluation reduces the significance of the conclusions. However, the problem is simplified if the rare-earth ions are introduced into the cubic sites since then only two parameters suffice to specify it. Lea et.al (131) discussed the effect of a cubic field on various rare-earth ions as a function of the ratio between the fourth and sixth degree CEF parameters. Recently, Segal and Wallace (132) carried out similar analysis for hexagonal systems with simplifying assumptions that only fourth and sixth degree terms are involved. But, only a few systems are realisable where the impurity ion sees an exactly cubic or simplified hexagonal coordination. Nonetheless, a number of

workers has discussed the optical spectra of various systems by approximating the low site symmetry to a field of higher one, particularly octahedral (O_h). In this section, we present the calculations of Schottky specific heat, paramagnetic susceptibility parameters, μ_{eff} and g-values of Er^{3+} ion in $CdIn_2S_4$, $CdInGaS_4$ and $ZnIn_2S_4$ systems, whose site symmetry can be approximated by O_h.

5.3.2 Crystal Structure

The thiocompounds $CdIn_2S_4$, $CdInGaS_4$ and $ZnIn_2S_4$ crystallize in the spinel structure and have been shown to have a structure typified by $Cd_{1/2}\ In_{1/2}[Cd_{12}\ In_{3/2}]\ S_4$(133-35). The rare-earth ion occupies the trivalent Indium site and thus goes to a cubic (O_h) site. Brown et al. (133) found that the rare earth ion site has a slight trigonal distortional on strongly cubic symmetry.

5.3.3 Calculations

In a cubic field, the $^4I_{15/2}$ ground term of Er^{3+} splits into a pair of Kramers doublets $2\Gamma_6$ and $2\Gamma_7$ and three $4\Gamma_8$ quartets. The calculations of Lea et al. (131) show that in an O_h field either $2\Gamma_7$ or $4\Gamma_8$ can be the ground level depending on the relative magnitudes of the Fourth and sixth degree terms. When such a system is subjected to an external magnetic field, the sixteen-fold degeneracy is completely lifted and for axis of quantization along one of the cubic axes, the Hamiltonian becomes (neglecting the rare-earth exchange interaction):

$$H = H_{Free} + A_4\langle r^4\rangle \beta_J (O_4^0 + 5\, O_4^4) + A_6^6\langle r^6\rangle \gamma_J (O_6^0 - 21\, O_5^4) + g_J \mu_B H J_Z. \quad (5.2)$$

Since the CEF mixing of multiplets in Er^{3+} is small, the calculations are carried within the ground J manifold. The optical spectra of Er^{3+} in the thiocompounds have been interpreted by Brown et al. (133) and Shand (135) assuming an O_h field with the CEF parameters listed below:

System	$A_4\langle r^4\rangle$ (cm^{-1})	$A_6\langle r^6\rangle$ (cm^{-1})	Ref.
$Er^{3+}:CdIn_2S_4$	195.	8.	133
$Er^{3+}:CdInGaS_4$	205.	6.	135
$Er^{3+}:ZnIn_2S_4$	205.	7.	135

The eigenvalues and eigenvectors of various Stark levels obtained with these parameters are:

E_i^o (cm^{-1})	Γ_n	Ψ_i^o $Er^{3+}:CdIn_2S_4$
-128.46	$^4\Gamma_8$	$0.039\|\pm15/2\rangle+0.480\|\pm7/2\rangle-0.452\|\mp1/2\rangle+0.750\|\mp9/2\rangle$
		$0.040\|\pm13/2\rangle+0.181\|\pm5/2\rangle-0.220\|\mp3/2\rangle+0.958\|\mp11/2\rangle$
- 85.12	$^2\Gamma_7$	$0.633\|\pm13/2\rangle+0.582\|\pm5/2\rangle-0.451\|\mp3/2\rangle-0.239\|\mp11/2\rangle$
- 67.01	$^4\Gamma_8$	$0.077\|\pm15/2\rangle+0.742\|\pm7/2\rangle-0.238\|\mp1/2\rangle-0.622\|\mp9/2\rangle$
		$0.772\|\pm13/2\rangle-0.460\|\pm5/2\rangle+0.413\|\mp3/2\rangle+0.149\|\mp11/2\rangle$
143.55	$^2\Gamma_6$	$0.582\|\pm15/2\rangle+0.331\|\pm7/2\rangle+0.718\|\mp1/2\rangle+0.191\|\mp9/2\rangle$

166.25	$^4\Gamma_8$	$0.809\|\pm15/2\rangle - 0.332\|\pm7/2\rangle - 0.472\|\mp1/2\rangle$
		$-0.114\|\mp9/2\rangle$.
		$0.032\|\pm13/2\rangle - 0.646\|\pm5/2\rangle - 0.760\|\mp3/2\rangle$
		$-0.054\|\mp11/2\rangle$

$Er^{3+}:CdInGaS_4$

-136.09	$^4\Gamma_8$	$0.017\|\pm15/2\rangle + 0.442\|\pm7/2\rangle - 0.427\|\mp1/2\rangle$
		$+0.789\|\mp9/2\rangle$
		$0.006\|\pm13/2\rangle - 0.194\|\pm5/2\rangle + 0.260\|\mp3/2\rangle$
		$-0.946\|\mp11/2\rangle$
- 71.14	$^4\Gamma_8$	$0.039\|\pm15/2\rangle + 0.784\|\pm7/2\rangle - 0.241\|\mp1/2\rangle$
		$-0.571\|\mp9/2\rangle$
		$0.774\|\pm13/2\rangle - 0.479\|\pm5/2\rangle + 0.361\|\mp3/2\rangle$
		$+0.203\|\mp11/2\rangle$
- 67.90	$^2\Gamma_7$	$0.633\|\pm13/2\rangle + 0.582\|\pm5/2\rangle - 0.451\|\mp3/2\rangle$
		$-0.239\|\mp11/2\rangle$
153.67	$^2\Gamma_6$	$0.582\|\pm15/2\rangle + 0.331\|\pm7/2\rangle + 0.718\|\mp1/2\rangle$
		$+0.191\|\mp9/2\rangle$
164.35	$^4\Gamma_8$	$0.312\|\pm15/2\rangle - 0.284\|\pm7/2\rangle - 0.494\|\mp1/2\rangle$
		$-0.126\|\mp9/2\rangle$
		$0.006\|\pm13/2\rangle + 0.628\|\pm5/2\rangle + 0.774\|\mp3/2\rangle$
		$+0.084\|\mp11/2\rangle$.

$Er^{3+}:ZnIn_2S_4$

-135.57	$^4\Gamma_8$	$0.026\|\pm15/2\rangle + 0.457\|\pm7/2\rangle - 0.437\|\mp1/2\rangle$
		$+0.774\|\mp9/2\rangle$
		$0.012\|\pm13/2\rangle + 0.189\|\pm5/2\rangle - 0.244\|\mp3/2\rangle$
		$+0.951\|\mp11/2\rangle$
- 76.86	$^2\Gamma_7$	$0.633\|\pm13/2\rangle + 0.582\|\pm5/2\rangle - 0.451\|\mp3/2\rangle$
		$-0.239\|\mp11/2\rangle$
- 70.77	$^4\Gamma_8$	$0.056\|\pm15/2\rangle + 0.767\|\pm7/2\rangle - 0.241\|\mp1/2\rangle$
		$-0.592\|\mp9/2\rangle$
		$0.774\|\pm13/2\rangle - 0.471\|\pm5/2\rangle + 0.383\|\mp3/2\rangle$
		$+0.182\|\mp11/2\rangle$

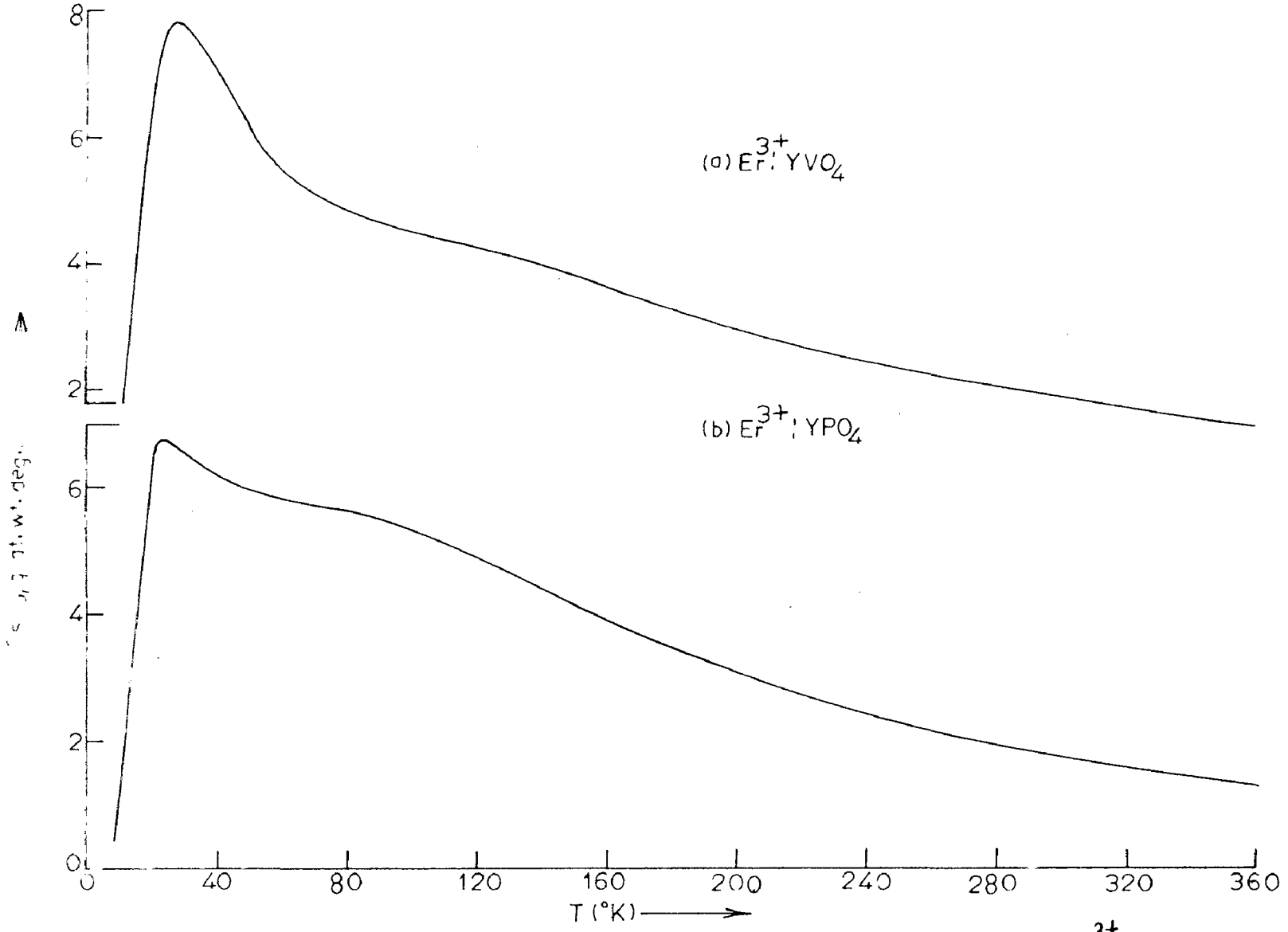

FIG: 5.4 Temperature variation of schottky specific heat of (a)Er^{3+} : YVO_4 and (b)Er^{3+} : YPO_4 systems.

$$168.50 \quad {}^4\Gamma_8 \qquad \begin{aligned} &0.811|\pm 15/2\rangle - 0.305|\pm 7/2\rangle - 0.485|\mp 1/2\rangle \\ &\qquad\qquad - 0.121|\mp 9/2\rangle \\ &0.010|\pm 13/2\rangle - 0.636|\pm 5/2\rangle - 0.768|\mp 3/2\rangle \\ &\qquad\qquad - 0.071|\mp 11/2\rangle \end{aligned}$$

The E_i^o values so obtained are used to get the Schottky specific heat and the results are shown in Fig.5.5.

Following Ayant (136) the eigenvectors of Stark levels in O_h field are designated by

$$\begin{aligned} &[\Gamma_i \pm 1/2\rangle : a_1|\pm 15/2\rangle + a_2|\pm 7/2\rangle + a_3|\mp 1/2\rangle + a_4|\mp 9/2\rangle \\ &\text{and} \qquad\qquad (5.3) \\ &[\Gamma_i \pm 3/2\rangle : b_1|\pm 13/2\rangle + b_2|\pm 5/2\rangle + b_3|\mp 3/2\rangle + b_4|\mp 11/2\rangle . \end{aligned}$$

The state represented by ${}^2\Gamma_6$ belongs to the first eigenvector, ${}^2\Gamma_7$ to the second and ${}^4\Gamma_8$ has both the eigenvectors. The Zeeman splitting of a Γ_8 quartet has been discussed by Ayant (136) and his studies are very useful when it is necessary to take into account small deviations from the cubic field. If the actual CEF has slight trigonal distortion, which is larger than Zeeman energy but smaller than the cubic field, as is the case in thiocompounds, then the Γ_8 quartet splits into two Kramers doublets and these can still be represented by the wavefunctions $|\Gamma_8 \pm 1/2\rangle$ and $|\Gamma_8 \pm 3/2\rangle$. The components of spectroscopic splitting factors are given by

transition	$g_{\parallel}$	$g_{\perp}$
$1/2 \rightleftharpoons -1/2$	$g_J(P-Q)$	$g_J(P+Q)$
$\pm 3/2 \rightleftharpoons \pm 1/2$	$0.5g_J\left[\left\{3(P^2+Q^2)+2PQ\right\}^{1/2} - (P-Q)\right]$	$0.5g_J(P+Q)$
$3/2 \rightleftharpoons -3/2$	$g_J\left\{3(P^2+Q^2)+2PQ\right\}^{1/2}$	0

(5.4)

where

$$P = \langle \Gamma_8\, 3/2 |\, J_z |\, \Gamma_8\, 3/2 \rangle$$

and

$$Q = \langle \Gamma_8 1/2 | J_z | \Gamma_8\, 1/2 \rangle . \qquad 5.5$$

The g-values for the lowest CEF level so generated are listed below:

Host	Transition	$g_{\parallel}$	$g_{\perp}$	$\bar{g}$
	$1/2 \rightleftharpoons -1/2$	3.85	8.21	6.76
$CdIn_2S_4$	$\pm 3/2 \rightleftharpoons \pm 1/2$	4.19	4.11	4.14
	$3/2 \rightleftharpoons -3/2$	12.24	0.0	4.08
	$1/2 \rightleftharpoons -1/2$	3.27	8.56	6.80
$CdInGaS_4$	$\pm 3/2 \rightleftharpoons \pm 1/2$	4.64	4.28	4.40
	$3/2 \rightleftharpoons -3/2$	12.54	0.0	4.18
	$1/2 \rightleftharpoons -1/2$	3.50	8.43	6.79
$ZnIn_2S_4$	$\pm 3/2 \rightleftharpoons \pm 1/2$	4.46	4.22	4.30
	$3/2 \rightleftharpoons -3/2$	12.43	0.0	4.14.

Next, the first and second order magnetic interaction perturbation energies are computed. The complete energy spectrum is as follows:

Unperturbed eigenfunctions Complete energy in magnetic field H

$\underline{Er^{3+}: CdIn_2S_4}$

$| \Gamma_8 \pm 1/2 \rangle$ $E_1^o \mp 1.817\ G - 0.1793\ G^2$

$| \Gamma_8 \pm 3/2 \rangle$ $E_1^o \mp 5.027\ G - 0.0619\ G^2$

$\|\Gamma_7 \pm 3/2\rangle$	$E_2^o \pm 2.833G - 0.4454\ G^2$
$\|\Gamma_8 \pm 1/2\rangle$	$E_3^o \pm 0.197\ G + 0.1609\ G^2$
$\|\Gamma_8 \pm 3/2\rangle$	$E_3^o \pm 4.026\ G + 0.4907\ G^2$
$\|\Gamma_6 \pm 1/2\rangle$	$E_4^o \pm 2.500\ G - 0.4971\ G^2$
$\|\Gamma_8 \pm 1/2\rangle$	$E_5^o \pm 5.120\ G + 0.5156\ G^2$
$\|\Gamma_8 \pm 3/2\rangle$	$E_5^o \pm 0.167\ G + 0.0166\ G^2$

$Er^{3+}:CdInGaS_4$

$\|\Gamma_8 \pm 1/2\rangle$	$E_1^o \mp 2.205\ G - 0.1568\ G^2$
$\|\Gamma_8 \pm 3/2\rangle$	$E_1^o \mp 4.927\ G - 0.0473\ G^2$
$\|\Gamma_8 \pm 1/2\rangle$	$E_2^o \pm 0.669\ G + 0.1409\ G^2$
$\|\Gamma_8 \pm 3/2\rangle$	$E_2^o \pm 4.045\ G - 2.7683\ G^2$
$\|\Gamma_7 \pm 3/2\rangle$	$E_3^o \pm 2.833\ G + 2.7984\ G^2$
$\|\Gamma_6 \pm 1/2\rangle$	$E_4^o \pm 2.500\ G - 1.1357\ G^2$
$\|\Gamma_8 \pm 1/2\rangle$	$E_5^o \pm 5.037\ G + 1.1515\ G^2$
$\|\Gamma_8 \pm 3/2\rangle$	$E_5^o \pm 0.049\ G + 0.0172\ G^2$

$Er^{3+}: ZnIn_2S_4$

$\|\Gamma_8 \pm 1/2\rangle$	$E_1^o \mp 2.054\ G - 0.1627\ G^2$
$\|\Gamma_8 \pm 3/2\rangle$	$E_1^o \mp 4.974\ G - 0.0487\ G^2$
$\|\Gamma_7 \pm 3/2\rangle$	$E_2^o \pm 2.833\ G - 1.4528\ G^2$
$\|\Gamma_8 \pm 1/2\rangle$	$E_3^o \pm 0.480\ G + 0.1462\ G^2$
$\|\Gamma_8 \pm 3/2\rangle$	$E_3^o \pm 4.042\ G + 1.4851\ G^2$
$\|\Gamma_6 \pm 1/2\rangle$	$E_4^o \pm 2.500\ G - 0.7379\ G^2$

$|\Gamma_8 \pm 1/2\rangle$ $\quad E_5^o \pm 5.074\ G + 0.7544\ G^2$

$|\Gamma_8 \pm 3/2\rangle$ $\quad E_5^o \pm 0.098\ G + 0.0165\ G^2$

These energy expressions are employed to extract the gram-atomic susceptibility from the Van Vleck formula and it is found that the results for the three host lattices are nearly same. The values of magnetic susceptibility and μ_{eff} for Er^{3+}:$CdIn_2S_4$ system as a typical case are given in Table 5.3.

5.3.4 Discussion

The Schottky specific heat of Er^{3+} in three thiocompounds shows two peaks:

Host	First peak		Second peak	
	Position T(°K)	magnitude (J/g.at.wt.deg)	Position T(°K)	magnitude (J/g.at.wt.deg.
$CdIn_2S_4$	36	4.88	130	3.02
$CdInGaS_4$	37	5.12	-	-
$ZnIn_2S_4$	36	5.03	120	3.19.

The first peak is relatively sharper than the second and the broadened peak can be attributed to a large separation (~210 cm^{-1}) between a quartet and a doublet resulting into two groups of Stark levels. The extra entropy associated with C_S upto 400°K, S = 10.7 e.u., compares well with the value 11.5 e.u. gotten from S = R ln(2J+1/4) for a quartet ground level.

Brown et al.(133) reported the EPR parameters of Er^{3+}:$CdIn_2S_4$ as $g_{||}$= 1.90±0.05 and $g_{\perp}$ = 9.0±0.2. According to the present calculations, the experimental findings correspond to the allowed transition $1/2 \rightleftharpoons -1/2$; the $\bar{g}_{exp}$=6.63 matches well with computed $\bar{g}$ = 6.76. Similar future experiments

TABLE 5.3: Temperature dependence of paramagnetic susceptibility and effective magnetic moment of $Er^{3+}:CdIn_2S_4$ system.

$T(^oK)$	$K.10^3$(cgs emu)	$\mu_{eff}(\mu_B)$
300	37.9	9.54
250	45.4	9.53
200	56.5	9.50
150	74.7	9.47
100	110.4	9.40
75	145.2	9.33
50	212.0	9.21
40	259.5	9.11
30	334.2	8.95
20	472.2	8.69
10	862.1	8.30

in other two systems for different transitions would provide a good check on the present calculations.

The paramagnetic susceptibility shows a Curie-Weiss dependence on temperature in accordance with the relation, $K = 11.54/(T+4.4)$ down to $10^{\circ}K$. The computed value of Curie constant, $C = 11.54$, is in good agreement with experimental 11.98 for erbium metal (64). Furthermore, the μ_{eff} values extracted from the K values, are nearly same for the three systems. The room temperature magnitude of $9.54\,\mu_B$ matches well with the free ion value $9.58\,\mu_B$ and $9.52\,\mu_B$ for metallic erbium (67). The KT as well as μ_{eff} values exhibit a decrease with decreasing temperature due to gradual emptying of higher CEF levels; it lies within 3% of the room temperature value down to about $60^{\circ}K$ in all the systems.

The agreement observed for g-values of $Er^{3+}: CdIn_2S_4$ with experiment and that for μ_{eff}, S and C of the three systems with the corresponding theoretical parameters and C for metal, shows that the approximation of low symmetry fields with higher ones, is acceptable for calculations of thermal and magnetic quantities.

REFERENCES

1. G.H. Dieke, Spectra and Energy levels of rare-earth ions in crystals, John Wiley and Sons, New York (1968).
2. W. G. Wybourne, Spectroscopic properties of rare-earths, John Wiley and Sons, New York (1965).
3. C.J. Ballhausen, Introduction to ligand field theory, McGraw-Hill Book Co., New York (1962).
4. J. Becquerel, Z. Phys. 58, 205 (1929).
5. H. Bethe, Ann. Physik 3, 133 (1929).
6. H.A. Kramers, Proc. Acad. Sci. Amsterdam 33, 953 (1930).
7. J.H. VanVleck, J. Chem. Phys. 3, 803 (1935); 807 (1935).
8. R. Schlapp and W.G. Penney, Phys. Rev. 42, 666 (1932).
9. W.Low, Solid State Physics Suppl.2, Academic Press (1960).
10. H. Watanabe, Operator methods in ligand field theory, Prentice-Hall Inc., Englewood Cliffs (1966).
11. T. Murao, F.H. Spedding and R.H. Good Jr., J. Chem. Phys. 42 993 (1965).
12. K.W.H. Stevens, Proc. Phys. Soc. A65, 209 (1952).
13. R.J. Elliot and K.W.H. Stevens, Proc. Roy. Soc. A218, 553(1953).
14. R.J. Elliot and K.W.H. Stevens, Proc. Roy. Soc. A219, 387(1953).
15. B.R. Judd, Proc. Roy. Soc. A227, 552(1955).
16. R. Orbach, Proc. Roy. Soc. A264, 458 (1961).
17. M.T. Hutchings, Solid State Physics Vol.16, 227, Academic Press, New York (1964).
18. K.H. Hellwege, Ann Physik 4, 95 (1949).
19. H.M. Rosenberg, Low Temperature Solid State Physics, Clarendon Press, Oxford (1963).

20. H. Meyer and P.L. Smith, J. Phys. Chem. Solids 9, 285 (1959).

21. W. Schottky, Z. Phys. 23, 448 (1922).

22. B.H. Justice and E.F. Westrum Jr., J. Phys. Chem. 67, 339 (1963).

23. J.H. VanVleck, Theory of electric and magnetic susceptibilities, University Press, Oxford (1932).

24. C.A. Hutchison and E.Y. Wong, J. Chem. Phys. 29, 754(1958).

25. E.H. Carlson and G.H. Dieke, J. Chem. Phys. 29, 229(1958).

26. B.R. Judd, Proc. Roy. Soc. A251, 134 (1959).

27. E.H. Carlson and G.H. Dieke, J. Chem. Phys. 34, 1602(1961).

28. H.M. Crosswhite and G.H. Dieke, J. Chem. Phys. 35, 1535(1961).

29. E.Y. Wong and I. Richman, J. Chem. Phys. 36, 1889(1962).

30. F. Varsanyi and G.H. Dieke, J. Chem. Phys. 36, 2951(1962).

31. K.S. Thomas, S.Singh and G.H. Dieke, J. Chem. Phys. 38, 2180(1963).

32. J.C. Eisenstein, J. Chem. Phys. 39, 2134 (1963).

33. G.H. Dieke and B. Pandey, J. Chem. Phys. 41, 1952(1964).

34. N.H. Kiess and G.H. Dieke, J. Chem. Phys. 45, 2729(1966).

35. D.J. Randazzo, J. Chem. Phys. 49, 1808 (1968).

36. W.G. Penney and R. Schlapp, Phys. Rev. 41, 194 (1932).

37. W.H. Zachariasen, J. Chem. Phys. 16, 254 (1948).

38. D.H. Templeton and C.H. Dauben, J. Am. Chem. Soc. 76, 5237 (1954).

39. H. Gobrecht, Ann Phys. (Germany)28, 673 (1937); 31, 755(1938)

40. B.R. Judd, Mol. Phys. 2, 407 (1959).

41. M.J.D. Powell and R. Orbach, Proc. Phys. Soc.78, 753(1961).

42. G.M. Zverev, L.V. Makarenko and A.I. Smirnov, Soviet Phys. - Solid State 9, 2883 (1968).

43. D. Brown, Halides of Lanthanides and Actinides, Interscience Pub., New York, (1968).

44. A.F. Wells, Structural Inorganic Chemistry, Clarendon Press, Oxford (1962).

45. D.H. Templeton and G.F. Carter, J. Phys. Chem. 58, 940 (1954).

46. J.D. Forrester, A. Zalkin, D.H. Templeton and J.C. Wallman, Inorganic Chemistry 3, 185 (1964).

47. R.W.G. Wyckoff, Crystal Structures, Vol.2, John Wiley and Sons, New York (1960).

48. E.Y. Wong, J. Chem. Phys. 35, 544 (1961).

49. M.H. Crozier and W.A. Runciman, J. Chem.Phys. 35, 1392 (1961).

50. K. Rajnak and W.F. Krupke, J. Chem. Phys. 46, 3532(1967).

51. B. G. Wybourne, J. Chem. Phys. 32, 639 (1960).

52. G.H. Dieke and S. Singh, J. Chem. Phys. 35, 555 (1961).

53. F.H. Spedding, Phys. Rev. 58, 255 (1940).

54. A.M. Hellwege and K.H. Hellwege, Z. Phys. 130, 549(1951); 135, 615 (1953).

55. E.V. Sayre, K.M. Sancier and S. Freed, J. Chem. Phys. 23, 2060 (1955).

56. G.H. Dieke and R. Sarup, J. Chem. Phys. 29, 741 (1958).

57. H.M. Crosswhite, G.H. Dieke and W.J. Carter, J. Chem. Phys. 43, 2047(1965).

58. D.R. Behrendt, S.Legvold and F.H. Spedding, Phys. Rev.106, 723 (1957).

59. M.S. Abu Elamayan, J. Chem. (U.A.R.)3, 75 (1960).

60. S. Arajs, R.V. Colvin, J. Appl. Phys. 32, 336S (1961).

61. K.L. Brower and H.J. Stapleton, J. Chem. Phys. 46, 888 (1967).

62. E.B. Kleber and B. Love, The Technology of Scandium, Yttrium andthe rare-earth metals (Pergamon Press, Oxford), p.76 (1963).

63. A.H. Cooke, R. Lazenby and M.J.M. Leask, Proc. Phys. Soc. 85, 767 (1965).

64. S. Arajs and D.S. Miller, J. Appl. Phys. 325 S(1960).

65. B.C. Gerstein, C.J. Penney and F.H. Spedding, J. Chem. Phys. 37, 2610 (1962).

66. R.W. Green, S. Legvold and F.H. Spedding, Phys. Rev. 122, 827(1961).

67. I. Pop, Studii Cercetari Fiz. 17, 755 (1965).

68. B. Schneider, Z. Phys. 177, 179 (1964).

69. J.M. Lock, Proc. Phys. Soc. 70B, 566 (1957).

70. H. Nagasawa and T. Sugawara, J. Phys. Soc. Japan 23, 701 (1967).

71. J.C. Eisenstein, R.P. Hudson and B.W. Magum, Phys. Rev. 137A, 1886 (1965).

72. G.H. Dieke and L. Heroux, Phys. Rev. 103, 1227(1956).

73. C.R. Viswanathan, K. Radisavljevis and E.Y. Wong, J. Chem. Phys. 46, 4231(1967).

74. D.R. Johnston and E.Y. Wong, J. Chem. Phys. 45, 1073(1966); 44, 2693 (1966).

75. V.I. Ivernova, V.P. Tarasova and M.M. Umanskij, Vestn. Mosk. Univ. 8, 37 (1951).

76. B. Bleaney, H.E.D. Scovil and R.S. Trenam, Proc. Roy. Soc. A223, 15 (1954).

77. R. Fricke and A. Seitz, Z.Anorg. Allgem. Chem. 254, 107 (1947).

78. W.P. Wolf, H.E. Meissner and C.A. Catanese, J. Appl. Phys. 39, 1134(1968).

79. P.D. Scott and W.P. Wolf, J. Appl. Phys. 40, 1031 (1969).

80. H.E. Meissner and W.P. Wolf, J. Appl. Phys. 40, 1038(1969).

81. R.W. Cochrane, C. Y.Wu and W.P. Wolf, Abst. EF-2, 16th Conference on Magnetism and Magnetic Material, Nov.16-20 (1970).

82. P.D. Scott, H.E. Meissner and H.M. Crosswhite, Phys. Letters 28A, 489(1969).

83. K. Schubert and A. Seitz, Z. Natureforsch 1, 321 (1946); Z. Anorg. Allgem. Chem. 254, 116 (1947).

84. G.S. Ofelt, J. Chem. Phys. 38, 2171 (1963).

85. W.C. Thoburn, S. Legvold and F.H. Spedding, Phys. Rev. 112, 56(1958).

86. J.H. Vanden Handel and J.C. Hupse, Physica 9, 225(1942).

87. J. Becquerel, W.J. deHass and J.H. Vanden Handel, Physica 5, 753(1938).

88. J.A.A. Ketelaar, Physica 4, 619 (1937).

89. R.J. Elliot, B.R. Judd and W.R. Runciman, Proc. Roy. Soc. A240, 509 (1957).

90. J.M. Baker and B.Bleaney, Proc. Roy. Soc. A245, 156 (1958).

91. E.H. Erath, J. Chem. Phys. 34, 1985 (1961).

92. S. Hüfner, Z.Phys. 169, 417, 427 (1962).

93. J.B. Gruber, J. Chem. Phys. 38, 946 (1963).

94. J.B. Gruber and R.A. Satten, J. Chem. Phys. 39, 1455(1963).

95. G.H. Dieke, Physica 33, 212 (1967).

96. F.H. Spedding, M.T. Rothwell, W.J. Hass and W.L. Sherland, J. Chem. Phys. 48, 4843 (1968).

97. A. Mahalanabis and S.P. Chachra, Indian J. Pure and Applied Phys. 6, 55 (1968).

98. T. Mookherji and A. Mookherji, Indian J. Pure and Appl. Phys. 4, 43(1966).

99. B.C. Gerstein, L.D. Jenning and F.H. Spedding, J. Chem. Phys. 37, 1496 (1962).

100 A.H. Cooke, F.R. Mckim, H. Mayer and W.P. Wolf, Phil. Mag. series 8, 2, 928 (1957).

101 A.H. Cooke, D.T. Edmonds, F.R. Mckim and W.P. Wolf, Proc. Roy. Soc. A252 46 (1959).

102. R.G. Wheeler, F.M. Rames and E.J. Wechtel, J. Appl. Phys. 39, 915 (1968).

103. G. Gremberg, Z. Phys. 159 , 125 (1960).

104. R. Pauthenet, Ann. Phys. 3, 424 (1958).

105. K.A. Wickersheim and R.L. White, Phys. Rev. Letters 8, 483(1962).

106. W.P. Wolf, M. Ball, M.T. Hutchings, M.J.M. Leask and A.F.G. Wyatt, J. Phys. Soc. Japan, Supp. B1, 17, 443 (1962).

107. J.W. Carson and R.L. White, J. Appl. Phys. 31 53S (1960).

108. J. Overmeyer et al., in Paramagnetic Resonanance, W. Low ed., Academic Press, New York (1963), Vol.I.

109. M. Ball, G. Gorton, M.J.M. Leask, D. Ryan and W.P. Wolf, J. Appl. Phys. 32, 267S (1961); 34, 1104 (1963).

110. B.E. Keen et al., J. Appl. Phys. 37, 1120 (1966).

111. D.G. Onn, H. Meyer and J.P. Remeika, Ann. Acad. Sci. Fenn. AVI 210, 218 (1966).

112. J.A. Koningstein, in Optical Properties of ions in Crystals edited by H.M. Crosswhite and H.W. Moos, Interscience Pub., New York (1967), and the references therein.

113. M.T. Hutchings and W.P. Wolf, J. Chem. Phys. 41, 617 (1964).

114. R.A. Buchanan, J.J. Pearson, K.A. Wickersheim and G.F. Hermann, Phys. Rev. 159, 245 (1967); 159, 251 (1967).

115. G.F. Hermann, J.J. Pearson, K.A. Wickersheim and R.A. Buchanan, J. Appl. Phys. 37, 1312 (1966).

116. J.A. Koningstein and J.E. Geusic, Phys. Rev. 136A, 711 (1964).

117. J.A. Koningstein and J.E. Geusic, Phys. Rev. 136A, 726 (1964).

118. P. Grunberg, S. Hüfner, E. Orlich and J. Schmitt, Phys. Rev. 184, 285 (1969).

119. J.A. Koningstein and G. Schaack, Phys. Rev. B2, 1242 (1970).

120. F. Euler and J. Bruce, Acta Cryst. 19, 971 (1965); and reference given there.

121. E.H. Erath, J. Chem. Phys. 34, 1985 (1961).

122. J. Hammann, J. Phys. (Paris) 29, 495 (1968).

123. C. Brecher, H. Samlson, A. Lempicki, R. Riley and T. Peters, Phys. Rev. 155, 178 (1967); also in Optical Properties of ions in crystals, edited by H.M. Grosswhite and H.W. Moos, Interscience Pub., New York (1967).

124. J. Rosenthal, Phys. Rev. 164, 363 (1967).

125. D. Kuse, Z. Phys. 203, 49 (1967).

126. U.Ranon, Phys. Letters 28A, 228 (1968).

127. J. Rosenthal, R.F. Riley and U. Ranon, Phys. Rev. 177, 625 (1969).

128. R.W. G. Wyckoff, Crystal Structures 2nd ed., Vol.3 Chap.VIII, Interscience Pub., New York (1965).

129. W.O. Milligan and L.W. Vernon, J. Phys. Chem. 56, 145 (1952).

130. A.J. Kassmann, J. Chem. Phys. 53, 4118 (1970).

131. K.R. Lea, M.J.M. Leask and W.P. Wolf, J. Phys. Chem. Solids 23, 1381 (1962).

132. E. Segal and W.E. Wallace, J. Solid State Chem. 2, 347 (1970).

133. M.R. Brown, K.G. Roots and W.A. Shand, J. Phys. C 3, 1323 (1970).

134. M.R. Brown, M.D. Martin and W.A. Shand, J. Phys. C 3, 1329 (1970).

135. W.A. Shand, J. Phys. C 3, L115 (1970).

136. Y. Ayant, in Paramagnetic Resonance edited by W. Low, Academic Press, New York (1963).

LIST OF PUBLICATIONS

1. S.P. Taneja, Magnetic Properties of $DyCl_3$ and $HoCl_3$ Single Crystals, J. Phys. Soc. Japan Vol.28, No.5, 1167 (1970).

2. S.P. Taneja, Magnetic Susceptibilities of Hexagonal $ErCl_3$, Phys. Letters Vol.29A, No.5, 253 (1969).

3. S.P. Taneja and S.P. Puri, Crystal Field Calculation of Principal Magnetic Susceptibilities and Anisotropy Variation with Temperature of Anhydrous Neodymium Chloride, Phys. Stat. Sol. Vol.30, No.1, 193 (1968).

4. S.P. Taneja and S.N. Singh, On the g-Tensor and Anisotropy of Paramagnetic Susceptibility of Nd^{3+} Ion in $La_2(SO_4)_3.9H_2O$, Chem. Phys. Letters Vol.4, No.4, 201 (1969).

5. S.P. Taneja, On the Magnetic Properties of Dy^{3+} Ion in Dysprosium Ethylsulphate Singh Crystal, Phys. Stat. Sol. Vol. 36, No.2, 525 (1969).

6. Vishwamittar, S.P. Taneja and S.P. Puri, Thermal and Magnetic Properties of Pr^{3+} and Er^{3+} Ions in a Crystal Field with C_{3h} Site Symmetry, J. Phys. C (in press).

7. Vishwamittar, S.P. Taneja and S.P. Puri, Crystal Field Calculations of Magnetic and Thermal Properties of Tb^{3+} Ion in C_{3h} Field, Chem. Phys. Letters (to appear in May/June 1971).

8. Vishwamittar, S.P. Taneja and S.P. Puri, On the Behavior of Er^{3+} Ion in Tetragonal Crystalline Fields., J. Phys. Chem. Solids (Communicated)
(Part of the work appeared in Bull. Am. Phys. Soc.Vol.16,

325 (1971)).

9. Vishwamittar, S.P. Taneja and S.P. Puri, Thermal and Magnetic Properties of Er^{3+} Ion in Nearly Cubic Crystalline Fields., Int. J. Magnetism (Communicated).

10. Vishwamittar, S.P. Taneja and S.P. Puri, Crystal Field Study of Er^{3+}:YAlG, J. Chem. Phys. (Communicated).

11. S.P. Taneja, Vishwamittar and S.P. Puri, Crystal Field Investigations of $Yb(C_2H_5SO_4)_3.9H_2O$, J. Appl. Phys. (Communicated).